POLITECNICO DI MILANO

DIPARTIMENTO DI ELETTRONICA, INFORMAZIONE E
BIOINGEGNERIA

DOTTORATO DI RICERCA IN BIOINGEGNERIA

Brain functional connectivity in resting state:
methods for networks identification and noise separation
in healthy subjects and Alzheimer's disease

Doctoral dissertation of:
Ludovica Griffanti

Advisors:

Prof. Giuseppe Baselli

Prof. Stephen M. Smith

Dr. Francesca Baglio

Tutor:

Prof. Andrea Aliverti

Chair of the PhD program:

Prof. Maria Gabriella Signorini

XXVI edition
2011-2013

Acknowledgements

Contents

Abstract - English

Aim - The aim of this study was to optimize and validate objective methods of signal detection vs. noise for the investigation of brain functional connectivity with resting state functional magnetic resonance imaging in healthy subjects and patients with Alzheimer's disease.

Background - Resting-state functional magnetic resonance imaging (RS-fMRI) is a widespread and powerful technique for investigating the functional connectivity (FC) of the human brain. With this technique it is possible to study different Resting State Networks (RSNs) that are associated with specific brain functions, and that can be altered in pathological conditions. Although several analysis methods are currently used for the analysis of RS-fMRI data, a common problem is the separation of noise from the neural-related signal of the RSNs, due to the absence of a model for neural activity. Hence, effective methods for the correct identification and removal of the artefacts from the data (*cleaning* or *clean-up*) are needed to obtain reliable FC analyses. This is particularly important in Alzheimer's disease (AD), as the decreased functional connectivity of the default mode network (DMN), quantified on RS-fMRI data, is becoming a possible new biomarker for this pathology. Therefore an early diagnosis and a detailed characterization of this alteration are crucial.

Protocols and results - (i) Methodological developments. The amount of FC estimation errors in seed-based FC analyses was quantified through surrogate data analysis and two approaches for FC maps thresholding have been introduced in order to increase the reliability of single-subject FC analyses. Further, an automated denoising method (FMRIB's ICA-based X-noisefier - FIX), developed in collaboration with the FMRIB (Functional Magnetic Resonance Imaging of the Brain) Centre (University of Oxford, UK), allowed to further improve the FC estimation as, through the cleaning of the raw single-subject data, it can be applied to any FC analysis. The cleaning procedure with FIX consists of the following major operations: single-subject spatial independent component analysis (ICA), component-wise feature extraction, classifier training, components classification, and removal of the artefactual components from the data. FIX achieved over 95% classification (signal vs noise) accuracy for the training sub-sets built by hand-labelling the single-subject independent components (ICs) in three different datasets. The procedure for artefact removal was then optimized, testing the efficacy of several cleaning options on different acquisition sequences (standard EPI and multi-band slice accelerated EPI) at two group ICA model orders (low- and high-dimensional ICA) by means of time series (time series amplitude and spectra), network matrices, and spatial maps analyses.

(ii) Applications. The impact of different data-driven cleaning approaches for RS-fMRI data was evaluated on a population of aged healthy controls and patients with mild to moderate Alzheimer's

disease (AD). Among the tested approaches, the cleaning procedure with FIX showed to be the most effective in correctly detecting the typical FC alteration of the default mode network (DMN) in AD patients. Finally, we obtained promising results for a better localisation and quantification of FC alterations in AD on two RSNs of interest through the combination of an effective cleaning procedure and high-dimensional spatial and temporal RSNs analyses.

Conclusion - The present work has demonstrated and validated both the optimization of known protocols and also novel approaches in basically two directions: 1) an effective cleaning of RS-fMRI data for reliable FC analyses; 2) a more detailed parcellation of the brain and the analysis of the temporal information with time series and network analyses. The discussed results are promising towards an early and accurate detection of FC alterations in pathological conditions and their monitoring at different stages, and support future developments for the definition of reliable non-invasive biomarkers for AD and other pathologies.

Abstract - Italiano

Scopo − Lo scopo di questa tesi è stato quello di ottimizzare e validare metodi obiettivi per l'identificazione del segnale riguardante l'attività neurale rispetto al rumore per lo studio della connettività funzionale cerebrale in soggetti sani e pazienti con malattia di Alzheimer.

Introduzione − La risonanza magnetica funzionale a riposo (*resting state functional magnetic resonance imaging*, RS-fMRI) è una tecnica molto diffusa e utilizzata per lo studio della connettività funzionale (CF) del cervello umano. Con questa tecnica è infatti possibile studiare diverse reti cerebrali, le cosiddette *Resting State Networks* (RSNs), che sono associate a specifiche funzioni e la cui attività può essere alterata in condizioni patologiche. Sebbene esistano attualmente diversi metodi per l'analisi dei dati di RS-fMRI, un problema comune è quello della difficile separazione del rumore dal segnale relativo all'attività neurale delle RSNs, a causa dell'assenza di un modello dell'attività neurale a riposo. Per questo motivo sono necessari metodi efficaci per la corretta identificazione e rimozione degli artefatti dai dati, al fine di ottenere analisi di CF affidabili. L'ottenimento di misure di CF affidabili è particolarmente importante nella malattia di Alzheimer (Alzheimer's disease, AD), poichè la diminuzione di FC osservata in pazienti con AD all'interno della cosiddetta *default mode network* (DMN) e quantificata in dati di RS-fMRI, sta diventando un possibile nuovo biomarker per questa patologia. Perciò una diagnosi precoce e una caratterizzazione dettagliata di questa alterazione sono di cruciale importanza.

Metodi e Risultati − (i) Sviluppi metodologici. E' stato quantificato l'errore di stima in analisi di CF *seed-based* (calcolata cioè come la correlazione tra il segnale in un'area specifica, detta *seed* e il resto del cervello) attraverso l'utilizzo di serie temporali surrogate e sono stati proposti due metodi di sogliatura delle mappe di CF, per aumentare l'affidabilità delle analisi di CF a singolo soggetto. Successivamente, l'introduzione di un metodo di rimozione (*cleaning*) di artefatti e rumore (FMRIB's ICA-based X-noisefier − FIX), sviluppato in collaborazione con il centro FMRIB (Functional Magnetic Resonance Imaging of the Brain) dell'Università di Oxford (Oxford, UK), ha permesso di migliorare ulteriormente la stima della CF poichè, rimuovendo gli artefatti direttamente dai dati grezzi, può essere applicato a qualsiasi analisi di CF. La procedura di *cleaning* consiste nei seguenti passaggi principali: analisi delle componenti indipendenti (*independent component analysis*, ICA), estrazione di caratteristiche spaziotemporali tipiche delle componenti (*features*), addestramento di un classificatore (*training*), classificazione delle componenti in segnale o rumore, rimozione delle componenti rumorose dai dati. FIX ha raggiunto una accuratezza di classificazione di oltre il 95% rispetto alla classificazione manuale in tre diversi dataset costruiti classificando manualmente le componenti (*independent components*, ICs) a singolo soggetto. E' stata poi

ottimizzata procedura per la rimozione degli artefatti, testando l'efficacia di diverse opzioni di *cleaning* su dati acquisiti con diverse sequenza (standard EPI e EPI accelerata multiband), usando due diverse dimensionalità per l'analisi ICA di gruppo (bassa e alta dimensionalità), attraverso analisi di serie temporali (ampiezza e spettro delle serie temporali), analisi di rete e analisi delle mappe spaziali.

(ii) Applicazioni. E' stato valutato l'impatto di diversi approcci di *cleaning* per i dati di RS-fMRI in una popolazione di soggetti sani anziani e pazienti con malattia di Alzheimer. Tra gli approcci testati, la procedura di *cleaning* con FIX si è rivelata la più efficace nell'identificare correttamente nei pazienti con AD la tipica alterazione di CF della DMN. Infine, combinando il *cleaning* con FIX all'analisi ICA di gruppo ad alta dimensionalità sono stati ottenuti risultati promettenti per una miglior localizzazione e quantificazione dell'alterazione funzionale nei pazienti AD in due RSNs di interesse (DMN e network sensorimotoria).

Conclusione – Il presente lavoro ha dimostrato e validato sia l'ottimizzazione di protocolli già disponibili, sia nuovi approcci, principalmente in due direzioni: 1) l'efficace rimozione del rumore dai dati di RS-fMRI per analisi di CF affidabili; 2) la dettagliata parcellizzazione del cervello e l'analisi dell'informazione temporale attraverso analisi delle serie temporali e analisi di rete. I risultati discussi si sono dimostrati promettenti per l'identificazione precoce ed accurata delle alterazioni di CF in condizioni patologiche e il loro monitoraggio a diversi stadi della patologia, con lo scopo ultimo di poter definire accurati biomarker non invasivi per la malattia di Alzheimer e altre patologie.

Parole chiave: risonanza magnetica funzionale a riposo; connettività funzionale; rimozione di artefatti; analisi delle componenti indipendenti; analisi di rete; malattia di Alzheimer.

Extended summary

The present work deals with the study of brain functional connectivity (FC) through resting state functional magnetic resonance imaging (RS-fMRI). This technique addresses Resting State Networks (RSNs) displaying coherent activity, associated with specific brain functions, and altered by pathological conditions. Although several analysis methods are currently used for its analysis, a common issue is the absence of a model for neural activity, which hinder the separation of noise from the neural-related signal from the RSNs. In this thesis this problem is firstly challenged by a preliminary estimation of errors in single-subject seed-based functional connectivity maps and its thresholding through surrogate data. Then, by the development of a tool for the automatic identification and removal of noise in raw single-subject data, by regressing out artefactual independent components (ICs), thus cleaning data prior to any further processing, including group ICA. As to the latter, high-dimensional ICA is used as a powerful approach for obtaining a more detailed parcellation of the brain that allows performing improved spatial, temporal, and network analyses. These methodological innovations are then applied in the challenging field of Alzheimer's disease, where anatomical, microstructural and behavioural abnormalities hinder the quantitative comparison with normal controls, which is aimed at evidence based diagnosis, follow-up, and prognosis.

Background and aim

Resting-state functional magnetic resonance imaging (RS-fMRI) is a widespread and powerful technique for investigating the functional connectivity (FC) of the human brain. In RS-fMRI studies, subjects are asked to rest quietly while brain images are acquired. The idea which stands behind this approach is that the brain regions similarly modulated by stimuli or tasks, rather than being idle during rest, display instead vigorous and persistent functional activity (Buckner et al., 2008), mainly detected as spontaneous though coherent low-frequency BOLD signal fluctuations. The similarity between the time series in different voxels can be estimated, thus providing measures of functional connectivity (FC, Friston et al., 1993; Biswal et al., 1995). In this way FC is suggested to describe the relationship between the neuronal activation patterns of anatomically separated brain regions, reflecting the level of functional communication between regions (Van Den Heuvel, 2010). With this technique it has been observed that, at rest, the brain is organized into Resting State Networks (RSNs) that can be associated with specific functions (Beckmann et al., 2005; Smith et al., 2009). Today the most studied RSNs are: the default mode network (DMN, the first discovered and most studied RSN), the sensory-motor network, the right and the left lateral networks, the

salience network, the ventral stream network, the task positive network, the primary, the medial and the lateral visual networks, and the auditory network.

Among the different available techniques for FC analysis of RS-fMRI data, the most widespread ones, used in this thesis, are seed-based correlation and independent component analysis. Seed-based correlation was the first method used for RS-fMRI FC analyses (Biswal et al., 1995): one or more regions of interest (ROIs) are *a priori* selected to evaluate the similarity (e.g., temporal correlation) of their average time course with each other area or single voxel in the brain. The result is a map of brain voxels significantly correlated with the chosen seed ROI or a quantitative assessment of the strength of correlation with the selected target ROI (Golestani and Goodyear, 2011). Independent Component Analysis (ICA) was introduced in fMRI analysis (McKeown et al., 1998) as a data-driven and hypothesis-free analysis method able to decompose RS-fMRI data into spatially independent components. In this way multiple RSNs can be studied simultaneously. ICA does not require RNS areas to be completely non-overlapping, but only that the different sources of signal change are not distributed in the same way, i.e. that knowledge about the spatial distribution of one does not provide any information on the spatial distribution of the other (Beckmann, 2012).

A common problem of all FC analysis methods is the lack of prior knowledge about the temporal signal of interest (no specific task during acquisition), which makes the RS-fMRI data analysis more challenging than task-based fMRI. This also hinders the correct separation of noise from the neural-related signal from the RSNs. In fact, several sources of noise are present in the data, many of which share some spatial or spectral overlap with RSNs. Spatially extended artefacts can be caused by the scanner (e.g., hardware instabilities), or, more frequently, they are caused by non-neuronal physiological mechanisms (head motion, cardiac and respiratory cycles) (Murphy et al., 2013). Their correct identification and removal (hereafter also called *denoising*, *cleaning* or *clean-up*) is therefore crucial for reliable FC analyses. Other important methodological issues addressed, at least partially, in this thesis were: the need to increase spatial and temporal resolution of fMRI data; the optimization of single-subject FC analyses in order to provide sensitive and accurate detection of FC alterations, to be used as non-invasive biomarkers; the need of a high-dimensionality parcellation of the brain in order to allow more detailed network analyses.

Certainly, the ultimate goal of the optimization of FC analysis methods is their clinical application, and the FC analysis of the RSNs is currently used to study a wide range of neurological and psychiatric disorders (Cole et al., 2010). In this thesis we focused on Alzheimer's disease, the most common cause of neurodegenerative dementia. In this pathology the study of one RSN in particular, the DMN, is especially important because the DMN structures are involved in the memory processes and are vulnerable to atrophy, deposition of the amyloid protein, and generally

show a reduced glucose metabolism (Buckner et al., 2005). Moreover, with RS-fMRI it has been consistently demonstrated a decreased functional connectivity of the DMN, and this is becoming a possible new biomarker for AD (Li et al., 2011; Greicius et al., 2004; Gili et al., 2011). Therefore an early detection and a detailed characterization of this alteration are crucial.

Aims of the study

The aim of this study was to optimize and validate objective methods for the investigation of the RSNs based on resting state fMRI, in healthy subjects and patients with Alzheimer's disease. In particular, once quantified the amount of FC estimation errors in seed-based FC analysis (one of the most common FC analysis techniques), the problem of artefact removal from the raw data was focused, in order to optimize any subsequent FC analysis. An automated denoising method (FMRIB's ICA-based X-noisefier - FIX), was developed in collaboration with the FMRIB (Functional Magnetic Resonance Imaging of the Brain) Centre (University of Oxford, UK), and was tested on different datasets (healthy controls and AD patients), acquisition sequences (standard EPI and multi-band accelerated EPI), and group ICA model orders (low- and high-dimensional group ICA) for spatial, temporal, and network analyses. Finally, through the combination of an effective cleaning procedure and high-dimensional RSNs analysis a better localisation and quantification of FC alterations in AD was aimed at.

Methods

Individual thresholding of seed-based FC maps.

A method for the evaluation of errors in single-subjects FC maps and their thresholding was proposed. It involved the steps summarised in Figure 1 and described below:
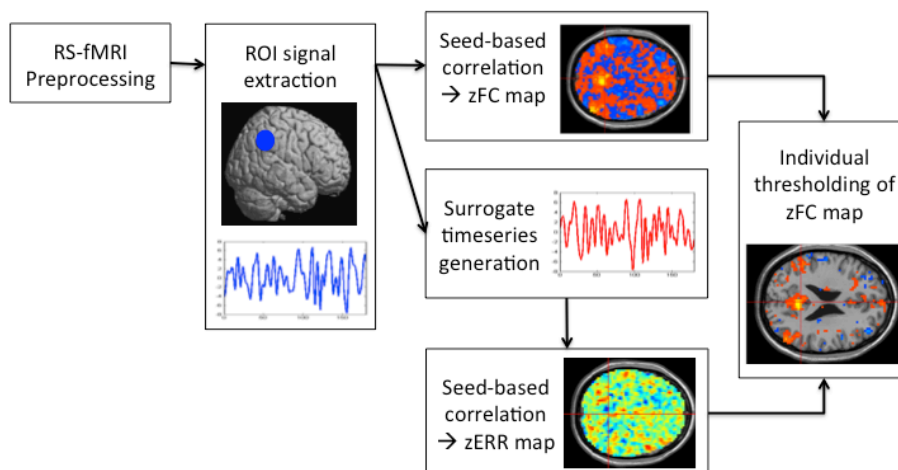
Fig. 1. Overall scheme of the methods used for the individual thresholding of seed-based FC maps

- preprocessing of RS-fMRI data (slice timing, motion correction, coregistration to MNI space, spatial smoothing, regression of nuisance variables, temporal band-pass filtering. See par. 2.2.2)

- extraction of the mean time course within a region of interest (ROI)

- linear correlation (followed by Fisher's r-to-z transformation) between the ROI-time course and the time courses of all acquired voxels in order to obtain the seed-based functional connectivity map (zFCmap)

- generation of surrogate phase-randomized time series of the ROI-time course with the iteratively refined amplitude adjusted Fourier transform (iAAFT) method (Schreiber and Schmitz, 2000)

- computation of seed-based functional connectivity maps using each surrogate time series as seed, in order to obtain error maps (zERRmaps, i.e. consisting only in random correlations)

- calculation of the mean and the standard deviation among the error maps, obtaining an error mean map (meanERRmap) and an error standard deviation map (stdERRmap) for each subject (the distributions of these two maps were fitted to theoretical sample distributions, respectively normal and chi-square distribution, in order to describe the characteristics of the random correlations (errors) within the brain FC maps)

- thresholding of the FC maps:

  o *global thresholding* method: computation of a 2*std (i.e., p<0.05) confidence interval (CI) as $CI_{global} = \overline{m} \pm 2 * \overline{std}$ (where $\overline{m}$ and $\overline{std}$ are the mean values of meanERRmap and stdERRmap distributions respectively), and application of IC_{global} to each voxel of the FC map (voxels showing a correlation value out of the CI are considered as significantly connected with the seed)

  o *local thresholding* method: computation of a 2*std (i.e., p<0.05) confidence interval for each brain voxel (*i*) as $CI_{local}(i) = mean(zERR(i)) \pm 2 * std(zERR(i))$, and application of IC_{local} to the *i*-th voxel of the FC map (voxels showing a correlation value out of the CI are considered as significantly connected with the seed)

This procedure was applied in 15 healthy controls to identify the default mode network (DMN) using a seed in the posterior cingulate cortex (PCC). We described the distribution of the random correlation within the brain, compared the two thresholding methods, and evaluated the intra-subject and inter-subject variability of the threshold.

ICA-based noise identification and removal

A tool for the automatic identification and removal of noise was developed in collaboration with the Functional Magnetic Resonance Imaging of the Brain (FMRIB) Centre (University of Oxford, UK). "FIX" (FMRIB's ICA-based X-noisefier) is an automated approach, once trained, for cleaning fMRI data of various types of noise. This tool is conceived to clean single-subject data before any further processing step (seed-based correlation, group-ICA, network analysis, or other approaches) exploiting a preliminary classification of single-subject independent components into signal or noise and regressing out the noise ones together with motion regressors. The major operations for FIX clean-up can be summarised as follows:

- preprocessing of RS-fMRI data (motion correction, EPI distortions correction, brain extraction, spatial smoothing, high-pass temporal filtering. See par. 3.3.2)
- single-subject ICA decomposition
- training dataset generation (training datasets):
    o manual labelling of the individual components in signal and noise
    o classifier training (using expert-/hand-labelled data)
- automatic classification of single-subject ICs in the test datasets (i.e., predicting components likelihood of being signal or noise)
- noise removal (removal of the artefactual components) (test datasets) – two options:
    o *aggressive* clean-up: regression of the full space of all artefacts (noise components and motion confounds) out of the 4D pre-processed data; however, signal power shared by signal and noise components is also cancelled out.
    o *soft* clean-up: regression of the full space of the motion parameters out of the data; estimation of the contribution of noise and signal components, thus preserving the shared signal power; subtraction of the contribution of the noise components only.

FIX cleaning was applied on three datasets (see details in Table 1) in order to: 1) test the classification accuracy, 2) test the efficacy of the noise removal procedure, and 3) evaluate the impact of the cleaning procedure in a clinical dataset (i.e. patients with Alzheimer's disease).

Table 1. Subjects recruited for FIX training dataset generation and corresponding test dataset used for the different studies evaluating FIX performance.

	Training dataset	**Test dataset**
Dataset 1	23 subjects (HC) – Standard EPI, 3T scanner	53 subject (HC) – Standard EPI, 3T scanner
Dataset 2	23 subjects (HC) – Multiband accelerated (MB6) EPI, 3T scanner	53 subject (HC) – Multiband accelerated (MB6) EPI, 3T scanner
Dataset 3	46 subjects (HC) – standard EPI, 1.5T scanner	41 subjects (20 HC, 21 AD patients) – standard EPI, 1.5T scanner

Legend: HC = healthy controls; AD = Alzheimer's disease patients; EPI = echo planar imaging; MB6 = multiband accelerated, factor 6

Below a summary of the methods applied in the three studies evaluating FIX performance is presented.

1) ICA-based noise identification: accuracy evaluation

On the training sub-sets respectively relevant to each of the three datasets the evaluation of the classification accuracy was tested with a leave-one-out test in terms of "true positive rate" (TPR, meaning the percentage of true signal components correctly detected with respect to manual labelling) and "true negative rate" (TNR, meaning the percentage of true artefact components correctly detected with respect to manual labelling).

2) ICA-based noise removal: efficacy evaluation on healthy controls

On the first two test datasets we tested the efficacy of the denoising procedure with different options. In particular, we compared the two *first-level* (within-subject) cleaning approaches (*soft* vs *aggressive*) for removing artefacts and motion-related parameters from the data and one *second-level* cleaning (*Nets clean-up*, applicable only for time series and network analyses).

With similar analyses we also investigated the combined effects of different cleanings and different acquisition sequences (test dataset 1 vs test dataset 2), in order to evaluate the benefits of the multiband slice accelerated sequence (Moeller et al. 2010; Feinberg et al., 2010) developed partly for the Human Connectome Project (HCP).

The methods are summarised in Figure 2 and described below.
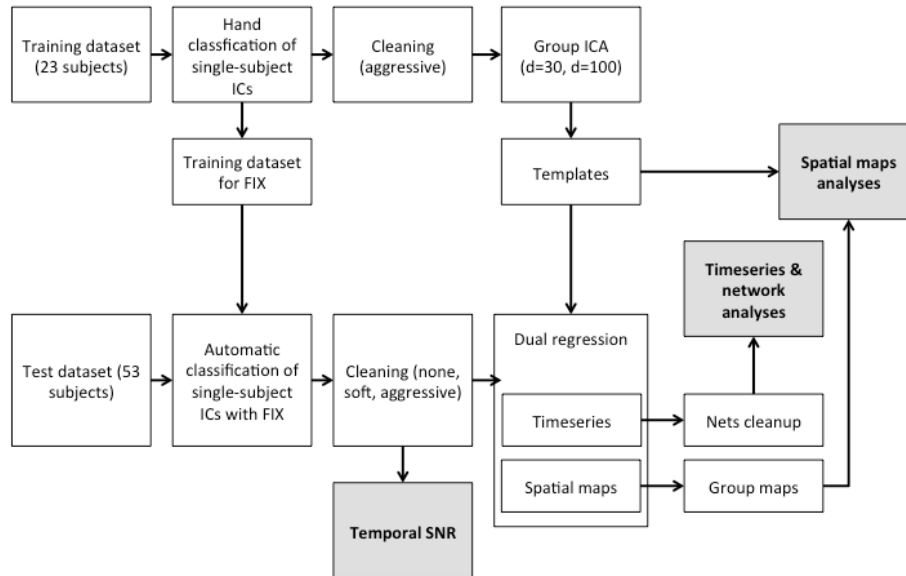
Fig. 2. Overall scheme of the methods used for the efficacy evaluation of FIX denoising on healthy controls

- Templates creation (from training datasets 1 and 2):
  o aggressive removal of the manually-labelled artefactual components
  o coregistration to MNI space
  o temporal concatenation and group ICA at low (d=30) and high (d=100) dimensionality
- preprocessing of test datasets 1 and 2 (motion correction, EPI distortions correction, brain extraction, high-pass temporal filtering. See par. 3.3.2) and ICA-based cleaning with two options (soft or aggressive), obtaining three sets of data: uncleaned data, softly cleaned data and aggressively cleaned data
- coregistration to MNI space
- dual regression using the templates as spatial regressors and generation of single-subject time series and spatial maps for each component
- efficacy evaluation of the different cleaning options and comparison of the two acquisition sequences and the two ICA model orders on:
  o temporal signal-to-noise ratio (SNR, average value within the brain of the image obtained as the ratio between the mean image across time standard deviation image across time).
  o time series amplitude (i.e. the time series standard deviation)
  o time series power spectra
  o network matrices (obtained with full correlation, partial correlation and regularised partial correlation): consistency across subjects

- group spatial maps: similarity with the template

<u>3) Impact of ICA-based noise removal in a clinical dataset (Alzheimer's disease)</u>

The denoising procedure with FIX was also applied to a group of elderly healthy controls and a group of patients with Alzheimer's disease (test dataset 3, using training dataset 3 as sequence-specific training dataset for FIX) and compared with other two common data-driven approaches for the cleaning of RS-fMRI data, in order to evaluate the impact of denoising on the identification of FC alterations in AD. The analyses involved the following steps:

- preprocessing of RS-fMRI data (motion correction, brain extraction, spatial smoothing, high-pass temporal filtering. See par. 5.2.3)
- cleaning with four cleaning options:
    - MOTreg: regression of motion parameters
    - MWCreg: regression of motion parameters, white matter spatial mean signal and CSF mean signal
    - FIXsoft: ICA-based denoising with FIX using the soft option
    - FIXagg: ICA-based denoising with FIX using the aggressive option
- on the data obtained after the different cleaning options (uncleaned, MOTreg, MWCreg, FIXsoft, FIXagg), calculation of:
    - temporal signal-to-noise ratio (SNR)
    - %ΔSTD: the reduction of BOLD signal fluctuations with respect to the uncleaned data.
    - seed-based correlation analysis with seed in the posterior cingulate cortex (PCC)
    - template-based dual regression (Khalili-Mahani et al., 2012; 2013)
- evaluation of the performance of the denoising procedures in terms of increase of within-group consistency and ability to detect the typical FC alteration in the DMN on AD patients (between-group differences).

Clinical application of ICA-based denoising and high-dimensional group ICA in Alzheimer's disease

The innovative combination of ICA-based cleaning and group ICA at high dimensionality introduced and validated on healthy subjects was applied in a preliminary clinical study on AD patients (test dataset 3, 20 HC and 21 AD), aiming at investigating in more detail the functional connectivity of two selected RSNs and their sub-networks. To achieve this, the following steps were performed:

- preprocessing of RS-fMRI data (motion correction, brain extraction, spatial smoothing, high-pass temporal filtering. See par. 6.2.1)

- ICA-based (FIX) aggressive cleaning and coregistration to MNI space.
- temporal concatenation of 4D RS-fMRI preprocessed data and group ICA decomposition at low dimensionality (d=25) and high dimensionality (d=70, as suggested by Abou Elseoud et al., (2010, 2011) and judged to be compatible with the number of temporal degrees of freedom in the data, in order to allow the combination of cleaning and high-dimensional ICA)
- dual regression to obtain single-subject time series and spatial maps for each component
- manual labelling of the low-dimensional components and selection of the RSNs of interest for the study (DMN and sensory-motor network, SMN)
- definition of a classification algorithm to label the high-dimensional components as belonging to the RSNs identified from low-dimensional ICA or as being residual noise; accuracy evaluation of the classification with respect to manual labelling; selection of the sub-networks of interest for the study
- evaluation of between-group differences (HC vs AD) with the two ICA dimensionalities on:
  o time series amplitude
  o network matrices (full correlation)
  o spatial maps

Results

Individual thresholding of seed-based FC maps.

The distribution of random errors within the brain was observed to be homogeneous and, after thresholding with either method, the default mode network areas were well identifiable (see Figure 3). The two methods yielded similar results (Dice index across subjects = 0.81±0.04), however the application of a global threshold to all brain voxels requires a reduced computational load. The inter-subject variability of the global threshold was observed to be very low and not correlated with age. Global threshold values reached a stable plateau with increasing surrogate and this low value can be suggested, with appreciable computational savings.
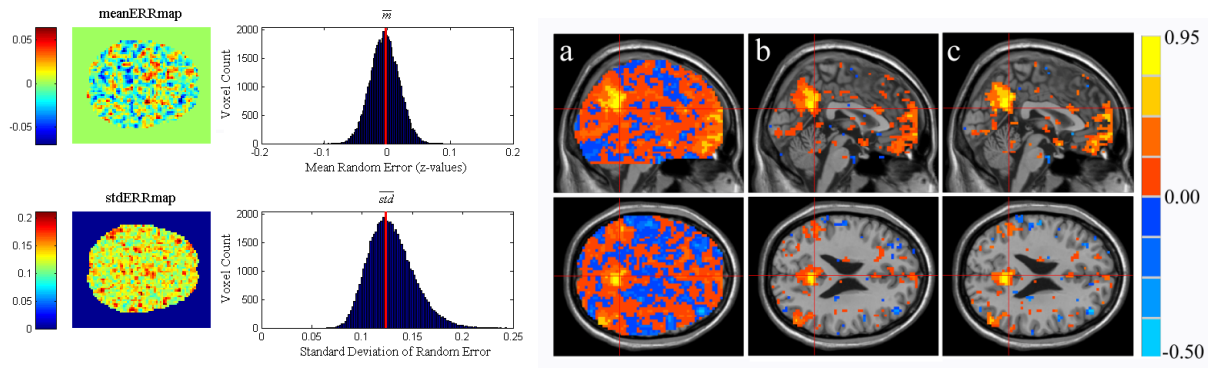
Fig. 3. Results of random error estimation (left, distributions of mean and standard deviation within the brain) and thresholding of a FC map (right, FC map before – a- and after global – b - and local – c - thresholding).

ICA-based noise identification: accuracy evaluation

From the training dataset built through manual labelling of the components, it emerged that the amount of noisy components is more than 70% of the estimated components for 1.5T images (which corresponds to the 30% of the total variance of the original data) and more than 85% (over 65% of the total variance) for 3T images. The best leave-one-out (LOO) results for the three training datasets are summarised in Table 2.

Table 2. FIX classification accuracy obtained with LOO test for the three datasets at the best threshold.

	Training dataset 1	Training dataset 2	Training dataset 3
TPR	97.8	96.5	95.8
TNR	92.2	97.2	79.4

Legend: TPR = True Positive Rate; TNR = True Negative Rate.

ICA-based noise removal: efficacy evaluation on healthy controls

Comparing the different cleaning approaches, the preferable balance between noise removal and signal loss was achieved by regressing out of the data the full space of motion-related parameters and only the unique variance of the artefact ICA components (FIX soft approach), without additional Nets clean-up (see, for example, the results obtained on the power spectra in Figure 4).
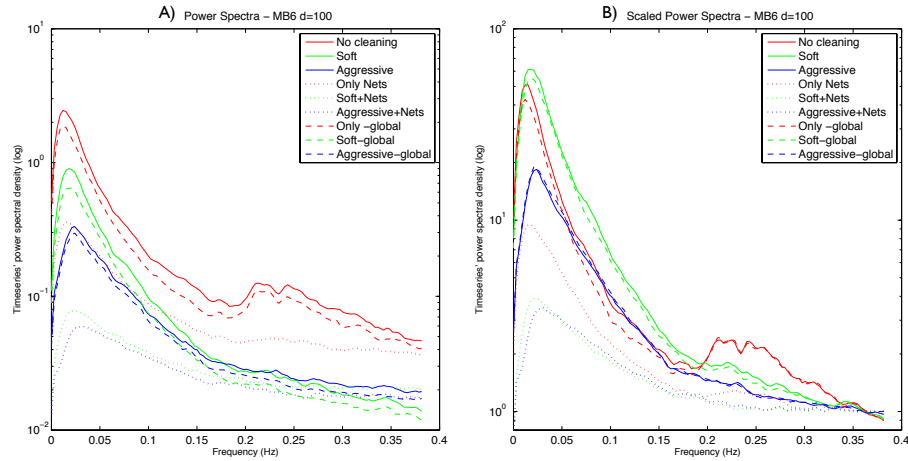
Fig. 4. Temporal power spectra (panel A) for different cleaning approaches, obtained from scaled time series (i.e., each normalised by the amplitude of the corresponding uncleaned time series), averaging the spectra across subjects and then calculating median spectra across components. Uncleaned data have the highest power both at low and high frequency; however, after normalising for power at the highest frequencies (where the content of thermal noise is higher than the content in signal) (panel B), it is clear that with soft clean-up we obtained the highest contrast-to-noise ratio. Results are shown for MB6 data, at d=100 (y axis in logarithmic scale), but were similar for the other protocols.

With the multiband accelerated sequence (MB6), after the optimal cleaning procedure, we achieved functional connectivity results that were statistically comparable or significantly better than the standard (un-accelerated) acquisition, and importantly, with higher spatial and temporal resolution (See Figure 5). Moreover, only with the accelerated data were able to successfully combine single-subject cleaning and high-dimensional ICA decompositions (d=100), which is highly valuable for detailed network analyses.
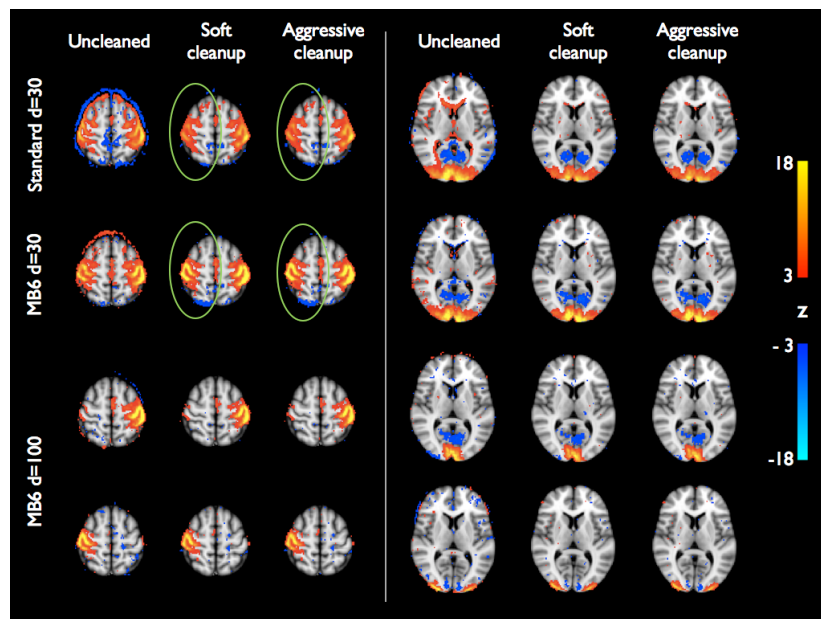
Fig. 5. Group-level z-statistic maps of two RSNs (sensory-motor network and visual network), derived from Standard (d=30) and MB6 (d=30 and d=100) datasets using the corresponding training data templates, without and with soft or aggressive FIX clean-up. Individual subjects' z-statistic maps were mixture model corrected and combined using fixed-effects averaging. Group maps are thresholded at abs(z)>3 (red-yellow colour coding for positive z values, blue-light

blue for negative ones). The effect of the cleaning is noticeably strong in terms of noise removal and more focal signal mapping (as highlighted with the ring around the right sensory-motor network). With high dimensionality the RSNs are split into multiple components, allowing a more detailed analysis of network connectivity.

Impact of ICA-based noise removal in a clinical dataset (Alzheimer's disease)

Figure 6 shows the probability maps of BOLD fluctuation reduction across subjects in the two groups: the reduction is localized at brain boundaries after MOTreg, a small further decrease involves the ventricles and the WM after MWCreg, a large reduction within ventricles and in areas corresponding to blood vessels can be observed after FIX clean-up.
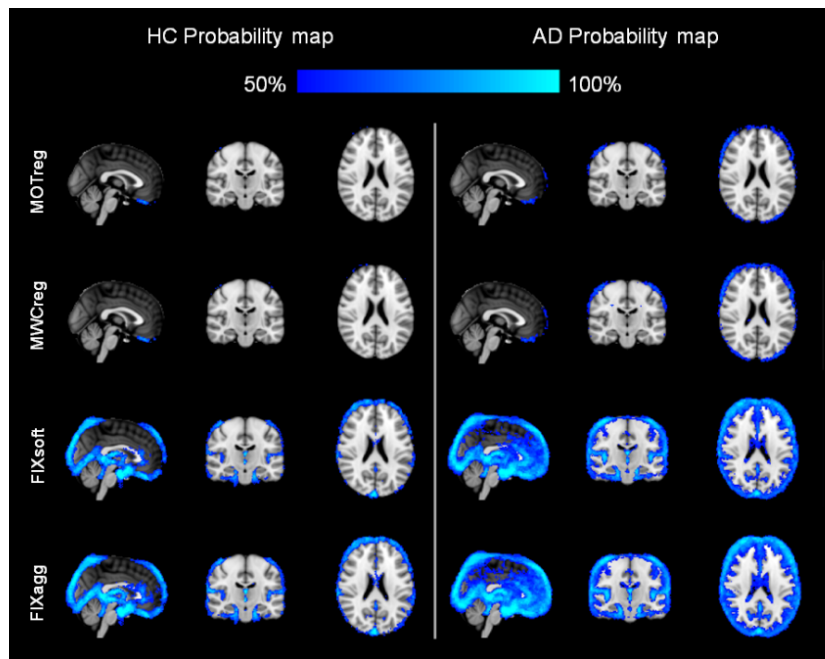
Fig. 6. Spatial pattern of change in BOLD signal standard deviation: probability map of areas where %ΔSTD>25% across all HC (left) or AD patients (right). Images are shown in radiological convention.

Regarding FC analyses, in both groups the consistency increased after cleaning (lower standard deviation across subjects). The consistency was, in general, higher within the HC group than in the AD group and the highest consistency was achieved with MWCreg and FIXagg. However, only after FIXagg a significant FC decrease within the DMN was observed in the AD group both with seed-based correlation and with template-based dual regression (see Figure 7).
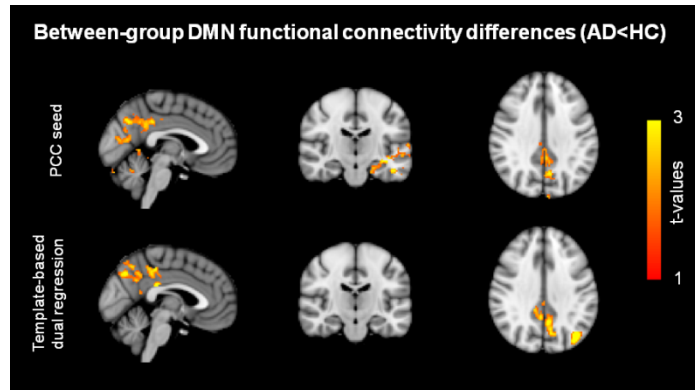
Fig. 7. Between-group differences in functional connectivity results using a seed in the PCC (top) or DMN template-based dual regression (bottom) on data cleaned with FIX aggressive clean-up. Images are shown in radiological convention.

Clinical application of ICA-based denoising and high-dimensional group ICA in Alzheimer's disease

Three low-dimensional components of interest were selected: the posterior and anterior part of the DMN (respectively the posterior cingulate cortex, PCC, and the medial prefrontal cortex, mPFC), and the sensory-motor network (SMN). The classification algorithm showed an accuracy of 95.7% with respect to manual labelling and the sub-networks of interest are showed in Figure 8.
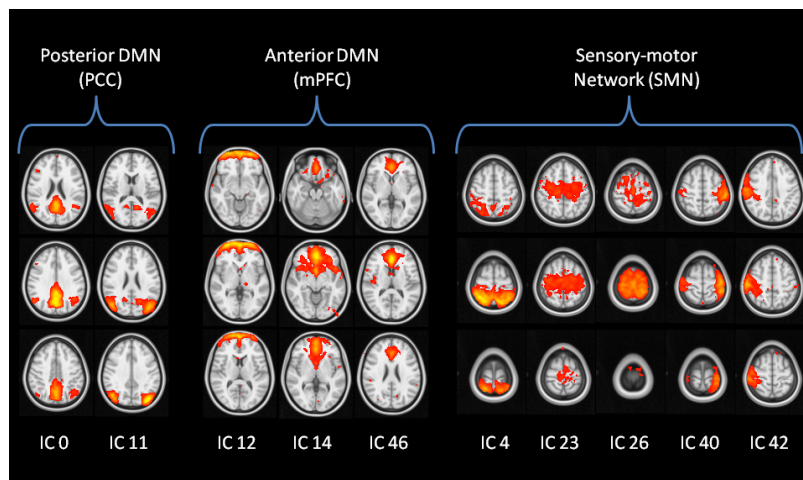
Fig. 8. High-dimensional components relative to the neworks of interest automatically selected by the labelling algorithm with the spatiotemporal-based criteria: the posterior default mode network (PCC) was identified in two components, the medial prefrontal cortex (mPFC) in three, and five components were labelled as belonging to the sensory-motor network (SMN). The number of each component was based on the ranking of variance explained by the component.

As regards low dimensionality results, the time series amplitude was significantly lower in AD patients in all the three components, while only the correlation between the PCC and mPFC components was altered in AD. The spatial analysis highlighted significantly lower activations in AD compared to HC only in the PCC component.

At high dimensionality, the time series amplitude was significantly decreased ($p<0.05$) in AD patients in both PCC sub-networks (PCC_0, PCC_{11}), but only in one component within the mPFC (the ventral mPFC, $mPFC_{14}$) and one in the SMN. The network analyses on the high-dimensional components of interest showed both within-network (mPFC and SMN) and between-network (mPFC-PCC) connectivity alterations in AD (AD<HC, $p<0.05$). Significantly lower activation in the spatial maps was found in AD patients in three high-dimensionality components (PCC_0, $mPFC_{14}$, SMN_{23}). In the PCC sub-network (PCC_0), the decreased activation was localised in the PCC and the precuneus; the alteration in the mPFC ($mPFC_{14}$) involved the ventral mPFC, while a decreased activation in the SMN was localized in the left precentral gyrus.

Discussion

In this work, optimized methods for the correct identification of the RSNs and the detection and removal of the artefacts from RS-fMRI data were proposed.

From the preliminary estimation of errors in the single-subject seed-based functional connectivity maps we observed a homogeneous distribution of random error within the brain, which suggests that this kind of error, although always present, is independent from the resting state activity itself. The proposed thresholding methods are promising for a better identification of the RSNs at single-subject level and, in future studies, they could be applied in a clinical setting to quantify the FC alterations with respect to a seed ROI through the definition of specific FC measures. Indeed, the availability of a reliable single-subject FC analysis could be particularly useful for rare case studies (when a group study is not feasible) and for the longitudinal evaluation of a single patient's disease progression or response to treatment or rehabilitation.

Subsequently, the developed tool (FMRIB's ICA-based Xnoisefier - FIX) for the automatic identification and removal of noise allowed to further improve the reliability of FC estimation since, through the cleaning of the single-subject raw data, it can be applied to any FC analysis. Regarding the classification of signal and noise, FIX achieved over 95% classification accuracy on the three datasets built by hand-labelling of the components, thus demonstrating to be a highly valuable tool for the identification of the artefacts in RS-fMRI data. Our results on the denoising efficacy showed that FIX cleaning is useful to obtain reliable temporal and spatial RS-fMRI analyses: if an artefact is not cleaned at the single subject level and its spatial pattern is overlapping one of the RSNs, it will generally influence both the single-subject RSN time series, (i.e. the output of the first stage of dual regression) and the RSN spatial maps (obtained from the second step of dual regression). In fact, the non-cleaned time series will have higher amplitude with respect to the cleaned data, often with high frequency confounds visible in the power spectra, and the presence of shared noise will in general

produce less consistent network matrices across subjects. The noise would also lead to noisy subject-level z-maps, and affects any following group-level analyses, ultimately reducing the ability to detect specific activation patterns within the RSNs. This problem also affects seed-based resting-state correlation maps for similar reasons, as demonstrated in the application on AD patients. In this population we observed the presence of a greater amount of artefacts, possibly due predominantly to atrophy, and the cleaning procedure with FIX revealed to be particularly useful to detect the typical alteration of the PCC in the DMN with two different FC analysis methods.

The comparison of two different acquisition sequences suggests that the use of multiband (MB) accelerated EPI is advantageous for RS-fMRI analysis for several reasons: i) the increased temporal and spatial resolution yielded a better FIX classification accuracy (98% for MB6 versus 95% for Standard, with leave-one-out testing); ii) a considerably higher proportion of non-artefactual group-ICA components was identified in the MB6 dataset, thus suggesting more successful ICA-based clean-up of MB data; iii) the MB accelerated data allowed a more detailed time series and network analyses through higher dimensionality decomposition (d=100), which was not achievable with the Standard sequence because of its lower temporal degrees of freedom; iv) MB time series spectra after cleaning showed considerably less structured artefact (i.e., deviation from the expected clean 1/f-like spectrum) though preserving mean total time series power; v) network patterns were more reproducible across subjects with MB6; vi) the results of spatial map analyses were not altered in MB data, notwithstanding the lower static image SNR of MB due to its higher resolution.

FIX is now publicly available; the current version (v1.06) is available as a "plugin" for FSL (the FMRIB Software Library) at link www.fmrib.ox.ac.uk/fslwiki/fsl/FIX. The FIX download includes training-weights files for "standard" fMRI acquisitions and for Human Connectome Project (HCP http://www.humanconnectomeproject.org/) RS-fMRI data. In fact, partly due to the study performed in this thesis, FIX is now in use as part of the default HCP analysis pipeline (Smith et al., 2013), and FIX-cleaned data is the recommended version of the resting-state fMRI data that is publicly available – already over 200 subjects' worth of hour-long datasets having been released to date.

Finally, the combined use of ICA-based denoising and high-dimensional group ICA was applied in Alzheimer's disease, in order to investigate in more detail the functional connectivity of two selected RSNs (the DMN and the SMN) and their sub-networks. The creation of an automatic labelling algorithm allowed to automatically identify the sub-networks of interest with an objective and quantitative criterion and to perform a high-dimensional analysis that added complementary information to the low-dimensional one. A future improvement of the algorithm could be the use of a standard template to avoid the need of manually label the low-dimensional components or the

development of an extension of the classifier used by FIX for the automated labelling of group-level components at low and high dimensionality. The study of the temporal information and the more detailed parcellation of the RSNs of interest allowed to detect FC changes in AD that were not detectable with the more common approach of low-dimensional spatial map analyses, thus suggesting that the optimized FC analysis could give further insight into the detection of functional connectivity alterations in pathological conditions for evidence based diagnosis, follow-up and prognosis (Abou Elseoud et al., 2011; Tian et al., 2013). Of course these results needs further research to be confirmed and the analysis on other resting state networks and at different model orders would be the natural progress of this study. Moreover, future studies including patients with Mild Cognitive Impairment (MCI) and severe AD patients, or longitudinal studies on AD patients would better clarify whether the early changes we observed with the temporal analyses truly anticipated changes detectable even in the low-dimensional spatial maps at more advanced disease stages.

Conclusion

The aim of this study was to optimize and validate objective methods for the investigation of the RSNs and the removal of artefacts in resting state fMRI data, applicable to the context of neurodegenerative diseases, especially Alzheimer's disease. With a preliminary study quantified the amount of FC estimation errors in one of the most common FC analysis techniques (seed-based FC) was quantified and a thresholding method was proposed for a reliable single-subject FC analysis. Through the development of FMRIB's ICA-based X-noisefier (FIX), we then demonstrated that, by combining an accurate ICA component classifier with an effective approach for noise removal, we were able to remove artefacts directly from the raw data, automatically, and that we were not removing significant amounts of non-artefactual signal. Moreover, with multiband accelerated sequences and effective cleaning, we were able to perform higher dimensionality decompositions and more detailed RSN analyses than with a standard EPI acquisition. The proposed denoising approach was also demonstrated to be particularly beneficial in clinical applications, as it allowed to correctly detect FC alterations in mild to moderate Alzheimer's disease (AD) patients. Finally, we showed that high-dimensional ICA, supported by a component classification based on low-dimensional ICA, could be successfully applied in clinical studies (e.g. in AD) to gain additional knowledge regarding brain functional connectivity changes in diseased populations. A detailed parcellation of the brain and the analysis of the temporal information (e.g. amplitude and networks analyses) could give further and earlier insight into the detection of functional connectivity alterations in pathological conditions and their monitoring at different stages. The promising results

obtained in describing the functional disconnections due to this neurodegenerative disease support further efforts in this investigation direction, towards the definition of reliable non-invasive biomarkers for AD.

Chapter 1- Background and aim

In this chapter, the scientific and clinical background of neuroimaging methods for the study of brain functional connectivity will be introduced, and both general and specific aims of optimizing these methodologies and applying them in the study of Alzheimer's disease will be described.

1.1. Functional MRI, Resting State functional MRI and functional connectivity

Contemporary functional neuroimaging techniques provide excellent opportunities for investigating the human brain in vivo. It was the advent of the functional imaging modalities of positron emission tomography (PET), single photon emission computed tomography (SPECT), functional magnetic resonance imaging (fMRI), high resolution EEG, and magnetoencephalography (MEG) that led to a new era in the study of brain function.

Throughout the last two decades, fMRI has developed into the most prominent method used for functional brain imaging (Bandettini et al., 2012; Howseman and Bowtell, 1999) and it is increasingly used to probe the functional integrity of brain networks. fMRI is a non-invasive technique for examining brain function through the use of blood oxygen level-dependent (BOLD) contrast. This contrast relies on two basic principles: i) hemoglobin has different properties according to its level of oxygenation (oxyhemoglobin is diamagnetic, while deoxyhemoglobin is paramagnetic) (Ogawa et al., 1990; Kim and Ogawa 2012); ii) regional blood oxygenation varies according to the levels of neural activity. These properties can be used to indirectly assess brain activity (Amaro and Barker, 2006) (Figure 1.1): the activation of a cortical area causes an increase of oxygenated blood inflow, higher than the strict metabolic consumption. This is indirectly sensed, since the arterial blood accelerates the hemodynamic mean transit time in the district, thus pushing away a portion of de-oxygenated blood in the venous capillaries. As deoxyhemoglobin is paramagnetic, it increases the local microscopic magnetic field inhomogeneity Δ B thus shortening the T_2* relaxation time thus accelerating signal fading. In this way, changes in BOLD signal can be used to identify areas of increased or decreased neuronal activity (Logothetis, 2004; Raichle and Mintun, 2006) while subjects perform motor, sensory, cognitive or emotion-provoking tasks (Drobyshevsky et al., 2006).
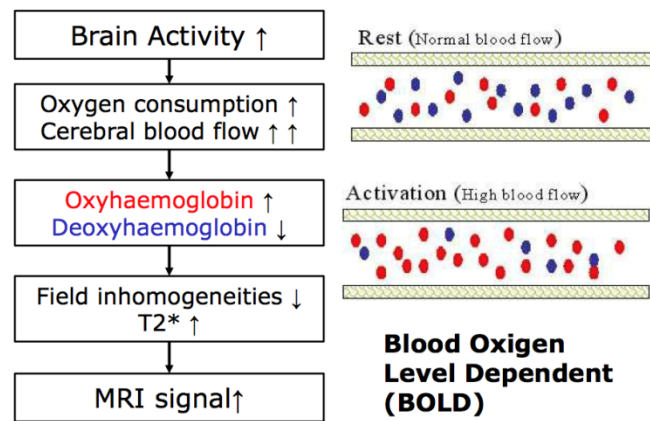
Figure 1.1. Brain activity and BOLD signal principles.

FMRI studies can be divided in two approaches: task-induced and task-independent protocols. The initial fMRI studies in humans focused on task-induced responses in the BOLD signal (Bandettini et al., 2012; Kwong et al., 1992). In standard task-induced fMRI, an experimental task of interest is presented alternately with a control condition (control task or rest) and the BOLD signal during the experimental task is compared to the BOLD signal during the control condition. As the difference between baseline and task-related activation accounts for about 1–5% of the total BOLD signal (Bandettini et al., 1992), statistics over repeated activations (either with a block design or event-related design) is necessary in order to provide response images as statistical parametric maps. In doing this, a parametric model linking the BOLD signal of each voxel to the experimental task is required (Stephan et al., 2006). The mainly adopted model is the general linear model (GLM) (Friston et al., 1995). Regressors are the model inputs (design of the experimental task), which include the expected hemodynamic response (or a set of possible responses, with more sophisticated approaches), and possible confounding factors (registered movements, slow drifts, average signal). A modified version, named event-related, considers events either randomly presented or *a-posteriori* registered, again compared to baseline.

One of the new trends in functional neuroimaging is studying human brain ongoing activity expressed by structured BOLD fluctuations when subjects are not performing any particular task. This practice is task-independent and is also known as *Resting State fMRI* (RS-fMRI). In RS-fMRI studies, subjects are asked to rest quietly for several minutes while brain images are acquired. Since no external time reference is available as in task induced protocols, detection of significant activity relies only on the mutual dependence of the ongoing activity in different areas. Yet, a strong link with task related activity is recognized and has had a primary role in the discovery and classification of RS networks (see below). In fact, the brain regions similarly modulated (i.e., either activated or inhibited) by stimuli or tasks, rather than being idle during rest, display instead vigorous and persistent functional activity (Buckner et al., 2008) detected as spontaneous low-frequency (<0.1

Hz) BOLD signal fluctuations. Interregional correlations of these fluctuations can be estimated, and these quantitative estimates provide measures of functional connectivity.

Functional connectivity (FC) is traditionally defined as the temporal dependency between spatially remote neurophysiological events (Friston 2011). In the context of functional neuroimaging, FC is suggested to describe the relationship between the neuronal activation patterns of anatomically separated brain regions, reflecting the level of functional communication between regions (Van Den Heuvel, 2010). The coherent activity of functionally related brain areas can be captured in BOLD signal during RS-fMRI acquisitions. The first RS-fMRI study was conducted by Biswal and colleagues (Biswal et al., 1995), who, correlating the time course of a seed region of interest (ROI) in the motor area with the time course of all other brain voxels, saw that during rest the left and right hemispheric regions of the primary motor network are not silent, but show a high correlation between their fMRI BOLD time series, suggesting ongoing information processing and ongoing functional connectivity between these regions during rest.

Several studies replicated these pioneering results, showing a high level of FC other regions. In fact, when fMRI studies started to examine the possibility of measuring FC between brain regions as the level of co-activation of spontaneous fMRI time series recorded during rest (Biswal et al., 1997; Cordes et al., 2000; Greicius et al., 2003), it was observed that, at rest, the brain is organized into networks, called Resting State Networks (RSNs), consistent across subjects and highly similar to networks of task-induced activations and deactivations (Beckmann et al., 2005; Damoiseaux et al., 2006; De Luca et al., 2006; Veer et al., 2010; Smith et al., 2009). They are believed to belong to distinct networks serving different functions such as vision, language, etc. Today the most studied RSNs are: the default mode network (DMN), the sensory motor network (SMN), the right and the left lateral networks, the salience network, the ventral stream network, the task positive network, the primary, the medial and the lateral visual networks and the auditory network (Figure 1.2).
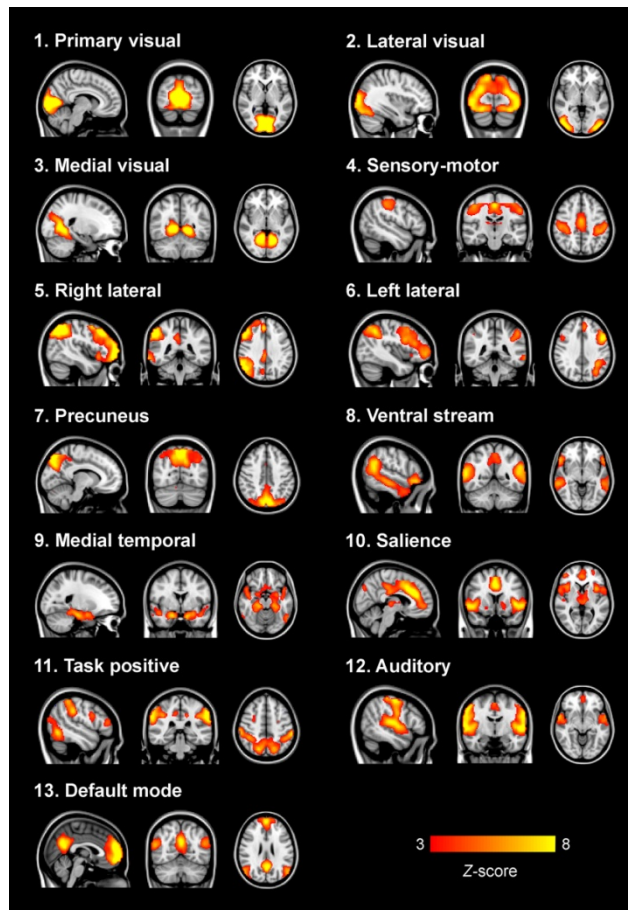
Figure 1.2. The principal and more investigated resting-state networks (Veer et al., 2010)

In particular, the first discovered and most studied RSN is the DMN, which was identified from PET data by Raichle et al. (2001). It includes the posterior and anterior cingulate cortex (PCC and ACC), the inferior parietal lobule (IPL), the medial prefrontal cortex (mPFC) and the hippocampus, regions that are known to show a high level of neuronal activity during rest and a deactivation in physiological conditions during the execution of cognitive tasks, suggesting that activity of this network is reflecting a default state of neuronal activity of the human brain (Gusnard et al., 2001; Raichle et al., 2001; Raichle and Snyder, 2007).

The FC analysis of the RSNs is currently used to study a wide range of neurological and psychiatric disorders, i.e. Alzheimer's disease (Damoiseaux et al., 2012; Sorg et al., 2009), dementia with Lewy bodies (Galvin et al., 2011), frontotemporal dementia (Farb et al., 2013), epilepsy (Cataldi et al., 2013), Parkinson's disease (Göttlich et al., 2013), stroke (Varsou et al., 2013), depression (Sambataro et al., 2013), and schizophrenia (Karbasforoushan and Woodward, 2012) among others. It is therefore of crucial importance the development of sensitive and accurate methods for the detection of FC alterations, to be used as non-invasive biomarkers.

1.2. Functional connectivity analysis methods

The lack of an a priori hypothesis about the brain activation (no specific task during acquisition) makes the RS-fMRI data analysis more challenging than the task-based fMRI. Various methods exist for analysing RS-fMRI FC, among which, the most widely used are: seed-based, model-free methods and network analysis methods.

Seed-based functional connectivity analysis

The first method used for RS-fMRI FC analyses is called seed-based or voxel-based (seed-based hereafter) technique. Firstly described by Biswal and colleagues (1995), it was subsequently applied in several studies (e.g. Raichle et al., 2001; Fox et al., 2005; Cordes et al., 2000; Taylor et al., 2009; Di Martino et al., 2008; Andrews-Hanna et al., 2007). In seed-based approaches one or more regions of interest (ROIs) are *a priori* selected to evaluate the similarity (e.g., temporal correlation) of their average time course with each other area or single voxel in the brain. The result is a map of brain voxels significantly correlated with the chosen seed ROI or a quantitative assessment of the strength of correlation within the target ROI (Golestani and Goodyear, 2011) (Figure 1.3).
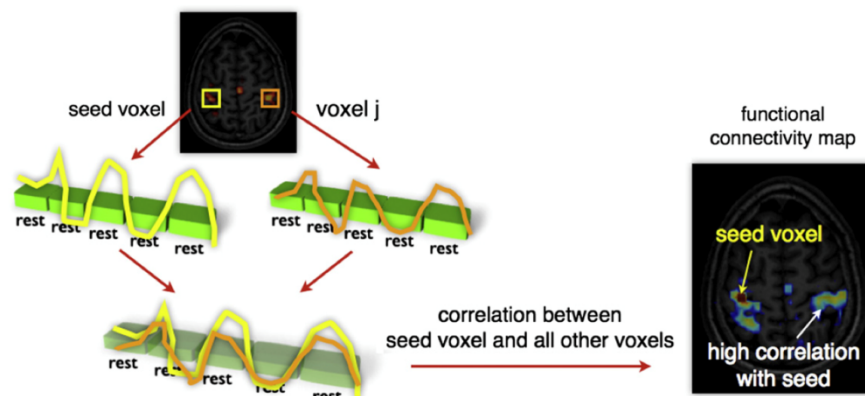
Figure 1.3. Seed-based FC. To examine the level of functional connectivity between the selected seed voxel and a second brain region j, the RS time series of the seed voxel is correlated with the RS time series of region j. A significant correlation between the time series of ROI and voxel j is reflecting a significant level of FC between these regions. Furthermore, to map out all functional connections of the selected seed region, the time series of the seed voxel can be correlated with the time series of all other voxels in the brain, resulting in a functional connectivity map that reflects the regions that show a high level of functional connectivity with the selected seed region (Van Den Heuvel and Hulshoff Pol, 2010).

Seed-based correlation has proven to be a powerful, easily interpretable, and effective tool in identifying and characterising the brain areas that show activity during the resting state. However, the networks obtained from seed-based method depend on the way the seed regions are defined (Cole et al., 2010). Typically, seeds are chosen based on the location of activity during a task (Biswal et al., 1995; Xiong et al., 1999), using anatomical images as a guide (Di Martino et al., 2008; Taylor et al., 2009), or based on standardized coordinates (Maldjian et al., 2003). However, the anatomical volume of known regions may vary between subjects, in the presence of

neurological disease, or with aging, and functional boundaries of brain regions may not be well defined. Hence, using this approach undesired voxels may be included, or functionally relevant voxels may be excluded. Moreover, the seed-based method only evaluates the relationship between the brain and the seed and considers one seed at a time, while, in absence of an *a priori* hypothesis, it might be more informative to simultaneously detect and characterise various different resting state networks from a single RS-fMRI acquisition.

Independent Component Analysis (ICA)

Data-driven methods, like principal component analysis (PCA) (Friston et al., 1993) and independent component analysis (ICA) (Beckmann et al., 2005; De Luca et al., 2006; Binnewijzend et al., 2012; Smith et al., 2009) were introduced as FC analysis methods to look for general connectivity patterns across brain regions. They aim to discover the underlying structure of the data rather than impose an *a-priori* knowledge on the model, with a blind separation of meaningful sources. In this case, instead of pointing a specific RSN by setting a seed, data analysis proceeds on indirect measurements, which are a mixture of true underlying source signals orthogonal (PCA) or maximally independent (ICA) one to each other (Fox and Grecius, 2010). Usually neither the original signals nor the mixing transformation is known and undoing this mixing process is a challenging problem known in the field of signal processing as the blind source separation (BSS) problem (Zarzoso and Nandi, 1999).

In this framework, ICA has therefore developed over the course of decades as an extension of PCA for investigating solutions to the BSS problem. ICA was introduced (McKeown et al., 1998) as an fMRI analysis method able to use decomposition into spatially independent components (Figure 1.4) in order to distinguish between non-task-related signal components, movements and other artefacts, as well as task-related activations. From clinical experience it was noted that psychomotor functions are performed in localized brain areas that can be inferred from specific deficits in patients. This led to the assumption that brain areas that respond to a psychomotor task are independently distributed from brain areas affected by other sources of variability. This does not require these areas to be completely non-overlapping, but only that other sources of signal change are not distributed in the same way as the task-related areas, i.e. that knowledge about the spatial distribution of one does not provide any information on the spatial distribution of the other (Beckmann, 2012).
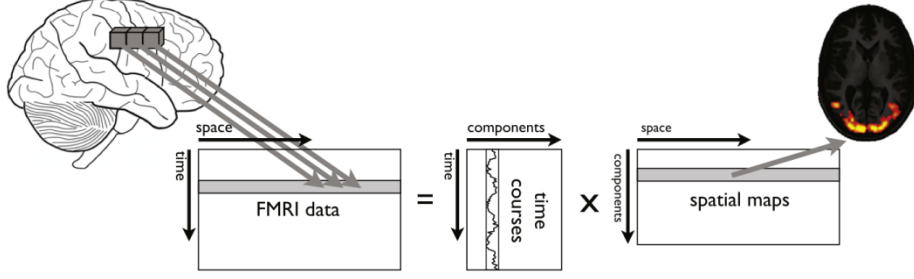
Figure 1.4. Schematic illustration of data representation and spatial decomposition with spatial ICA on fMRI data. The volumes obtained with functional image acquisition are rearranged into a 2D matrix by arranging all voxel for each 3D functional image into a single row. Then, ICA decomposes this dataset into two new matrices, the first one containing a component time course in each column and the second one containing a component spatial map in each row. The i-th time course and the i-th spatial map belong to the i-th component and they jointly describe the temporal and spatial characteristics of underlying hidden signals (Beckmann, 2012).

Mathematically, the ICA model can be expressed as:

$$X = AS \tag{1.1}$$

where the fMRI data are represented by the matrix X p x n (where n is the number of voxels belonging to the volume analysed at p different time points), the matrix S contains statistically independent spatial maps in its rows (which are the spatial areas in the brain, each with an internally consistent temporal dynamic) (Beckmann, 2012), and A is the mixing matrix which contains in its columns the time courses associated to the maps. The sources S are estimated by iteratively optimising the unmixing matrix $W = A^{-1}$, so that $S = WX$ contains mutually independent rows, using the information-maximization (Infomax) algorithm (Bell and Sejnowski, 1995).

An extension of the Independent Component Analysis is the probabilistic ICA (pICA) model, which assumes that the p-dimensional vectors of observations (time series) are generated from a set of q < p (i.e., there are fewer source processes than observations in time) statistically independent non-Gaussian sources (spatial maps) via a linear and instantaneous "mixing" process corrupted by additive Gaussian noise, $\eta(t)$:

$$x_i = As_i + \mu + \eta_i \tag{1.2}$$

x_i denotes the individual measurements at voxel location i, s_i denotes the non-Gaussian source signals contained in the data and η_i denoted Gaussian noise $\eta_i \sim \mathcal{N}(0, \sigma^2 \Sigma_i)$. The covariance of the noise is allowed to be voxel dependent in order to allow for the vastly different noise covariances observed in different tissue types (Woolrich et al., 2005). The vector μ defines the mean of the observations x_i and the matrix A p x q is assumed to be non-degenerate, i.e. of rank q. Solving the blind separation problem requires finding a linear transformation matrix W such that $\hat{s} = Wx$ is a good approximation to the true source signals s (Beckmann, 2012).

The detailed steps involved in estimating the pICA model, described by Beckmann and Smith (2004), implemented in the FSL's tool MELODIC (www.fmrib.ox.ac.uk/fsl/, University of Oxford), and used in this thesis, are schematically illustrated in figure 1.5.
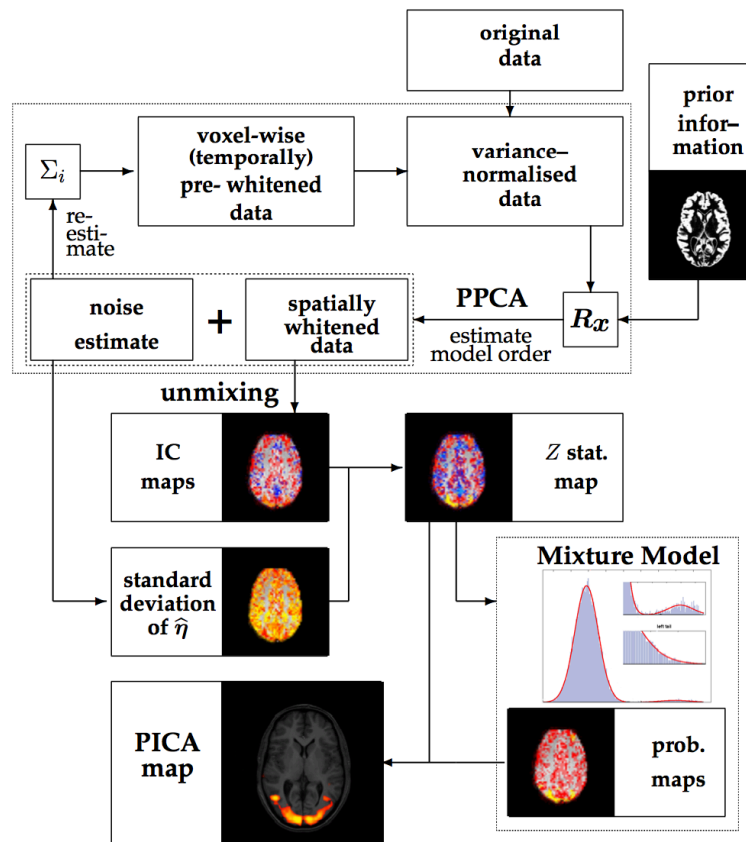
Figure 1.5. Schematic view of the probabilistic ICA model (Beckmann and Smith, 2004).

Network analysis

An alternative to seed-based and model-free analyses is provided by network analyses. In fact, one area of rapidly increasing interest is the mapping of functional networks. Such mapping typically starts by identifying a set of functional "nodes", and then attempts to estimate the set of connections or "edges" between these nodes, based on an analysis of the fMRI time series associated with the nodes (Smith et al., 2011; Smith 2012).

There are many ways to define network nodes from fMRI; nodes are often defined as spatial regions of interest, for example, as obtained from task-fMRI activation or from brain atlases. Alternatively, parcellation via a data-driven clustering of the fMRI data itself (e.g., hierarchical clustering or independent component analysis) can be run to define clusters or components (spatial maps with associated timecourses), which can be considered network nodes. In this case, although the extent of the clusters/components depends on the number of components extracted (e.g. ICA dimensionality), if a higher number of components is estimated (Kiviniemi et al., 2009), these are

more likely to be smaller, isolated regions (parcels), which can more sensibly be then considered as nodes for use in network analysis.

Once the nodes are defined, each has its own associated timecourse (e.g., the average time series from all voxels within the node). These are then used to estimate the connections (edges) between nodes: in general, the more similar the timecourses are between any given pair of nodes, the more likely it is that there is a functional connection between those nodes. Of course, full correlation (between two nodes' time series) is the simplest measure for estimating the connections between nodes, but it does not imply either causality (in itself it tells one nothing about the direction of information flow), or even whether the functional connection between two nodes is direct (there may be a third node "in-between" the two under consideration, or a third node may be feeding into the two, without a direct, or even causally-indirect, connection existing between them). Partial correlation (and regularised partial correlation), can correctly estimate the direct connections (Marrelec et al., 2006; Smith et al., 2011; Smith, 2012), while the study of directionality of the connections can be addressed with effective connectivity approaches (Friston 2011), not addressed in this thesis.

After the network matrix estimation, higher-level analyses based on graph theory (Bullmore and Sporns, 2009), allow to study the topological characteristics. Although not used in this thesis, these analyses include the study of network clustering and hierarchies, the study of network hubs (nodes or clusters that are particularly highly connected to other parts of the network), and deriving network summary statistical measures such as small-worldness (looking at how the clustering acts over multiple scales), and measures of general network efficiency (Rubinov and Sporns, 2010; Van Den Heuvel et al., 2008; Van Den Heuvel and Hulshoff Pol, 2010).

With the growing interest in this field and the huge amount of possible approaches, the scope of network-related research almost falls onto a one-dimensional continuum that starts with neural-level simulations at one end, passes through network modelling methods that are applied to real fMRI data, and ends with the most abstract of the graph-theoretic summaries of a network matrix (Figure 1.6). The various distinctions between the different levels relate to many of the respective strengths and weaknesses of different approaches, and also inform some thoughts about valuable future directions (Smith 2012).
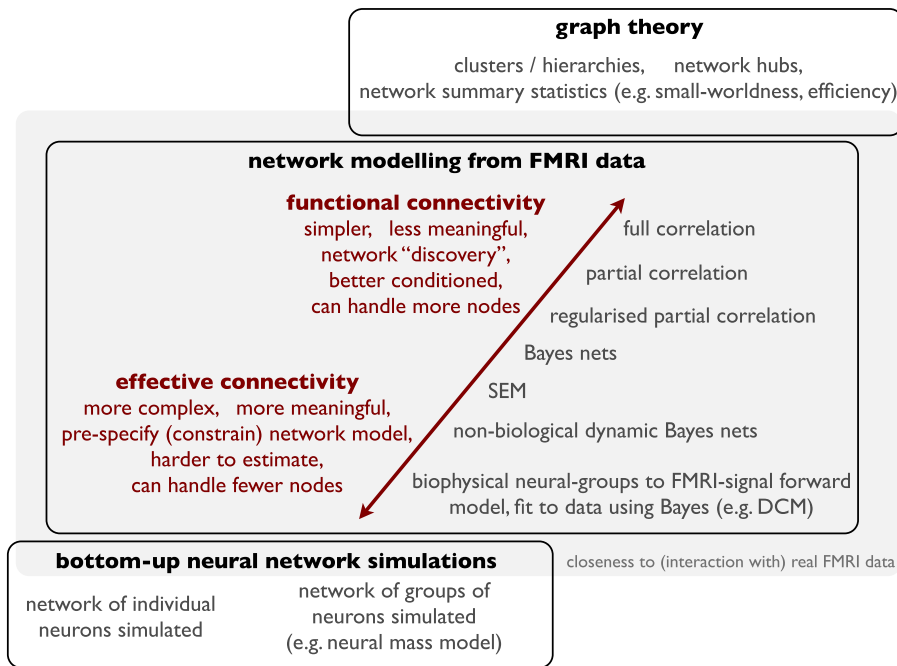
Figure 1.6. Oversimplified schematic of relationships between various network modelling analyses for/from fMRI (Smith 2012).

1.3. Limitations and future perspectives of RS-fMRI functional connectivity analyses

RS-fMRI has its inherent advantages and disadvantages. It avoids performance-related variability of task-induced fMRI studies and the acquisition protocol is easy and quite standard. Furthermore, asking no voluntary task to the subject may be an advantage in cases where the subject active interaction is impaired (e.g. Alzheimer's disease considered in this thesis). RS-fMRI also allows studying different characteristics (spatial, temporal, network properties) of the brain networks and evaluating different functions in a single acquisition.

On the other hand, this technique has its limitations, both relative to the fMRI technique itself (acquisition sequence and preprocessing steps) and specific for the different analysis methods. The methodological issues that will be addressed, at least partially, in this thesis are:

- The need to increase spatial and temporal resolution of fMRI data in order to allow a better localisation of the activations and a detailed temporal, spectral and dynamic analysis of the BOLD signal.

- The development of an effective method for artefact identification and removal that conversely retains as much neuronally-related signal as possible.

- The optimization of single-subject FC analyses in order to provide sensitive and accurate methods for the detection of FC alterations, to be used as non-invasive biomarkers.

- The need of a high-dimensionality parcellation of the brain in order to allow more detailed

network analyses.

For a more complete overview, please refer to (Smith 2012; Beckmann 2012; Bullmore 2012; Feinberg and Yacoub 2012; Van Essen and Ugurbil 2012).

1.4. Functional connectivity changes in Alzheimer's disease

Dementia is one of the main disorders associated with disability, institutionalization, and mortality among elderly individuals. The prevalence of dementia in western developed countries has been reported to be approximately 4% to 8% among people aged 65 years and older (Berr et al., 2005; Lobo et al., 2000). Today the most common cause of neurodegenerative dementia is Alzheimer's disease (AD). The typical clinical presentation of AD is characterized by an early and prominent impairment of memory functions, followed by a progressive accumulation of additional cognitive deficits, eventually resulting in dementia.

Modern research is increasingly focused on AD and much progress has been made in refining the understanding of research. In this framework, imaging techniques have become a major support for the clinical diagnosis of neurodegenerative diseases, as they play a key role as a "window on the brain" (Johnson et al., 2012). Nowadays, in fact, new neuroimaging biomarkers of this brain disorder are available (McKhann et al., 2011); e.g.: structural brain changes visible on MRI with early and extensive involvement of the hippocampus and the medial temporal lobe in Alzheimer's disease (AD); molecular neuroimaging changes seen with PET or fMRI with hypo-metabolism or hypo-perfusion in specific areas.

RS-fMRI, though used only in research so far, is most likely one of the instruments with highest potential as a new biomarker for this neurodegenerative disease (Li et al., 2011; Greicius et al., 2004; Gili et al., 2011), since it is able to detect subtle functional abnormalities in brain networks supporting complex cognitive processes that are progressively impaired over the course of neurodegenerative pathologies (Damoiseaux 2012; Brier et al., 2012).

In the reach scenario of the RSNs, the DMN is particularly relevant for AD patients since many studies have showed that DMN structures, involved in the memory processes, are vulnerable to atrophy, deposition of the amyloid protein (Figure 1.7, panel a), and generally show a reduced glucose metabolism (Figure 1.7, panel b) (Minoshima et al., 1997; Buckner et al., 2005). With RS-fMRI it has been consistently demonstrated a decreased functional connectivity of the DMN in its posterior portion (precuneus, posterior cingulate cortex) to the anterior portion (anterior cingulate and medial prefrontal cortex) also involving medial temporal lobe structures (Figure 1.7, panel c) (Brier et al., 2012; Hafkemeijer et al., 2012; Gili et al., 2011) Moreover, changes in functional connectivity of regions within the DMN, have been found in patients with Mild Cognitive

Impairment (MCI) (Esposito et al., 2013; Gili et al., 2011;Cha et al., 2013; Wang et al., 2013) and in healthy individuals at high risk for developing dementia (Sorg et al, 2009; Filippini et al., 2009; Hafkemeijer et al., 2012).
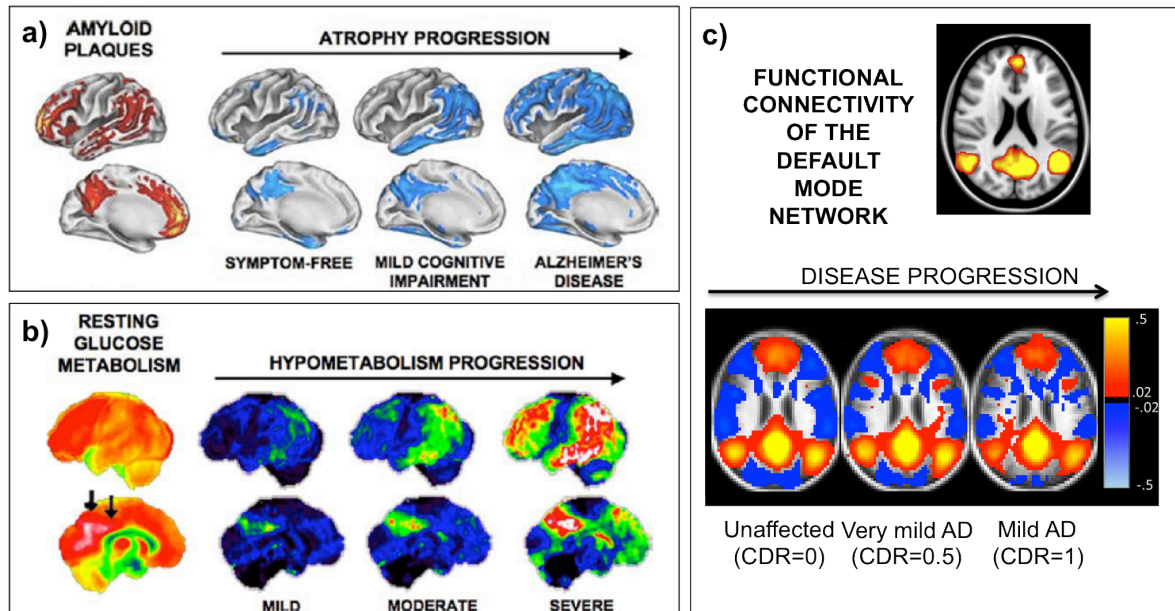
Figure 1.7. Default mode network alterations in Alzheimer's disease. a) Deposition of amyloid plaques and atrophy progression in Alzheimer's Disease (AD) as measured respectively by molecular imaging of amyloid plaques using PET (left) and by longitudinal MRI (right) (adapted from Buckner et al., 2005). b) Glucose metabolism within the DMN. Normal resting glucose metabolism shows a disproportionately high level of metabolism in healthy individuals as measured by FDG-PET (left). Arrows indicate high metabolism near the PCC. AD is consistently associated with progressive reduction in glucose metabolism (hypo-metabolism) in specific regions that overlap the DMN (right). (Minoshima et al., 1997). c) RS-fMRI maps using the PCC as a seed region for cognitive normal subjects (clinical dementia rating - CDR 0), very mild (CDR 0.5), and mild (CDR 1) AD patients. Reduced correlations (less orange and red) and anti-correlations (blue) were seen with increasing disease severity. (Adapted from Brier et al., 2012)

Recently, RS-fMRI studies have investigated the effects of AD also in other RSNs (Brier et al., 2012; Agosta et al., 2012; Li et al., 2012; He et al., 2013), in order to study possible additional FC changes beyond the default mode network and the memory function.

1.5. Aims of the Study

The aim of this study was to optimize and validate objective methods for the investigation of the RSNs based on resting state fMRI, applicable to the context of neurodegenerative diseases, focusing Alzheimer's disease for a pilot clinical validation. In particular, once quantified the amount of FC estimation errors in one of the most common FC analysis techniques (seed-based FC), the wider problem of artefact removal from the raw data in order to optimize any FC analysis was faced. The proposed method (FMRIB's ICA-based X-noisefier - FIX), developed in collaboration with the FMRIB (Functional Magnetic Resonance Imaging of the Brain) Centre (University of Oxford, UK), was validated on different datasets (healthy controls and AD patients), acquisition sequences

(standard EPI and multi-band accelerated EPI), and network dimensionalities (low- and high-dimensional ICA). Finally, we obtained promising results for a better localisation and quantification of FC alterations in AD through the combination of an effective cleaning procedure and high-dimensional network analysis.

The specific objectives of this doctoral thesis were:

- To study the amount of spurious correlations in single subject seed-based FC maps by means of surrogate time series and to calculate a confidence interval for reliable single-subject FC analyses (Chapter 2).

- To test the accuracy in noise identification of a recently developed tool for the cleaning of RS-fMRI data, based on single-subject ICA decomposition (FMRIB's ICA-based X-noisefier - FIX) (Chapter 3).

- To evaluate the effectiveness of FIX in noise removal, testing different cleaning approaches on spatial maps, temporal characteristics and brain networks (Chapter 4).

- To investigate the impact of FIX clean-up on data acquired with an accelerated sequence, in order to optimize this preprocessing step for the analysis of the Human Connectome Project data (Chapter 4).

- To evaluate the feasibility and the impact of low versus high dimensional network analyses using group-ICA. (Chapter 4).

- To apply the cleaning algorithm to a dataset of elderly healthy subjects and a group of patients affected by Alzheimer's disease (AD) in order to evaluate the impact of different cleaning procedures on the within-group consistency of FC results and on the ability to discriminate FC alterations in AD within the DMN (Chapter 5).

- To apply the high-dimensional ICA analysis on elderly healthy subjects and AD patients for a better localisation of the FC alterations in dementia (Chapter 6).

1.6. Thesis structure and author's personal contribution

In this paragraph the structure of the whole thesis work is summarized, recalling its development and highlighting author's personal contribution.

Chapter 2 describes an exploratory evaluation of the errors that affect seed-based FC analyses and two methods for single subject FC analyses. A preliminary phase of the work was the collection of the data and the author was entitled to contribute to the acquisitions (15 healthy subjects) that were performed at the Fondazione don Carlo Gnocchi, IRCCS Santa Maria Nascente (Milano, Italy). Regarding the methods of Chapter 2, the analysis pipeline is mainly based on

existing processing and visualisation tools, with novel contributions relevant to: i) optimal order selection in preprocessing steps, ii) error distribution estimation by phase randomisation, and iii) proposal of two confidence thresholding methods for single-subject FC mappping. The preliminary results of this study are reported in two conference proceedings (Griffanti et al., GNB 2012; Griffanti et al., BSI 2012), while the final work has now been accepted for publication as a full paper (Griffanti et al., *Methods of Information in Medicine*, in press).

During the internship at the Functional Magnetic Resonance Imaging of the Brain (FMRIB) Centre (University of Oxford, UK), the author collaborated at the development of the tool "FIX" (FMRIB's ICA-based X-noisefier). FIX is an automated approach, once trained, for cleaning fMRI data of various types of noise and it consists of several major operations: spatial ICA, component-wise feature extraction, classifier training (using expert-/hand-labelled data), components classification (i.e., predicting components likelihood of being signal vs. noise) and denoising (removal of the artefactual components).

Chapter 3 describes the first four steps, from the theoretical basis of the features extraction and the classification algorithm, to the tests for classification accuracy. In particular, in this phase the author was entitled to build three training datasets and test the classification accuracy of the tool. The first two datasets of RS-fMRI data (25 subjects acquired with standard EPI and multiband slice accelerated EPI) had been previously acquired with standard EPI and multiband accelerated EPI at FMIRB centre, while the author personally contributed to all the acquisitions of the third dataset (42 subjects, 1.5 T Siemens Avanto MRI scanner), that were performed at the Fondazione don Carlo Gnocchi, IRCCS Santa Maria Nascente (Milano, Italy). On these data the author manually classified all the single subject components (on average 70 components per subject for dataset 1, 130 for dataset 2 and 18 for dataset 3, as automatically estimated by the ICA tool used for the decomposition) in signal or noise and performed the classification accuracy tests. The results of these analyses are reported in a paper (Salimi-Khorshidi et al., 2014).

Chapter 4 addresses the improvement of the last step of denoising starting from the actual FIX procedure; i.e., the removal of the artefactual components identified by the classifier. Under the supervision of Prof. Stephen M. Smith, different approaches for artefact removal were developed and tested on 76 healthy subjects, previously acquired at FMIRB centre both by standard EPI and by multiband accelerated EPI. The author carried out all analyses for the optimisation of the cleaning method on time series, network matrices, and spatial maps. The preliminary results are reported in a conference proceeding (Griffanti et al., OHBM 2013) and the final work is now submitted for publication (Griffanti et al., under review). Partially due to the obtained results, FIX is now in use as part of the default Human Connectome Project analysis pipeline (Smith et al., 2013),

and FIX-cleaned data with the optimized options described in Chapter 4 is the recommended version of the resting-state fMRI data that is publicly available – already over 200 subjects' worth of hour-long datasets.

In Chapter 5 and 6, the methods described in Chapter 4 (cleaning procedure and high dimensional ICA network analysis) and optimized on healthy subjects, are applied in a clinical setting for the study of functional connectivity alterations in patients with Alzheimer's disease (AD), compared to a group of age-matched elderly healthy subjects. The author contributed to the acquisition of all the subjects (41 subjects: 21 AD and 20 controls) and personally cured all the image processing and computations both for the cleaning optimization (Chapter 5) and for the high dimensional ICA (Chapter 6). The results are presented in two conference proceedings (Griffanti et al., ISMRM 2014; Griffanti, Dipasquale et al., ISMRM 2014) and a full paper is currently in preparation (Griffanti et al.).

The existing tools for image processing were the basis for a successful analysis of the images and a list of the used software is reported in the Appendix. However, these were combined with in-house scripts coded in Matlab/shell scripting.

1.7. Scientific publications

1.7.1. Publications based on this study

Papers:

Griffanti L, Dipasquale O, Laganà MM, Nemni R, Baselli G, Baglio F. The impact of data-driven cleaning procedures for resting state fMRI on the detection of DMN functional connectivity alterations in Alzheimer's disease. (In preparation)

Griffanti L, Salimi-Khorshidi G, Beckmann CF, Auerbach EJ, Douaud G, Sexton C, Zsoldos E, Ebmeier KP, Filippini N, Mackay CE, Moeller S, Xu J, Yacoub E, Baselli G, Uğurbil K, Miller KL, Smith SM. ICA-based artefact removal and accelerated fMRI acquisition for improved Resting State Network imaging. (Under review)

Salimi-Khorshidi G, Douaud G, Beckmann CF, Glasser MF, **Griffanti L**, Smith SM. Automatic Denoising of Functional MRI Data: Combining Independent Component Analysis and Hierarchical Fusion of Classifiers. *NeuroImage* 2014; 90C 449-468.

Smith SM, Beckmann CF, Andersson J, Auerbach EJ, Bijsterbosch J, Douaud G, Duff E, Feinberg DA, **Griffanti L**, Harms MP, Kelly M, Laumann T, Miller KL, Moeller S, Petersen S,

Power J, Salimi-Khorshidi G, Snyder AZ, Vu AT, Woolrich MW, Xu J, Yacoub E, Uğurbil K, Van Essen DC, Glasser MF; WU-Minn HCP Consortium. Resting-state fMRI in the Human Connectome Project. *Neuroimage* 2013; 80:144-168

Griffanti L, Baglio F, Laganà MM, Preti MG, Cecconi P, Clerici M, Nemni R, Baselli G. Individual thresholding of voxel-based Functional Connectivity maps: estimation of Random Errors by means of Surrogate Time Series. *Methods of Information in Medicine* (In press)

Conference Proceedings:

Griffanti L, Dipasquale O, Laganà MM, Nemni R, Baselli G, Baglio F. How the cleaning of resting state fMRI data affects the detection of functional connectivity alterations in Alzheimer's disease. (Accepted as PowerPoster at ISMRM 2014, Milan)

Griffanti L*, Dipasquale O*, Baglio F, Nemni R, Baselli G. Analysis of resting state brain subnetworks from high dimensional ICA: disconnections in Alzheimer's disease. (Accepted as E-poster at ISMRM 2014, Milan)

Griffanti L, Salimi-Khorshidi G, Beckmann CF, Auerbach EJ, Douaud G, Ebmeier KP, Filippini N, Mackay CE, Moeller S, Xu J, Yacoub E, Baselli G, Ugurbil K, Miller KL, Smith SM. Improving resting state fMRI data quality through accelerated acquisition and automatic denoising. 19th Annual Meeting of the Organization for Human Brain Mapping (OHBM) June 16-20 2013, Washington State Convention Center, Seattle, WA, USA.

Griffanti L, Baglio F, Laganà MM, Preti MG, Cecconi P, Clerici M, Nemni R, Baselli G. Individual thresholding of voxel-based Functional Connectivity maps: estimation of Random Errors by means of Surrogate Time Series. Oral presentation at 7th International Workshop on Biosignal Interpretation (BSI 2012), 7th International Workshop on Biosignal Interpretation 2-4/7/2012. Conf. Proc. 21-24

Griffanti L, Baglio F, Laganà MM, Preti MG, Cecconi P, Clerici M, Nemni R, Baselli G. Stima dell'errore casuale in analisi di connettività funzionale voxel-based: un metodo per la selezione di una soglia individuale. III Congresso Gruppo Nazionale di Bioingegneria (GNB), Roma, 26-29/06/2012. ISBN:978 88 555 3182-5.

1.7.2. Other scientific publications

<u>Papers:</u>

Baglio F, **Griffanti L**, Saibene FL, Ricci C, Alberoni M, Critelli R, Villanelli F, Fioravanti R, Mantovani F, D'Amico A, Cabinio M, Preti MG, Nemni R, Farina E. Multistimulation therapy in Alzheimer's disease promotes changes in brain functioning (Under review)

Preti MG, Makris N, Papadimitriou G, Laganà MM, **Griffanti L,** Clerici M, Nemni R, Westin C, Baglio F, Baselli G. A novel approach of fMRI-guided tractography at the group level allowing to characterize the clinical evolution of Alzheimer's disease. PlosOne (In press)

Baglio F, Cabinio M, Ricci C, Baglio G, Lipari S, **Griffanti L**, Preti MG, Nemni R, Clerici M, Zanette M, Blasi V. Abnormal cortical and subcortical gray matter development in Borderline Intellectual Functioning (Under review).

Baglio F, Saresella M, Preti MG, Cabinio M, **Griffanti L**, Marventano I, Piancone F, Calabrese E, Nemni R, Clerici M. Neuroinflammation and brain functional disconnection in Alzheimer's disease. Frontiers in Aging Neuroscience 2013, 5(81) doi: 10.3389/fnagi.2013.00081

Cagliani R, Guerini FR, Rubio-Acero R, Baglio F, Forni D, Agliardi C, **Griffanti L**, Fumagalli M, Pozzoli U, Riva S, Calabrese E, Sikora M, Casals F, Comi GP, Bresolin N, Cáceres M, Clerici M, Sironi M. Long-Standing Balancing Selection in the THBS4 Gene: Influence on Sex-Specific Brain Expression and Gray Matter Volumes in Alzheimer Disease. Human Mutation 2013 May; 34(5):743-753. doi: 10.1002/humu.22301

Lipari S, Baglio F, **Griffanti L**, Mendozzi L, Garegnani M, Motta A, Cecconi P, Pugnetti L. Commentary on "Altered and asymmetric default mode network activity in a "hypnotic virtuoso": an fMRI and EEG study" - Reply. Consciousness and Cognition 2013 Feb; 22(2): 385-387. doi:10.1016/j.concog.2013.01.005

Lipari S, Baglio F, **Griffanti L**, Mendozzi L, Garegnani M, Motta A, Cecconi P, Pugnetti L. Altered and asymmetric default mode network activity in a "hypnotic virtuoso": an fMRI and EEG study. Consciousness and Cognition 2012 Mar; 21(1):393-400. Epub 2011 Dec 16.

Griffanti L, Baglio F, Preti MG, Cecconi P, Rovaris M, Baselli G, Laganà MM. Signal-to-Noise Ratio of Diffusion Weighted Magnetic Resonance Imaging: estimation methods and in-vivo application to spinal cord. Biomedical Signal Processing and Control 2012, doi:10.1016/j.bspc.2011.06.003

Preti MG, Baglio F, Laganà MM, **Griffanti L**, Nemni R, Clerici M, Bozzali M, Baselli G. Assessing Corpus Callosum Changes in Alzheimer's Disease: Comparison between Tract-Based Spatial Statistics and Atlas-Based Tractography. PlosOne 2012;7(4):e35856. Epub 2012 Apr 24

Baglio F, Castelli I, Alberoni M, Blasi V, **Griffanti L**, Falini A, Nemni R, Marchetti A. Theory of Mind in Amnestic Mild Cognitive Impairment: An fMRI Study. Journal of Alzheimer's disease 2012 Jan 1; 29(1):25-37.

Conference Proceedings:

Baglio F, **Griffanti L**, Saibene FL, D'Amico A, Baselli G, Nemni R. Altered connectivity in ventral stream and medial temporal lobe reflects deficits in Parkinson's disease. Neurological Sciences 2013; 34(S1): S297; ISSN 1590-1874. XLIV Congress of the Italian Society of Neurology. Milan, 2 - 5 november 2013

Tortorella P, **Griffanti L**, Baglio F, Cabinio M, Cecconi P, Caputo D, Rovaris M. Effects of Glatiramer Acetate on cortical functions and fatigue in multiple sclerosis: a morpho-functional MRI study. Neurological Sciences 2013; 34(S1): S165; ISSN 1590-1874. XLIV Congress of the Italian Society of Neurology. Milan, 2 - 5 november 2013

Laganà MM, Tavazzi E, Margaritella N, **Griffanti L**, Garegnani M, Tortorella P, Bergsland N, Cecconi P, Caputo D, Clerici M, Baselli G, Pugnetti L, Rovaris M. Evaluation of spinal cord damage in Multiple Sclerosis patients: a diffusion MRI and somatosensory evoked potential study. Neurological Sciences 2013; 34(S1): S394; ISSN 1590-1874. XLIV Congress of the Italian Society of Neurology. Milan, 2 - 5 november 2013

Baglio F, Cabinio M, Ricci C, Baglio G, Lipari S, **Griffanti L**, Nemni R, Clerici M, Zanette M, Blasi V. The relationship between brain volume and IQ profile in Borderline Intellectual Functioning. Neurological Sciences 2013; 34(S1): S205-S206; ISSN 1590-1874. XLIV Congress of the Italian Society of Neurology. Milan, 2 - 5 november 2013

Tortorella P, Laganà MM, Saresella M, **Griffanti L**, Tavazzi E, Marventano I, Pinardi G, Corbo M, Lunetta C, Cecconi P, Caputo D, Clerici M, Rovaris M. Pathophysiology of tissue damage in progressive multiple sclerosis: an immunological and MRI comparative study versus motor neuron disease. Neurological Sciences 2013; 34(S1): S313 XLIV Congress of the Italian Society of Neurology. Milan, 2 - 5 november 2013

Preti MG, Baglio F, Laganà MM, **Griffanti L**, Saibene FL, Cecconi P, Nemni R, Makris N, Baselli G. FMRI-guided tractography reveals functional and structural brain changes in amnestic MCI. 19th Annual Meeting of the Organization for Human Brain Mapping (OHBM) June 16-20 2013, Washington State Convention Center, Seattle, WA, USA.

Cabinio M, Baglio F, Ricci C, Baglio G, Preti MG, **Griffanti L**, Clerici M, Zanette M, Blasi V. Borderline Intellectual Functioning: the relationship between brain volume and IQ profile. 19th Annual Meeting of the Organization for Human Brain Mapping (OHBM) June 16-20 2013, Washington State Convention Center, Seattle, WA, USA.

Tortorella P, Laganà MM, Saresella M, Tavazzi E, **Griffanti L**, Marventano I, Pinardi G, Corbo M, Lunetta C, Cecconi P, Caputo D, Clerici M, Rovaris M. Pathophysiology of tissue damage in progressive multiple sclerosis: an immunological and MRI comparative study versus motor neuron disease.29th Congress of the European Committee for treatment and research in multiple sclerosis (ECTRIMS). Copenhagen 2-5 October 2013.

Preti MG, Makris N, Papadimitriou GM, Laganà MM, Baglio F, **Griffanti L**, Clerici M, Baselli G. A novel approach of fMRI-guided tractography analysis within a group: construction of an fMRI-guided tractographic atlas. 34th Annual International Conference of the IEEE Engineering in Medicine and Biology Society, San Diego, 2012

Baglio F, **Griffanti L**, Saibene F, Cabinio M, Preti MG, D'amico A, Critelli R, Alberoni M, Cecconi P, Baselli G, Nemni R, Farina E. The impact of two Different Cognitive Training Programs in Outpatienes affected by Mild Cognitive Impairment: a Pilot Study with fMRI. XLIII Congress of the Italian Society of Neurology 2012. It J Neurol Sci 2012

Tortorella P, Lagana MM, Saresella M, **Griffanti L**, Marventano I, Pinardi G, Corbo M, Lunetta C, Cecconi P, Caputo D, Clerici M, Rovaris M. Pathophysiology of tissue damage in progressive multiple sclerosis: an immunological and MRI comparative study versus motor neuron disease. American Academy of Neurology, 2012

Baglio F, **Griffanti L**, Preti MG, Laganà MM, Alberoni M, Villanelli F, Carelli L, Saibene F, Critelli R, Cecconi P, Baselli G, Nemni R, Farina E. Potential neuroprotective effect of non-pharmacological interventions in promoting cognitive and physical well-being in MCI and AD. Oral Presentation at Preconference Meeting 7th Panhellenic Conference on Alzheimer's disease, 15/02/2011.

Baglio F, **Griffanti L**, Preti MG, Laganà MM, Alberoni M, Villanelli F, Carelli L, Saibene F, Critelli R, Cecconi P, Baselli G, Nemni R, Farina E. The Efficacy of Multidimensional Stimulation Theraphy in People Living with Alzheimer: a Randomized Controlled Trial with Fmri. The journal of Nutrition, Health and Aging 2011; 14(4) pp. 317. (International Academy on Nutrition and Aging Meeting)

Baglio F, Preti MG, Saresella M, Laganà MM, **Griffanti L**, Farina E, Calabrese E, Alberoni M, Piancone F, Baselli G, Clerici M, Nemni R. Neuroimmunological and MRI analysis for the detection of prognostic biomarkers in Alzheimer's Disease and Mild Cognitive Impairment. It J Neurol Sci 2011; Congress of the Italian Neurological Society, SIN

Baglio F, **Griffanti L**, Preti MG, Laganà MM, Alberoni M, Villanelli F, Carelli L, Saibene F, Critelli R, Cecconi P, Baselli G, Nemni R, Farina E. The Efficacy of Multidimensional Stimulation Therapy in Mild to Moderate Alzheimer's Disease Patients: a Randomized Controlled Trial with fMRI. Journal of Alzheimer's disease 2011 Feb; 23 (S1): S47. Epub 2011 Feb 18. ISSN 1387-2877. Sindem Meeting: Italian Association for the Study of Dementia linked to the Italian Neurological Society, SIN

Baglio F, **Griffanti L**, Preti MG, Laganà MM, Alberoni M, Critelli R, D'amico A, Pini A, Cecconi P, Baselli G, Nemni R, Farina E. Cognitive Training in Outpatients Affected by Mild Cognitive Impairment: a Longitudinal Study with fMRI. Journal of Alzheimer's disease 2011 Feb; 23 (S1): S47-S48. Epub 2011 Feb 18. ISSN 1387-2877. Sindem Meeting: Italian Association for the Study of Dementia linked to the Italian Neurological Society, SIN

Baglio F, Preti MG, **Griffanti L**, Pugnetti L, Farina E, Garegnani M, Laganà MM, Cecconi P, Baselli G, Nemni R. fMRI, Tractography and EEG Analysis Integrated into Neurological Diagnosis of Corticobasal Degeneration. A Case Study. Journal of Alzheimer's disease 2011 Feb; 23 (S1): S46-S47. Epub 2011 Feb 18. ISSN 1387-2877. Sindem Meeting: Italian Association for the Study of Dementia linked to the Italian Neurological Society, SIN

Farina E, Baglio F, **Griffanti L**, Preti MG, Laganà MM, Alberoni M, Villanelli F, Carelli L, Saibene F, Critelli R, Cecconi P, Baselli G, Nemni R. Les maladies apparentées à la maladie d'Alzheimer, diagnostic et soins à l'hôpital de jour. Poster at 31ème Congrès National des Hôpitaux de Jour Gériatriques 26 et 27 May 2011 – Lyon.

Preti MG, Laganà MM, Baglio F, **Griffanti L**, Nemni R, Cecconi P, Baselli G. Comparison between skeleton-based and atlas-based approach in the assessment of corpus callosum damages in Mild Cognitive Impairment and Alzheimer Disease. Conf Proc IEEE Eng Med Biol Soc. 2011.

Tortorella P, Preti M, Saresella M, Lagana M, Baglio F, **Griffanti L**, Marventano I, Mendozzi L, Cecconi P, Dinacci D, Clerici M, Caputo D, Rovaris M. Determinants of locomotor disability in multiple sclerosis: an immunological and diffusion tensor MRI study. Journal of Neurology 2011. 258 (S1): 205-205. ISSN 0340-5354

Tortorella P, Lagana M, Saresella M, **Griffanti L**, Baglio F, Marventano I, Mendozzi L, Cecconi P, Dinacci D, Clerici M, Caputo D, Rovaris M. Determinants of locomotor disability in multiple sclerosis: an immunological and diffusion tensor MRI study. Conf Proc ENS, 2011.

Tortorella P, **Griffanti L**, Saresella M, Lagana M, Marventano I, Pinardi G, Corbo M, Lunetta C, Cecconi P, Caputo D, Clerici M, Rovaris M. Pathophysiology of tissue damage in progressive multiple sclerosis: an immunological and MRI comparative study versus motor neuron disease. Conf Proc ECTRIMS, 2011.

Chapter 2 - Individual thresholding of seed-based functional connectivity maps: estimation of random errors by means of surrogate time series.

In this explorative study, an evaluation of the errors that affect seed-based functional connectivity analyses is performed through the generation of surrogate time series by phase randomisation. Two thresholding methods for the functional connectivity maps are then proposed and validated on a group of healthy controls, in order to improve the reliability of single-subject results. The proposed method considers that FC is based on linear correlation in time to which corresponds phase coherence in the frequency domain. Hence, the null hypothesis can be simulated by destroying phase coherence by randomization at equal amplitude distribution. As in any bootstrap (surrogate data analysis), confidence intervals are drawn by numerous extractions of surrogate data satisfying the null hypothesis.

The preliminary results of this study are reported in two conference proceedings (Griffanti et al., GNB 2012; Griffanti et al., BSI 2012), while the final work has now been accepted for publication as a full paper (Griffanti et al., *Methods of Information in Medicine*, in press).

2.1. Introduction

Seed-based functional connectivity (FC) analysis (also called voxel-based FC) was the first technique used for the analysis of resting state functional MRI (RS-fMRI) data (see par. 1.2 and Biswal et al., 1995) and it is still extensively applied (Cole et al., 2010; Fox and Greicius 2010). The simplicity of the method, its straightforward interpretability with respect to the other methods, and its moderate to high reliability (Shehzad et al., 2009), make seed-based FC an attractive and useful approach.

The functional connectivity map (FCmap) is usually computed as Pearson's linear correlation between the signal extracted from a specific region of interest (seed) and all the other brain voxels, showing the network of regions functionally connected with the seed (Fox and Raichle 2007). In a recent study, Hlinka and colleagues (Hlinka et al., 2011) demonstrated that, after standard fMRI preprocessing steps, linear correlation well captures the full functional connectivity. Additionally, spatial and temporal filtering further diminishes small nonlinearities in the data. However, some

linear correlations could be artefactual, i.e. due to chance and not to real FC, and the p-value associated to Pearson's correlation coefficient, although significant *per se*, is not independent from this random error.

To our knowledge, these random errors are usually ignored and significant connected voxels are detected only at group level. At single-subject level, the use of an arbitrary threshold without a quantification of the random error size could lead to misinterpretation of the FC especially for rare case studies and clinical applications.

For this reason, in seed-based FC analyses, a more reliable method is needed for the identification of voxels significantly connected with the seed, taking into account for random errors.

In this work we describe a method for the estimation of this random error by using surrogate time series. Moreover, two thresholding methods are proposed for a reliable analysis of single-subject FC maps.

2.2. Materials and methods

2.2.1. Subjects and MRI data acquisition

Data were acquired from 15 healthy subjects (age: 46.6±23.0 years; M/F = 6/9). MRI acquisitions were performed in the Radiology Department of Fondazione don Carlo Gnocchi IRCCS in Milan, using a 1.5 T Siemens Magnetom Avanto (Erlangen, Germany) scanner with 8-channel head coil. RS-fMRI BOLD EPI images (TR/TE = 2500/30 ms; resolution = 3.1 x 3.1 x 2.5 mm^3; matrix size = 64 x 64; number of axial slices = 39; number of volumes = 160) were collected at rest (the participants were instructed to be relaxed, with eyes closed, not to think anything in particular and not to fall asleep). T1-weighted 3D scans were also acquired (TR/TE = 1900/3.37 ms; resolution = 1 x 1 x 1 mm^3; matrix size = 192 x 256; number of axial slices = 176). All subjects provided written informed consent to participate in the study according to the recommendations of the declaration of Helsinki.

2.2.2. RS-fMRI data preprocessing and generation of seed-based FC maps

The starting preprocessing steps, performed with SPM8, involved the following: 1) correction for slice-timing differences; 2) correction of head motion across functional images; 3) coregistration to the anatomical image and spatial normalization to the MNI space with a voxel size of 3 x 3 x 3 mm^3; 4) spatial smoothing with a 4 mm full-with at half-maximum Gaussian kernel. Then, further steps specific for RS-fMRI were: 5) regression of nuisance variables (head motion, mean white matter signal and mean cerebrospinal fluid signal); 6) temporal pass-band filtering (0.01-0.08 Hz) to remove linear trends and constant offsets over each run. For these operations we used REST

toolbox (Song et al., 2011).

For each subject, a region of interest (ROI) of 6 mm radius was positioned in the posterior cingulate cortex (with centre at MNI coordinates: 0 -53 26) based on previous studies (Van Dijk et al., 2010; Andrews-Hanna et al., 2007). This area plays a central role in the default mode network (DMN), the principal and more investigated resting state network (see par. 1.1). The corresponding time series (PCC-time course) was extracted as the mean signal within the ROI. Seed-based functional connectivity map (FCmap) was then obtained by computing the linear correlation between the PCC-time course and the time courses of all acquired voxels. Correlation maps were then converted to z-maps using Fisher's r-to-z transformation (zFCmap).

2.2.3. Estimation of random errors by means of surrogate time series

Surrogate time series of the PCC-time course were constructed with the iteratively refined amplitude adjusted Fourier transform (iAAFT) method, proposed by Schreiber and Schmitz (2000). According to this method, the Fourier transform of the series is computed, thus representing second order properties in the frequency domain. Next, the substitution of true phases by randomly extracted ones (uniform 0-2π distribution) maintains spectrum but alters the probability distribution of amplitude in time samples. Deviations in spectrum and distribution from the starting set are iteratively corrected. In this way, the obtained iAAFT surrogates preserved both amplitude distribution and spectral shape of the original time series, but phases were randomized.

From the PCC-time course of each subject, 39 surrogate series were generated. The choice of generating 39 surrogates is somewhat arbitrary. Basically we started adopting the minimum number of surrogates M needed to perform a two-tailed rank-order test (Schreiber and Schmidt 2000), calculated as $M = 2 K/ \alpha - 1$, selecting $\alpha = 5\%$ as residual probability of false rejection (95% level of significance) and $K=1$. We than verified that this choice did not influence the overall results by calculating the CI using different number of surrogates (see section 2.2.4). After surrogate generation, the mean correlation between the surrogates and the seed was computed and verified not to be significantly different from 0. Seed-based functional connectivity was then computed using each surrogate time series as seed. Since the temporal information of the PCC-time course has been destroyed in the surrogates, no more correlation is expected between brain voxels and the seed. Any correlation in the new FCmap is due to chance, so we obtained a set of 39 random error maps and the corresponding z-maps (zERR).

For each brain voxel, the mean and the standard deviation of the random error among the 39 maps was computed. Thus, we obtained an error mean map (meanERRmap) and an error standard deviation map (stdERRmap) for each subject, whose distributions were fitted to theoretical sample distributions, respectively the normal distribution and the chi-square distribution, using maximum

likelihood estimation method on shape parameters.

2.2.4. Thresholding methods for single-subject FCmaps

The mean values of meanERRmap and stdERRmap distributions (respectively $\overline{m}$ and $\overline{std}$) were then used to compute a 2*std (i.e., p<0.05) confidence interval (CI) with Eq.2.1:

$$CI_{global} = \overline{m} \pm 2 * \overline{std} \qquad (2.1)$$

The boundaries of this CI (Tsup and Tinf) were then used as threshold values and applied to all voxels of zFCmaps (global thresholding): only voxels showing a correlation value higher than Tsup or lower than Tinf were considered as significantly connected with the seed.

A possible alternative to this thresholding method was to apply a different threshold to each voxel, according to the local amount of random error.

For this local thresholding, the 2*std (p<0.05) CI was computed for each brain voxel (i) using Eq. 2.2:

$$CI_{local}(i) = mean(zERR(i)) \pm 2 * std(zERR(i)) \qquad (2.2)$$

In this way, two additional maps were generated for each subject: the superior confidence interval map (supCImap) and the inferior confidence interval map (infCImap). Finally, zFCmaps were thresholded using supCImap and infCImap: voxels showing a correlation value out of the CI were considered as significantly connected with the seed.

The thresholded maps obtained with the two methods were compared by calculating the Dice index as similarity measure:

$$\text{Dice} = \frac{2|tFCmap_{GLOB} \cap tFCmap_{LOC}|}{|tFCmap_{GLOB}| + |tFCmap_{LOC}|} \qquad (2.3)$$

where $tFCmap_{GLOB}$ is the binary map obtained with global thresholding and $tFCmap_{LOC}$ is the binary map obtained with local thresholding. Moreover, the difference in the number of voxels that passed the thresholds was evaluated through a paired t-test.

For global thresholding, mean and standard deviation of T_{sup} and T_{inf} across subjects were computed and their correlation with age was tested in order to evaluate the inter-subject variability of CI_{global}. Finally, the variability due to the number (N) of surrogates used, was assessed repeating the computation of random error and CI_{global} values with N=2:39.

2.3. Results

In Fig. 2.1, the meanERRmap and stdERRmap of one subject are shown as examples, as well as their distributions. The mean and standard deviation values of random error are spatially homogeneous within the brain and the relative distributions were found to be well fitted by corresponding theoretical distributions.
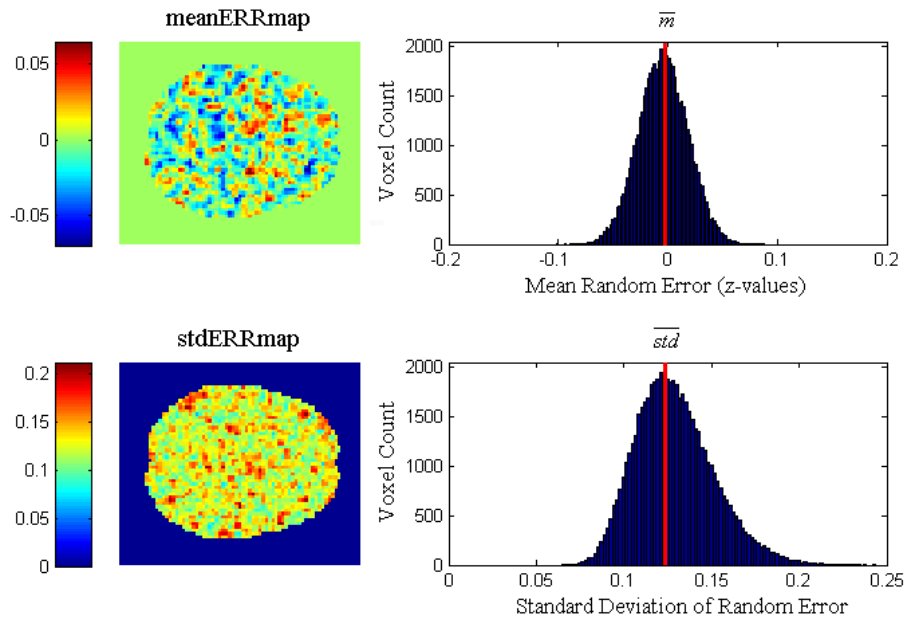
Figure 2.1. Random Error estimation. The mean random error (top panel) is spatially homogeneous within the brain and the distribution is Gaussian-shaped centered in zero. Also the standard deviation of the random error (bottom panel) is homogeneous with chi-square distribution. Data relative to a 20-year female healthy subject.

The PCC-zFCmap of one subject before (a) and after global (b) and local (c) random error thresholding is illustrated in Fig. 2.2. With both methods, the principal DMN areas (posterior cingulate cortex, medial prefrontal cortex and inferior parietal lobule) are well identifiable. Comparing the two thresholded maps, the mean Dice index across subjects was 0.81±0.04 and the number of voxels significantly connected with the seed obtained using global and local thresholding was not significantly different (N voxel after global thresholding = 9144.400 ± 3522.104; N voxel after local thresholding = 9322.330 ± 3755.627; p=0.429, paired t-test).
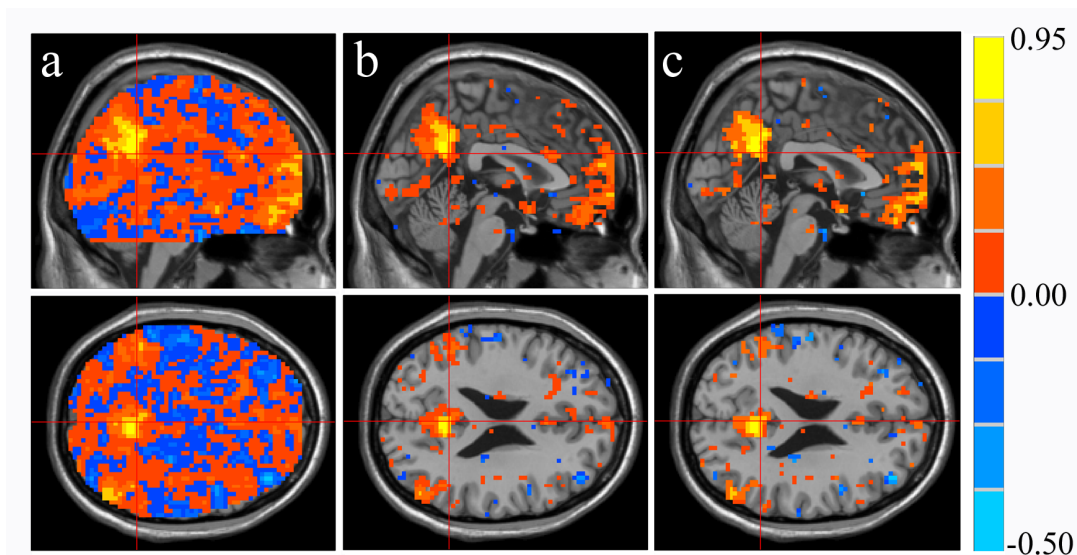
Figure 2.2. Random error thresholding. The single-subject PCC-FCmap is shown before (a) and after global (b) and local (c) random error thresholding. It can be observed that, after thresholding, DMN areas are well identifiable.

Regarding inter-subjects variability of global threshold, CI_{global} standard deviation across subjects was very low compared to its mean value (Tsup(z) = 0.252±0.008, Tinf(z) = -0.254±0.005) and not correlated with age (correlation Tsup-age: p=0.28; correlation Tinf-age: p=0.34). Obtaining a mean global threshold of z=± 0.25 (corresponding to a correlation coefficient r = 0.245), the associated p-value for a Pearson probability distribution is p<0.001. As shown in Fig. 2.3, this small variability is almost independent from the number of surrogates and CI_{global} boundaries reach stable values using a small number of surrogates (N ≈ 10), thus setting the minimal requirement of computational effort for surrogate data production.
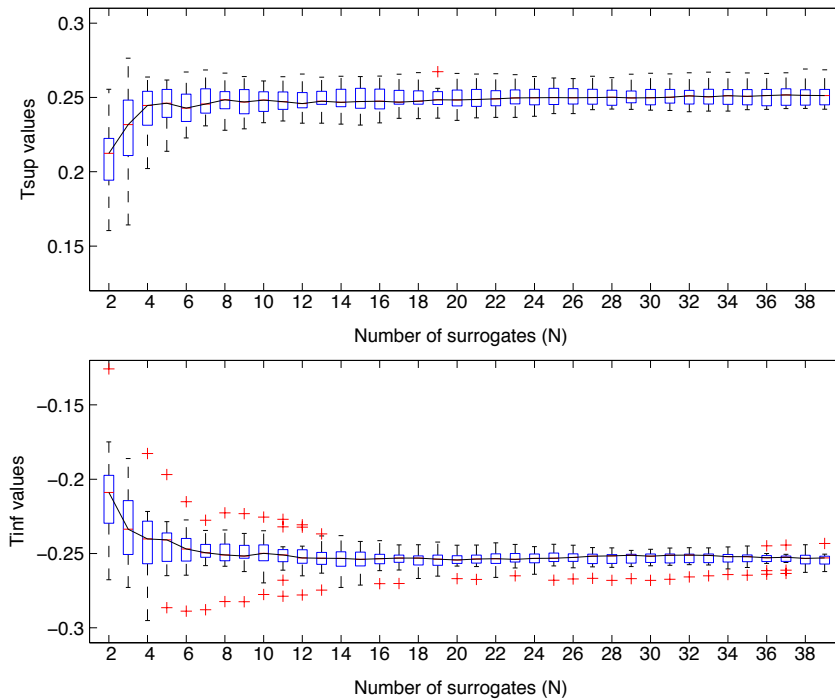
Figure 2.3. Global confidence interval (CI_{global}) variability. The boxplots illustrate the distribution across subjects of the upper boundary (Tsup, top panel) and lower boundary (Tinf, bottom panel) of CI_{global}, for different number of surrogates used for their computation.

2.4. Discussion and Conclusions

In this work we examined the problem of random errors in seed-based functional connectivity analyses and proposed a method for error evaluation based on surrogate time series. Observing a homogeneous distribution of random error within the brain, we can infer that there are no regions more influenced by random error than others and that this kind of error is independent from the resting state activity.

Random errors are usually ignored in this kind of analysis and correction is only performed at group level. In order to perform a reliable single-subject analysis, we proposed two individual thresholding methods, which allow the identification of voxels significantly connected with the seed

region. The two methods have been proven to be effective in identifying the DMN areas and are substantially equivalent, although the global thresholding approach requires a reduced computational load and may be preferable for further analyses. The boundary values of the CI_{global} have a low inter-subject variability not depending from subjects' age. Moreover the number of surrogates needed for the analysis can be remarkably reduced to small values as 10 extractions or less, further decreasing the computational load required for the analyses without significant changes in the results.

The analyses presented in this study were performed on data preprocessed with the same pipeline, therefore an influence of the preprocessing steps (especially regarding spatial and temporal filtering) can not be excluded. A possible future development of this study could be a detailed analysis of the effect of each preprocessing step and its effect on the final threshold

The proposed method is promising for an application in a clinical setting to quantify the FC alterations with respect to a seed ROI. Indeed, the availability of a reliable single-subject FC analysis could be particularly useful for rare case studies (when a group study is not feasible) and for the longitudinal evaluation of a single patient's disease progression or response to treatment or rehabilitation.

Chapter 3 - Automated artefact detection based on Independent Component Analysis and hierarchical fusion of classifiers: evaluation of accuracy

In this chapter an innovative method for the identification and removal of artefacts from RS-fMRI data is introduced. The proposed denoising method, called FIX (FMRIB's ICA-based X-noisefier), was developed in collaboration with the FMRIB (Functional Magnetic Resonance Imaging of the Brain) Centre (University of Oxford, UK), and consists of several major operations: single-subject spatial independent component analysis, component-wise feature extraction, classifier training, components classification, and removal of the artefactual components from the data. This chapter covers the first four steps, while the last FIX step, the removal of the nuisance components, will be described in detail in Chapter 4. In particular the first theoretical part (par. 3.2) illustrates the methodological basis of the cleaning algorithm; the second experimental part (par. 3.3-3.5) describes the training dataset I built and the tests I performed for classification accuracy.

The results of these analyses are reported in a paper (Salimi-Khorshidi et al., 2014).

3.1. Introduction

Functional magnetic resonance imaging (fMRI) has become a widely used approach for mapping brain function. In most fMRI experiments, however, many sources of temporal fluctuation (e.g., head movement, respiratory motion, scanner artefacts, etc.) do corrupt the recorded voxel-wise time series. Such artefacts reduce the signal-to-noise ratio, complicate the interpretation of the data, and can mislead statistical analyses (in both subject- and group-level inference) addressing neuronally-related brain activation.

The main disadvantages of the Resting State fMRI (RS-fMRI), compared to a standard task-induced fMRI, are the absence of a priori hypothesis of activation and externally triggered temporal references. In this way is more difficult to distinguish the signal related to neural activity from non-neural sources of noise, when the latter are (spatially or temporally) correlated. Moreover, the artefacts may share some spatial or spectral overlap with the RSNs and affect their correct

identification and quantification of their connectivity. In addition, recent developments in MRI acquisition generate ever-better data, but may increase some associated artefacts. Hence the correct identification and removal of non-neural fluctuations is crucial.

Spatially extended artefacts can be caused by the scanner (e.g., hardware instabilities), or, more frequently, they are caused by non-neuronal physiological/subject effects (Murphy et al., 2013). For example, it is well known that even relatively small amounts of head motion represent a significant confound for RS-fMRI network identification (Van Dijk et al., 2012; Power et al., 2012; Satterthwaite et al., 2012). Other confounds are related to physiological noise, including: cardiac and respiratory cycles (Birn et al. 2006; Shmueli et al., 2007), which occur at relatively high frequency ($\approx$ 1 Hz and $\approx$ 0.3 Hz, respectively) but are generally aliased into lower frequencies at standard TR (2-3 s) (Lowe et al., 1998) and appear in resting BOLD signals through arterial CO_2 concentration variations, blood pressure changes and movements (e.g. pulse related). Vascular tone also represents a source of physiological noise, generating low-frequency oscillations (<0.1 Hz) in absence of stimulus (Aalkjaer et al., 2011). Only by removing such confounds is it possible to obtain reliable functional connectivity measures. For this reason, there is increasingly growing interest in the development of an effective method for artefact identification and removal that retains as much neural-related signal as possible.

Current noise removal methods for individual resting dataset clean-up can be divided into two main categories (see Murphy et al., 2013 for a detailed review): those that use external physiological recordings and those that are data-driven. In the former category, with techniques like retrospective image correction (RETROICOR – Glover et al., 2000), low-order Fourier series are fit to the image data based on the time of each image acquisition relative to the phase of the cardiac and respiratory cycles. This approach has been extended to include the regression of low-frequency changes in heart rate (Shmueli et al., 2007), while Birn and colleagues (2006) developed a method to remove the variance of respiration-induced changes from the data through the regression of the respiration volume per time (RVT).

However, physiological monitoring data are often not available, and are not expected to relate to all common forms of artefact; hence, several methods have been proposed to estimate and remove the artefacts using only the fMRI data itself. The simplest approach is to apply temporal filtering (e.g., a band-pass filter keeping frequencies 0.01-0.08 Hz) that removes the primary cardiac and respiration frequencies if the TR is short enough, but not their aliased lower-frequency components with more standard TR. Moreover, the removal of high frequency signals through bandpass filtering may remove signal that contributes to resting state networks (Niazy et al., 2011). Another standard preprocessing step for fMRI analyses is rigid-body head motion correction. Usually, all the volumes

are aligned to a reference volume, with the volume-to-volume movement of the head described by three translations and three rotations. However, even with perfect geometric correction of head motion, spin history effects result in residual motion-related artefacts; it is common to attempt to remove these from the data using a multiple linear regression, with the confound regressors derived from the estimated motion parameters. However, it has been shown (Power et al., 2012; Satterthwaite et al., 2013) that such approaches are often not capable of completely removing the effects of motion. Power and colleagues (Power et al., 2012) described a technique called "scrubbing" to deal with remaining artefacts: volumes (time points) affected by excessive motion are simply excluded from the functional connectivity analyses. In another study (Satterthwaite et al., 2013) the authors proposed an improved preprocessing procedure by removing a higher number of motion-derived regressors (24 regressors, derived from the temporal derivatives of the 6 motion parameters, their square, and the combination of both). Further nuisance regressors can be derived from the resting data itself. Under the assumption that any process that affects all brain voxels is unrelated to the neural activity, global signal regression removes the global mean signal computed across all voxels in the brain (Desjardins et al., 2001; Greicius et al., 2003). However, it has been demonstrated (Murphy et al., 2009; Saad et al., 2012) that the global regression process also introduces spurious anti-correlations that are difficult to interpret. Some studies (Popa et al., 2009; de Pasquale et al., 2010) indicate that the global signal can include a significant amount of neural activity; therefore, many argue that its removal should be avoided. As BOLD signal related to neural activity should be predominantly in the grey matter, an alternative method is to regress out of the time series derived from just the white matter and/or CSF voxels (Weissenbacher et al., 2009).

Confound removal can also be performed through a modification of the acquisition sequence. The dual echo approach proposed by Bright and Murphy (Bright and Murphy, 2013) consists of simultaneous acquisitions of a short echo time (TE) and a BOLD-weighted (standard TE) fMRI data, followed by voxelwise regression of the short TE data from the BOLD-weighted data, to remove noise variance. A related method uses a multi-echo approach that allows separation of BOLD and non-BOLD signal components based on TE-dependence (Kundu et al., 2012). Multi-echo data at 3 TEs were acquired and fed into independent component analysis. Components were analyzed for the degree to which their signal changes fit models for relaxation-rate (R_2*) and initial signal intensity (when the TE=0) change, and summary scores were developed to characterize each component as BOLD-like or not BOLD-like. These scores clearly differentiated BOLD-like RSN components from non BOLD-like components (related to motion, pulsatility, and other nuisance effects), and non BOLD-like component timecourses were used as noise regressors to improve seed-based correlation mapping.

Independent component analysis (ICA) (McKeown et al., 1998) has proven to be a successful technique for detecting consistent spatial components and separating signal from noise. ICA decomposes the 4D (space x time) data into multiple components, each described by a single 3D spatial map and an associated timecourse. Ideally, some components purely reflect BOLD signal, and others purely reflect artefactual processes. If the latter can be identified then they can be subtracted from (or regressed out of) the data. Identification of artefactual components by hand is time-consuming, operator dependent, and requires expert knowledge about signal and noise fluctuations' spatial and temporal characteristics. Thus, there have been several approaches proposed that attempt to automate ICA-based denoising using different strategies to classify the components as signal or noise. To mention a few examples in addition to the work of Kundu et al. (2012): Thomas et al., (2002) identify the noise components to remove using an unsupervised algorithm that examines the Fourier decomposition of the time series obtained after principal components analysis or ICA; Kochiyama and colleagues (2005) proposed an automatic solution for removing the effects of task-related motion, characterising the non-artefactual ICs by virtue of their task-related signal changes; Perlbarg et al. (2007) remove signal fluctuations that match known spatial patterns of physiological noise; similarly, Beall and Lowe (2007) estimated cardiac and respiratory fluctuations from resting state data with temporal ICA and generated spatial weight matrices applicable to other resting data.

However, none of these approaches are comprehensive enough for RS-fMRI denoising.

The presence of multiple distinct kinds of artefacts in RS-fMRI data requires the identification and removal of a wide range of component types (i.e., having potentially quite varied artefactual spatial and/or temporal characteristics). Therefore, Tohka et al. (2008) proposed a richer set of spatial and temporal features that capture a wider range of ICs' characteristics, while De Martino et al., (2007) used a representation of the components in a multidimensional space of descriptive measures (IC-fingerprints), which are then used to classify the components by feeding the features into a support vector machine. The "features" are quantities derived from the ICA spatial maps and/or timecourses; for example, one feature might be the fraction of the supra-threshold spatial map overlaying grey matter, and another might be the fraction of power in the time series spectrum lying above 0.05Hz. A set of distinct features can be fed into a trained multivariate classifier in order to attempt to classify each ICA component as "good" or "bad".

The Oxford University Centre for Functional MRI of the Brain (FMRIB) recently developed FMRIB's ICA-based X-noisefier (FIX) tool (Salimi-Khorshidi et al., 2014), which is a fully automated (once hand-trained) approach for cleaning fMRI data of various types of noise. The general cleaning procedure in FIX, consists of several major operations: spatial ICA, component-

wise feature extraction, classifier training (using expert-/hand-labelled data), components classification (i.e., predicting components likelihood of being signal vs. noise) and denoising (removal of the artefactual components). The feature selection/extraction and the hierarchical fusion of classifiers (K-nearest neighbour, support vector machines and decision trees) used for the classifier training and prediction phase (the components' classification) are extensively described in Salimi-Khorshidi et al., (2014) and will be summarised in the next paragraph.

In this work the performance of FIX against manual component classifications was assessed across various fMRI datasets and evidence of good to excellent performance across three resting fMRI datasets was provided. The last step of the denoising procedure with FIX, the removal of the nuisance components, will be described in detail in the next chapter (chapter 4).

3.2. Methodological basis of the cleaning algorithm (FIX)

In this paragraph the methodological basis of the first operations of the cleaning procedure with FIX, developed by the analysis group of the Oxford University Centre for Functional MRI of the Brain (FMRIB), is summarised, while reference is made to Salimi-Khorshidi et al., (2014) for a detailed presentation. These operations are: spatial ICA, component-wise feature extraction and selection, classifier training (using expert-/hand-labelled data), components classification (i.e., predicting components likelihood of being signal vs. noise).

Independent Component Analysis. Firstly, each single run of fMRI space-time data is decomposed into multiple components using probabilistic independent component analysis (pICA) implemented in MELODIC (Beckmann and Smith, 2004). The details of pICA are illustrated in detail in paragraph 1.2.

Hand-labelling: criteria for the classification of "good" and "bad" components. Independent components were manually labelled into three different classes:

- "good", predominantly signal;

- "bad", predominantly noise;

- "unknown" , not unambiguously identifiable as good or bad (in such cases, FIX treats these components as "good", as the desired final behaviour is generally to be conservative with respect to minimising the chance of incorrectly removing valid neuronal signal).

The manual identification of each component was carried out by first looking at the thresholded spatial map (typically abs(Z)>2.3), then at the temporal power spectrum, and finally at the time series. When necessary, the unthresholded spatial map of the component was viewed.

In the following figures several examples of "good" (Figure 3.1) and "bad" (Figures 3.2-3.6) ICA components from typical fMRI datasets are shown, primarily in order to help clarifying the

criteria used for hand-labelling and the following descriptions of FIX's spatial and temporal features.

Briefly, the typical characteristics of signal components are:

- spatial maps with well-defined grey matter clusters;
- spatial pattern attributable to the RSNs' patterns described in literature (Beckmann 2005; De Luca 2006; Rytty et al., 2013);
- predominantly low-frequency (<0.1 Hz) power spectra;

while noise components can have:

- spatial overlap with white matter, CSF, or blood vessels;
- signal localised at the edges of the brain (motion) or in areas of signal drop (susceptibility);
- spatial maps with irregular/not well-defined clusters;
- non-predominantly low-frequency (<0.1 Hz) power spectra;
- spikes in the time series.

Figure 3.1 illustrates an example components identified as good for a standard EPI acquisition sequence (top) and for a multi-band accelerated EPI sequence (bottom), respectively.
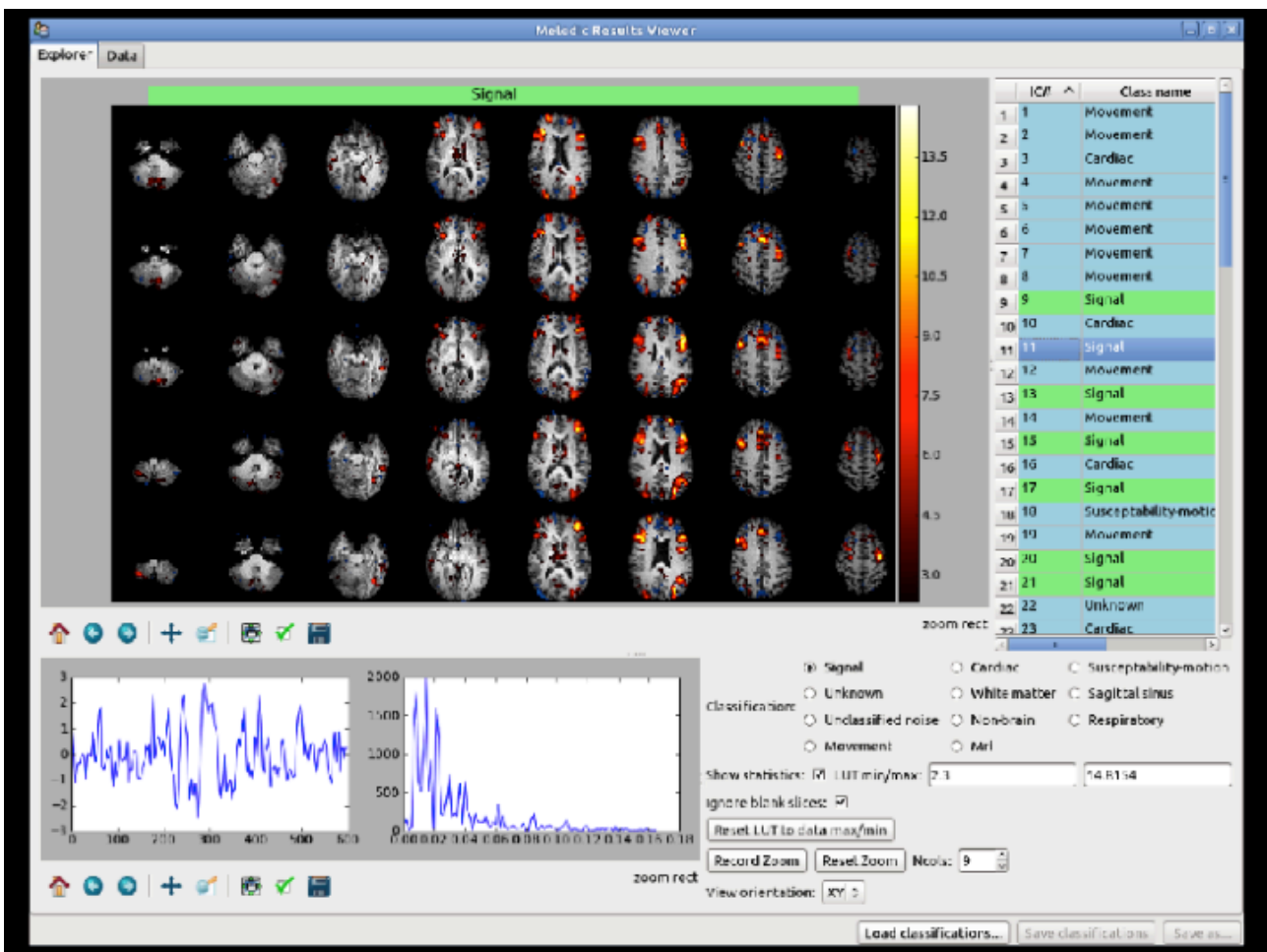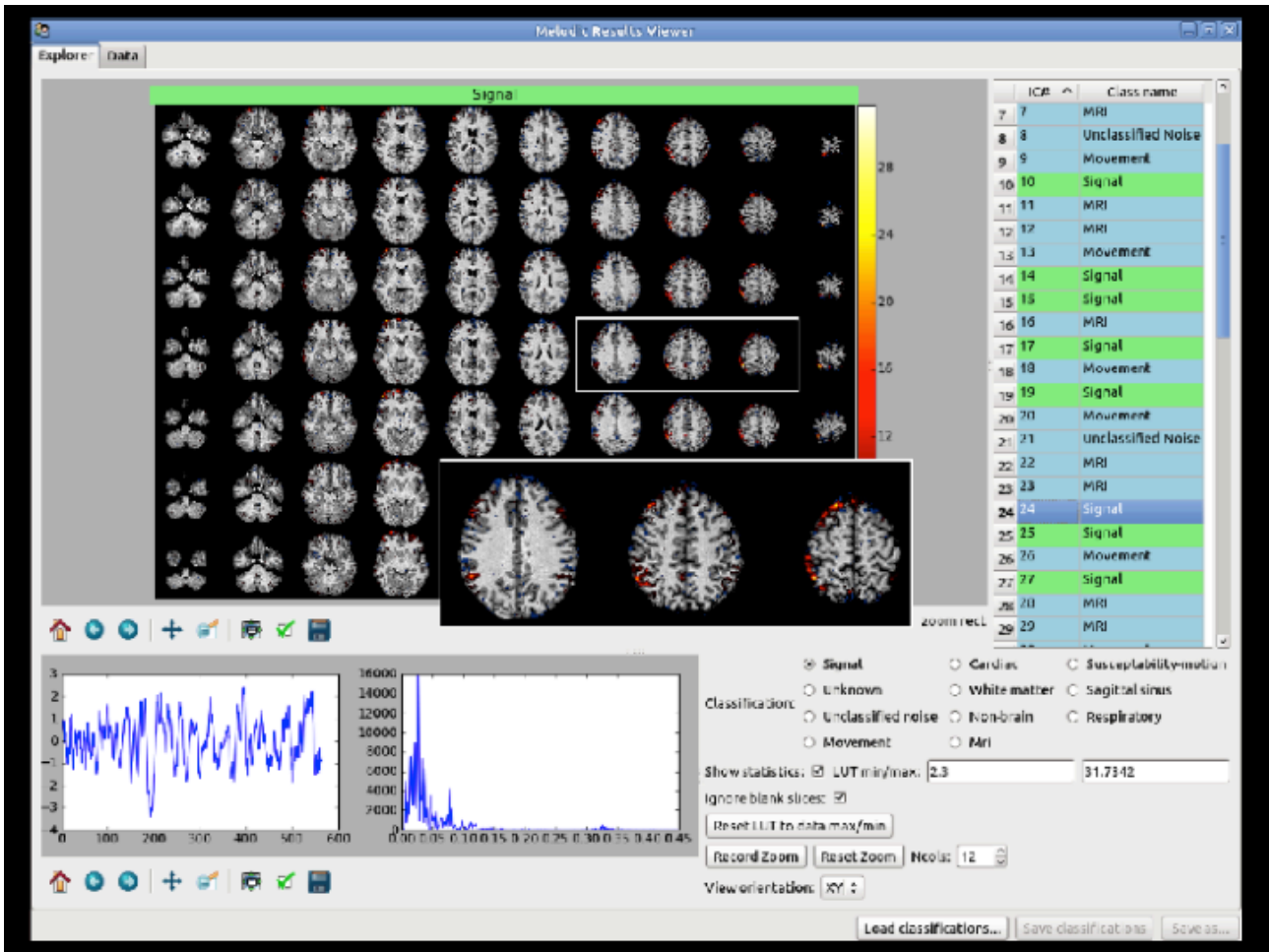
Figure 3.1: Examples of "good" components from two different acquisitions. The spatial map for a high resolution, short TR acquisition (bottom) is visually strikingly different from a more standard acquisition (top), with the signal above threshold following very closely the cortical gyrification. The spectral power lies primarily between 0 and 0.05 Hz for each component. The examples are shown as viewed by the "Melview" program developed by the FMRIB centre specifically to display and hand-classify ICA components for FIX training. The list of components (and their assigned classifications) appears on the right, and, for the currently selected component, the spatial map, temporal power spectrum and time course are displayed.

Conversely, figure 3.2 shows an example of movement-related bad components. Figure 3.3 demonstrates that two more noise components (respectively, white matter –WM – movement-related partial volume fluctuations and susceptibility-related artefact) are clearly artefacts as judged spatially, though the spectrum of the second example does not look clearly artefactual. Figure 3.4 shows sample cardiac pulsation (artery) bad components, identified in the cerebrospinal fluid (CSF) in the ventricles in one case, and anatomically following arteries (most commonly around the posterior cerebral artery and middle cerebral branches) in the other. Figure 3.5, left panel, shows components relating to major veins - in these cases, the sagittal sinus vein. Vein components tend to

have similar temporal characteristics (including power spectra) to those of good components. The right panel instead, shows an example of MRI acquisition/reconstruction related artefact - it does not look like artefacts arising directly from any aspect of physiology. Figure 3.6 shows two examples of "unknown" components, which do not look like clean neuronal-related signal, but may contain some aspects of it.
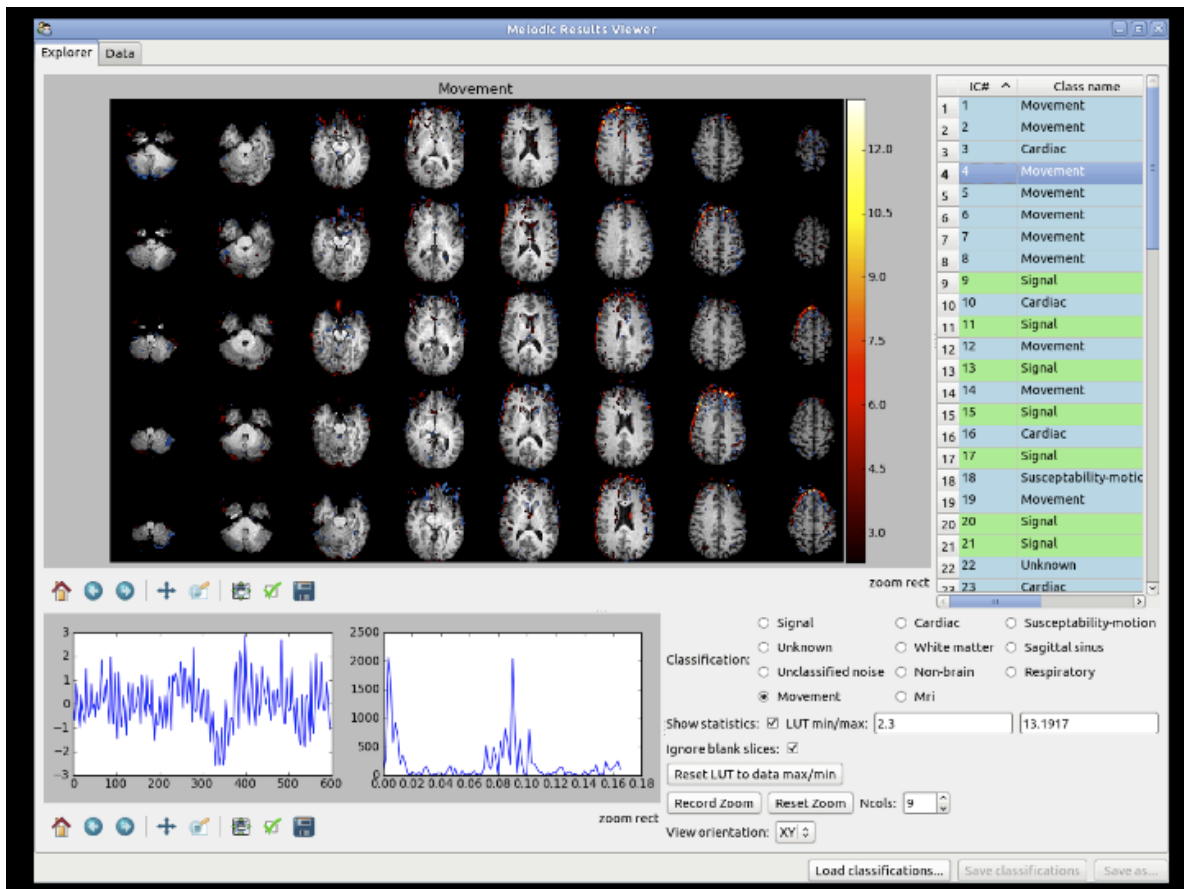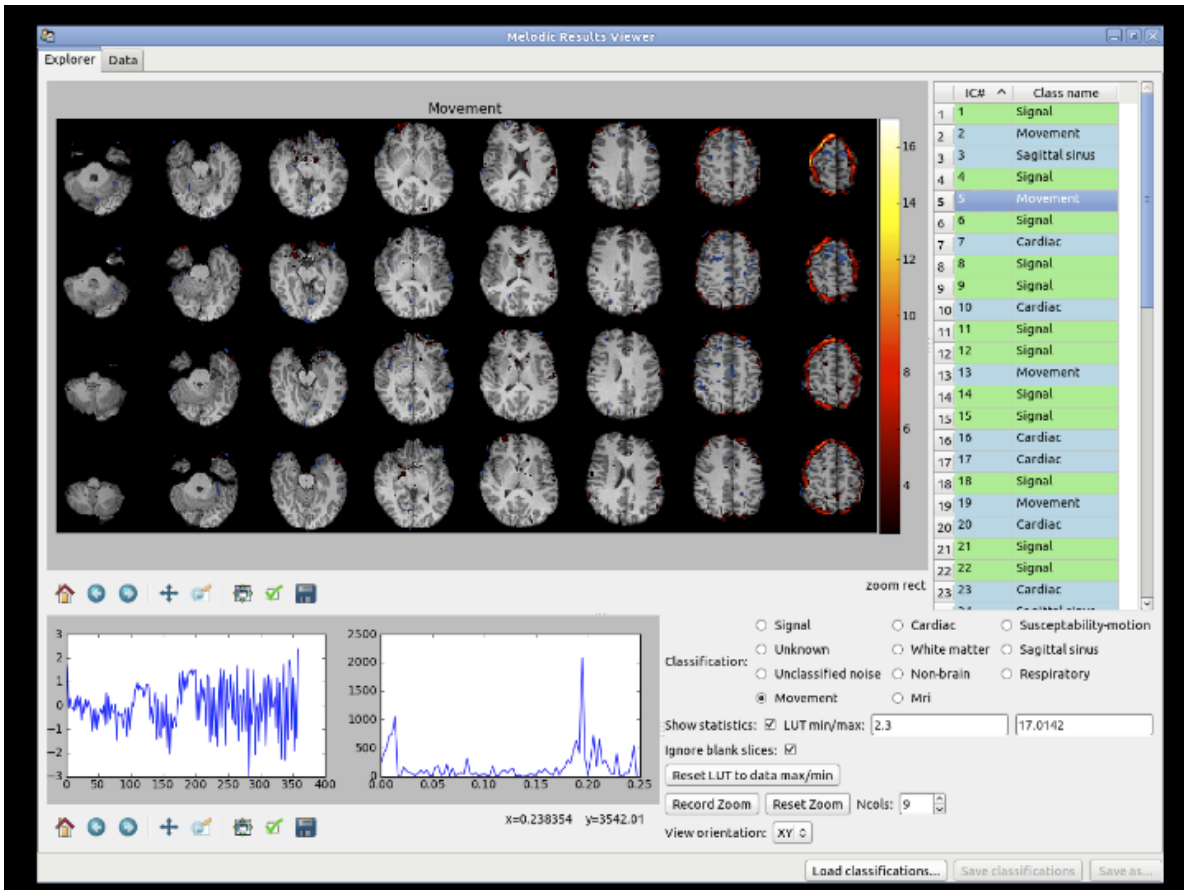
Figure 3.2. Examples of movement-related artefacts. The signal above threshold in the spatial maps is essentially at the edges of the brain. The frequencies of the power spectra are disparately distributed and the time courses visually dissimilar.
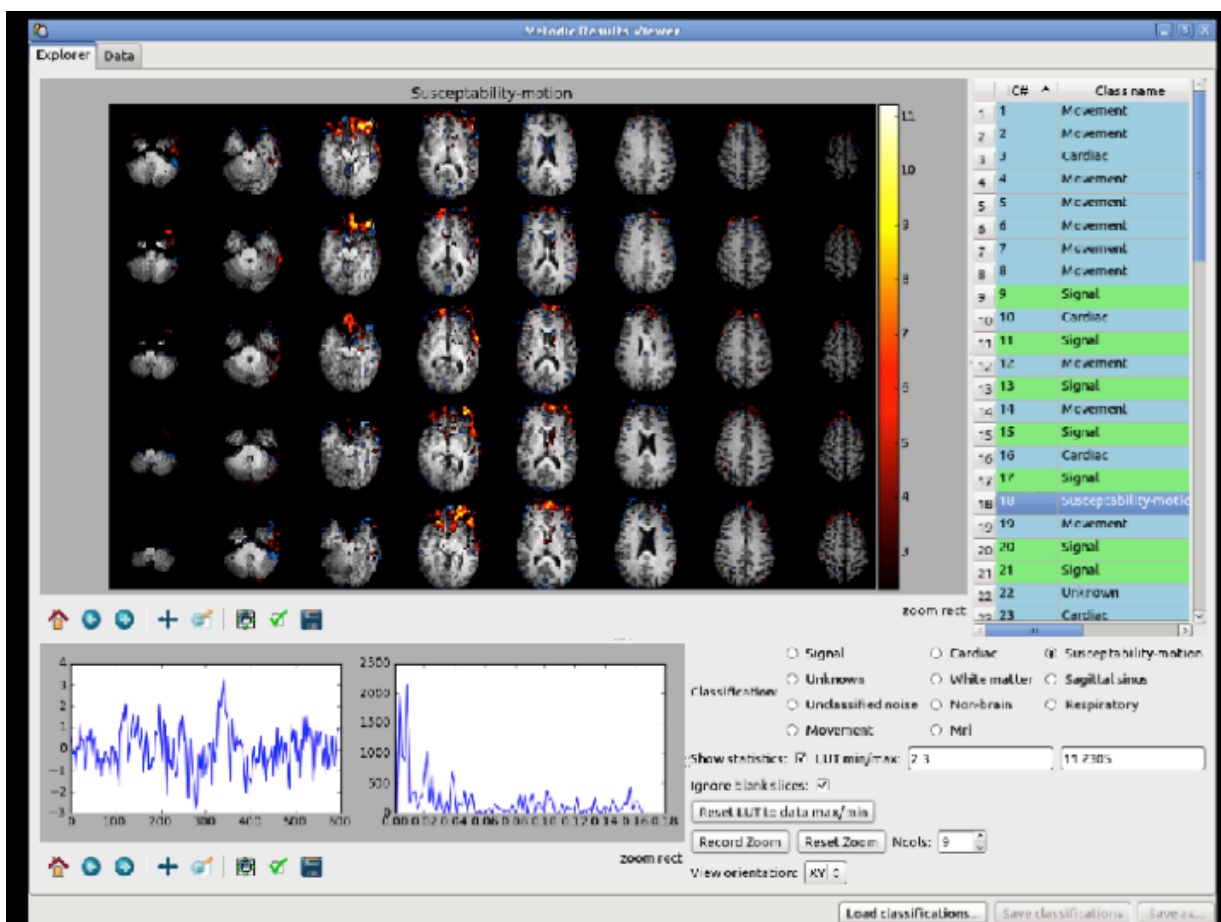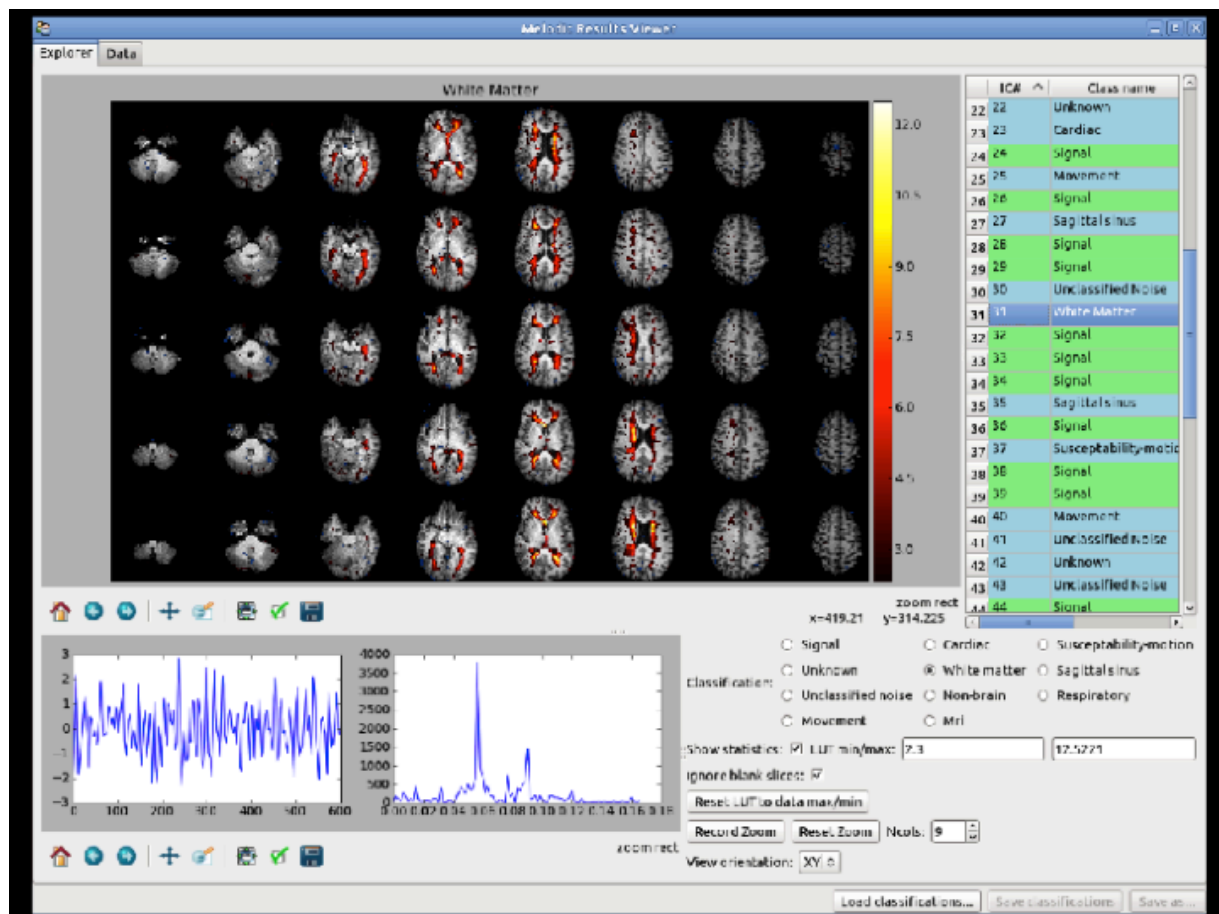
Figure 3.3. Two further noise components: "white matter" and "susceptibility-motion".
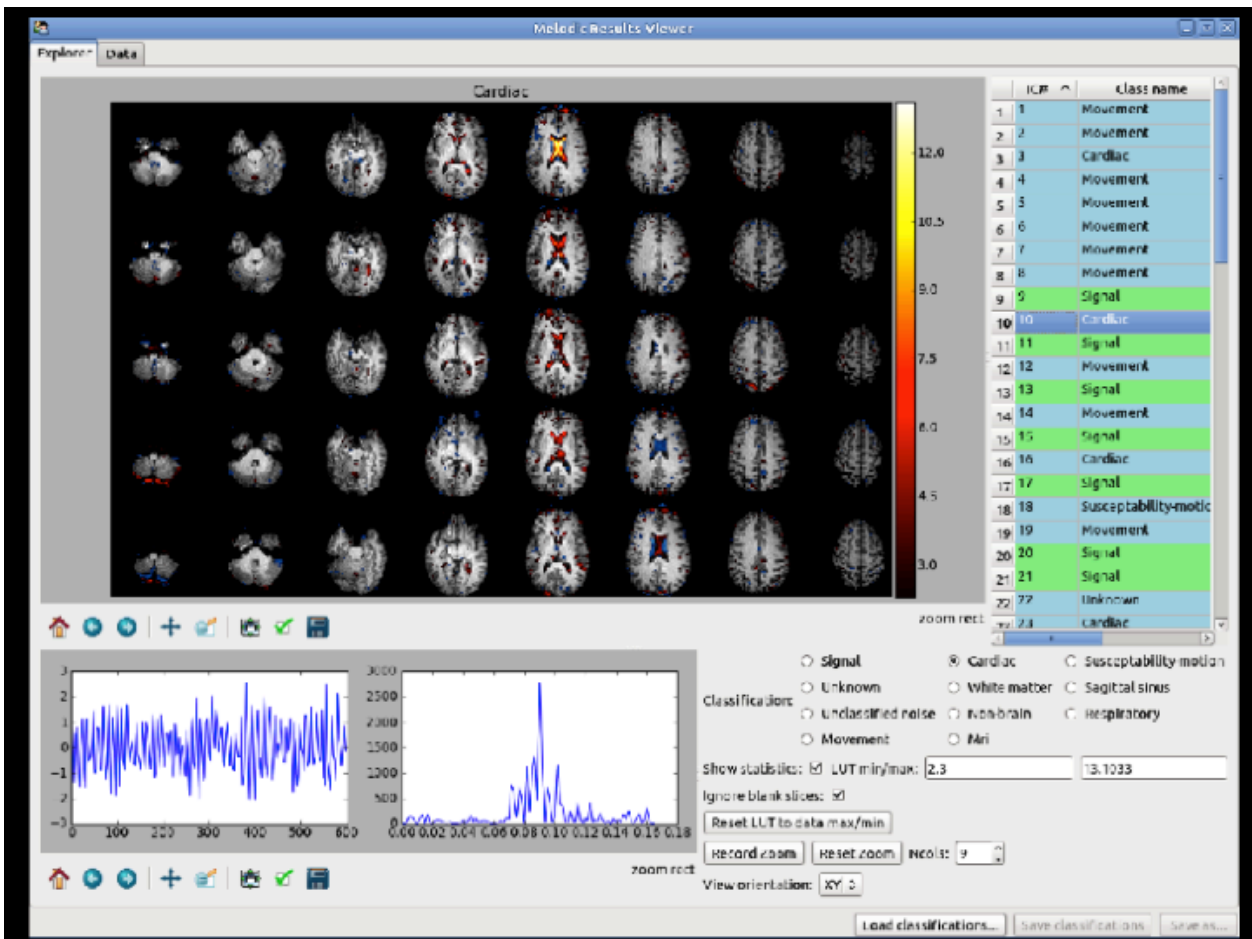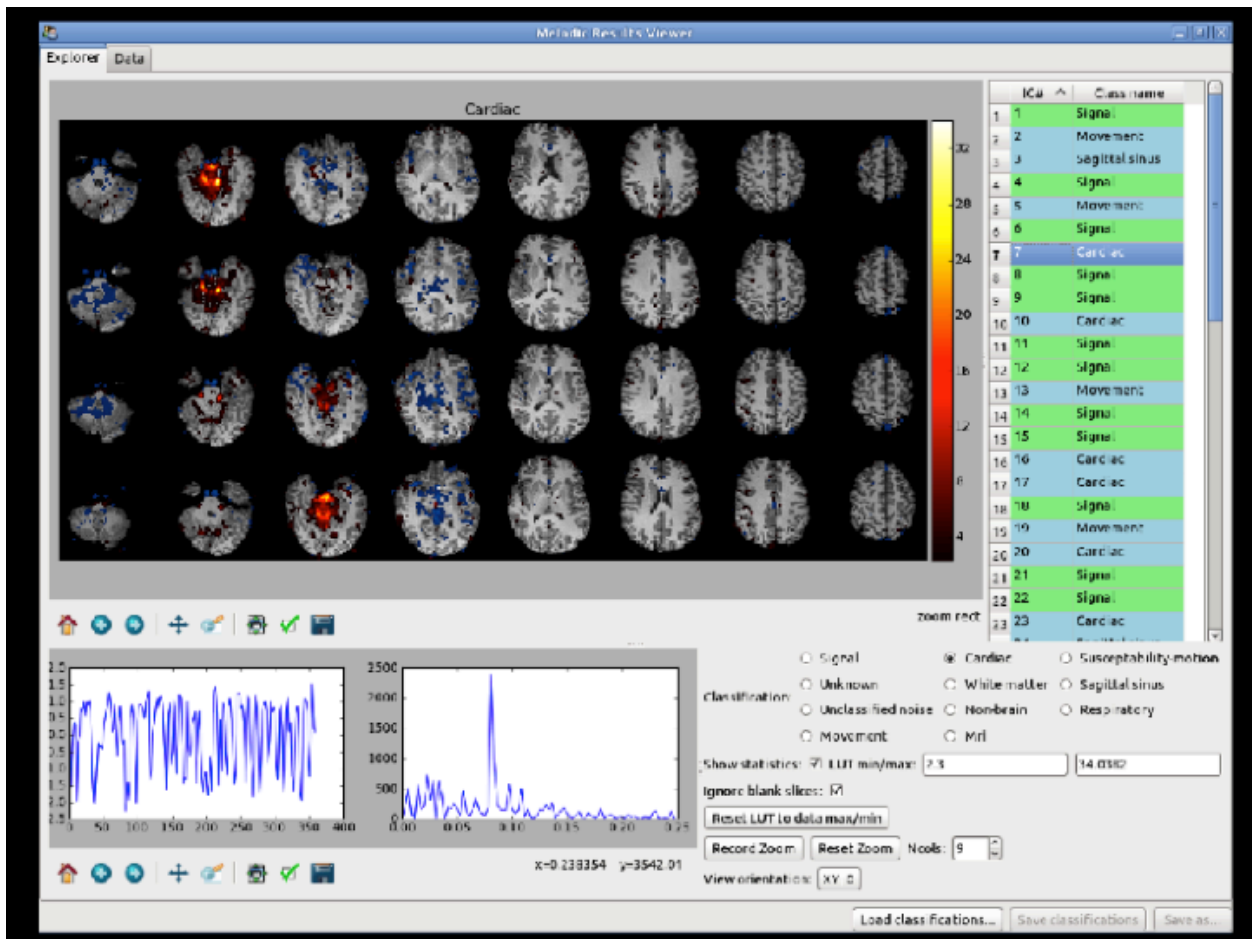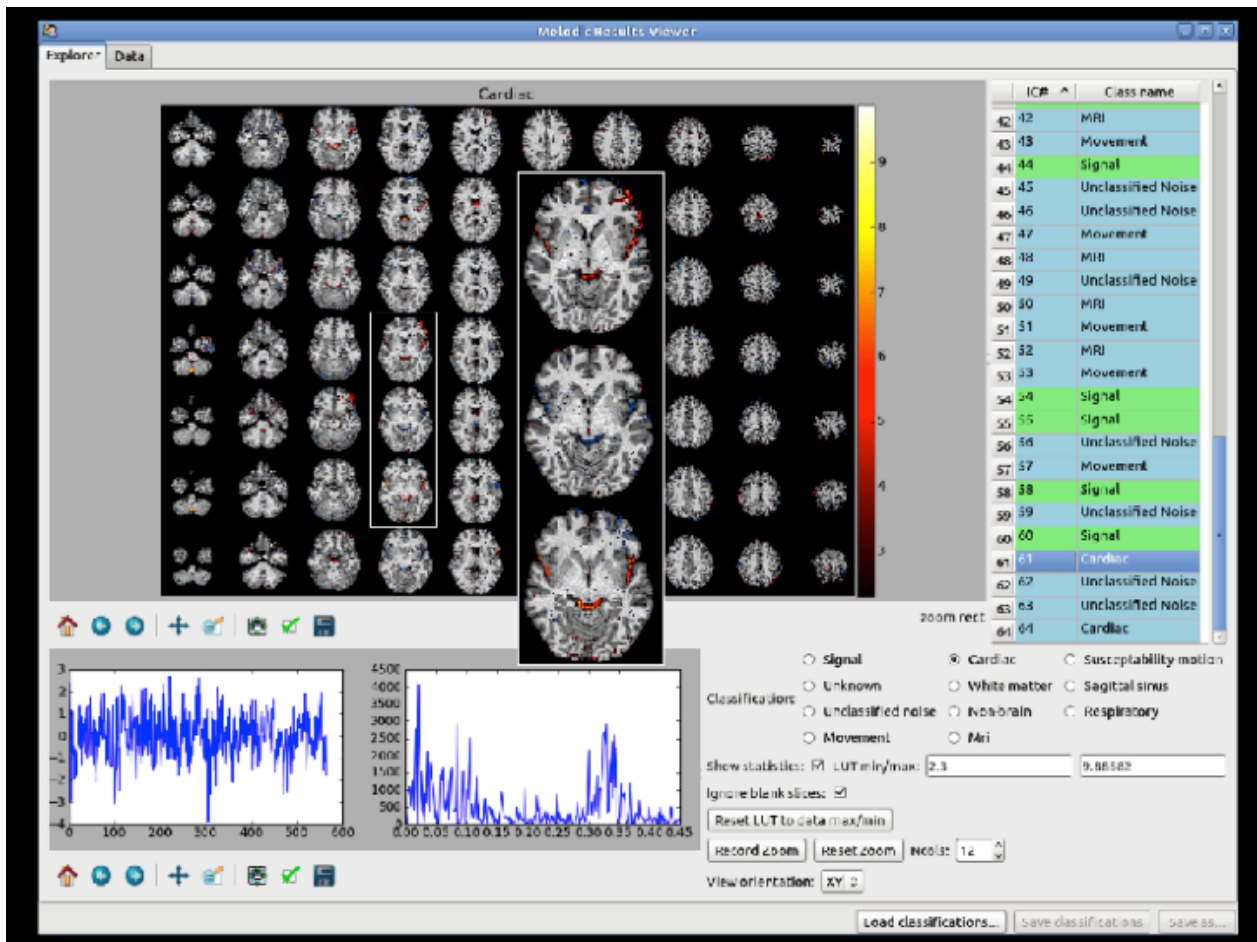
Figure 3.4. Examples of cardiac-related components. This includes components due to cardiac pulsation and arterial contribution. The signal above threshold in the spatial maps is essentially located in the ventricles, or following the main arteries (posterior cerebral artery, middle cerebral branches).
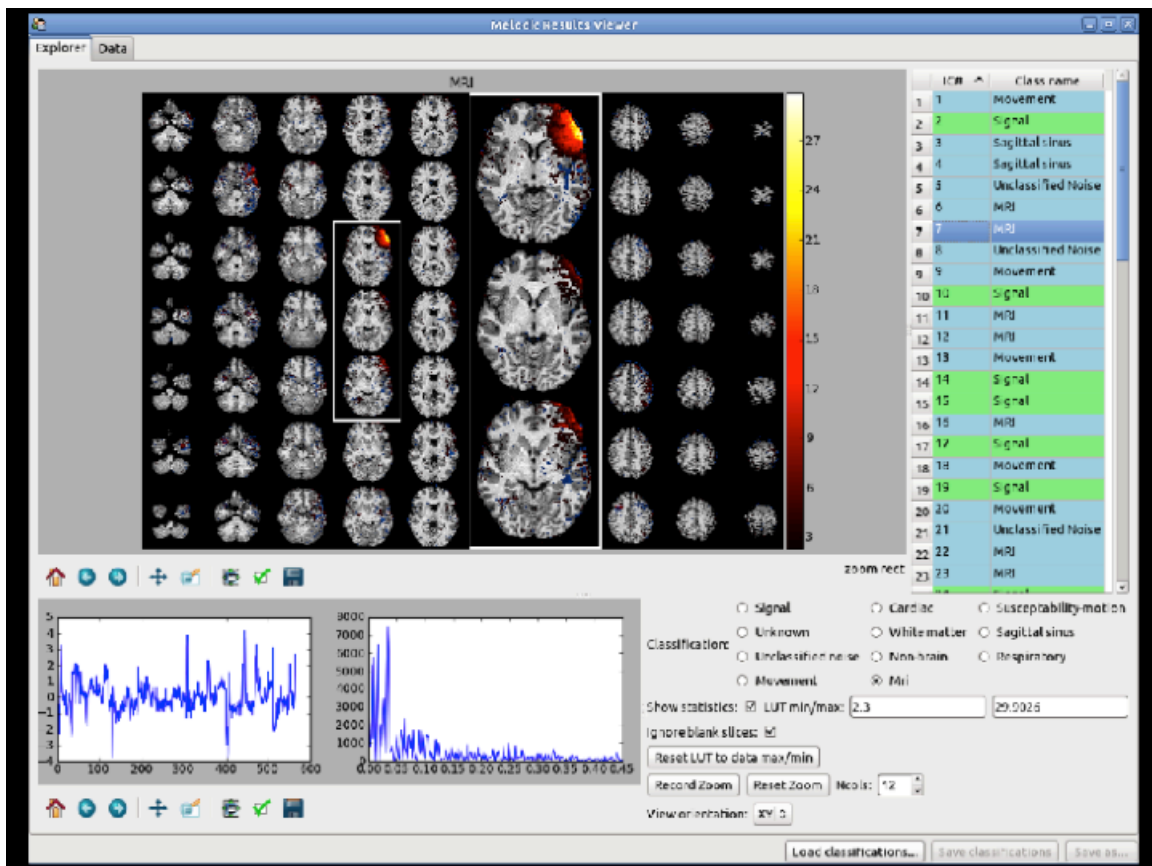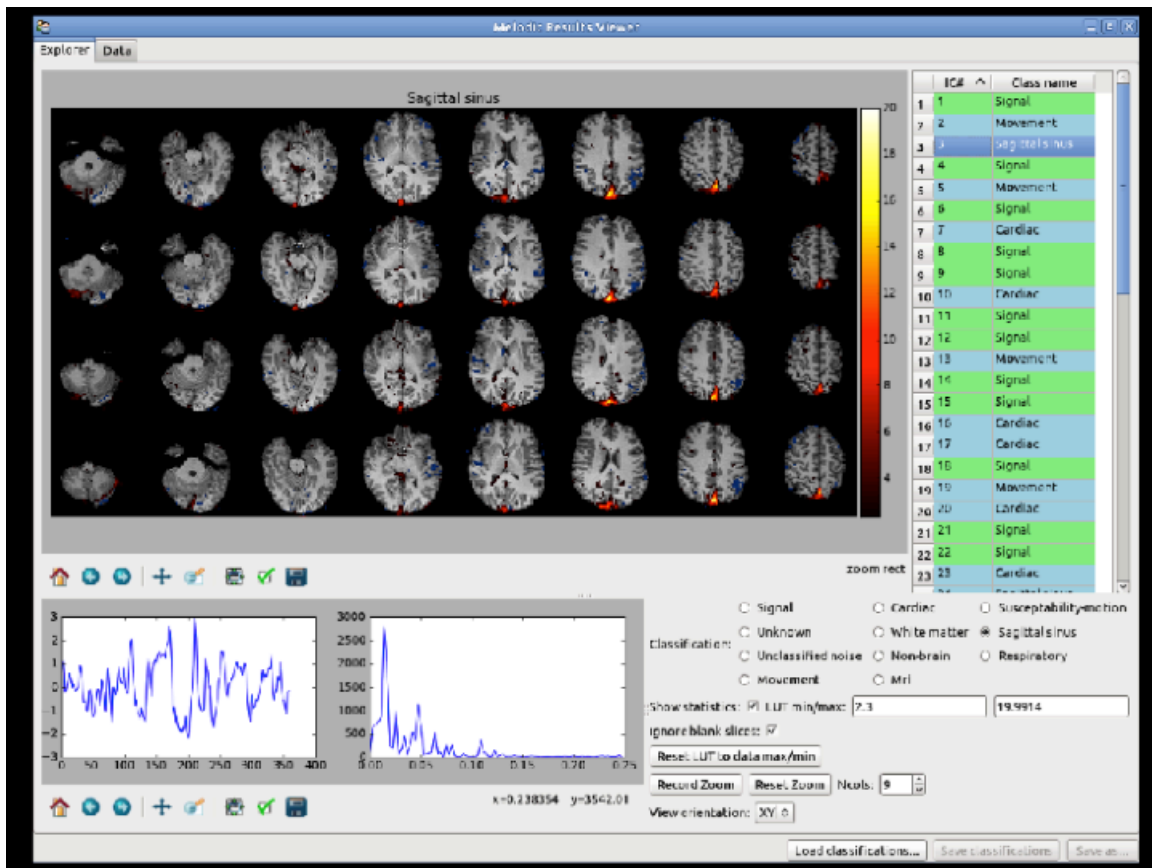
Figure 3.5. Example of two more artefact components. In the top panel the component is related to large veins and the signal above threshold in the spatial maps is essentially following the sagittal sinus. In the bottom panel the artefact is related to MRI acquisition/reconstruction.
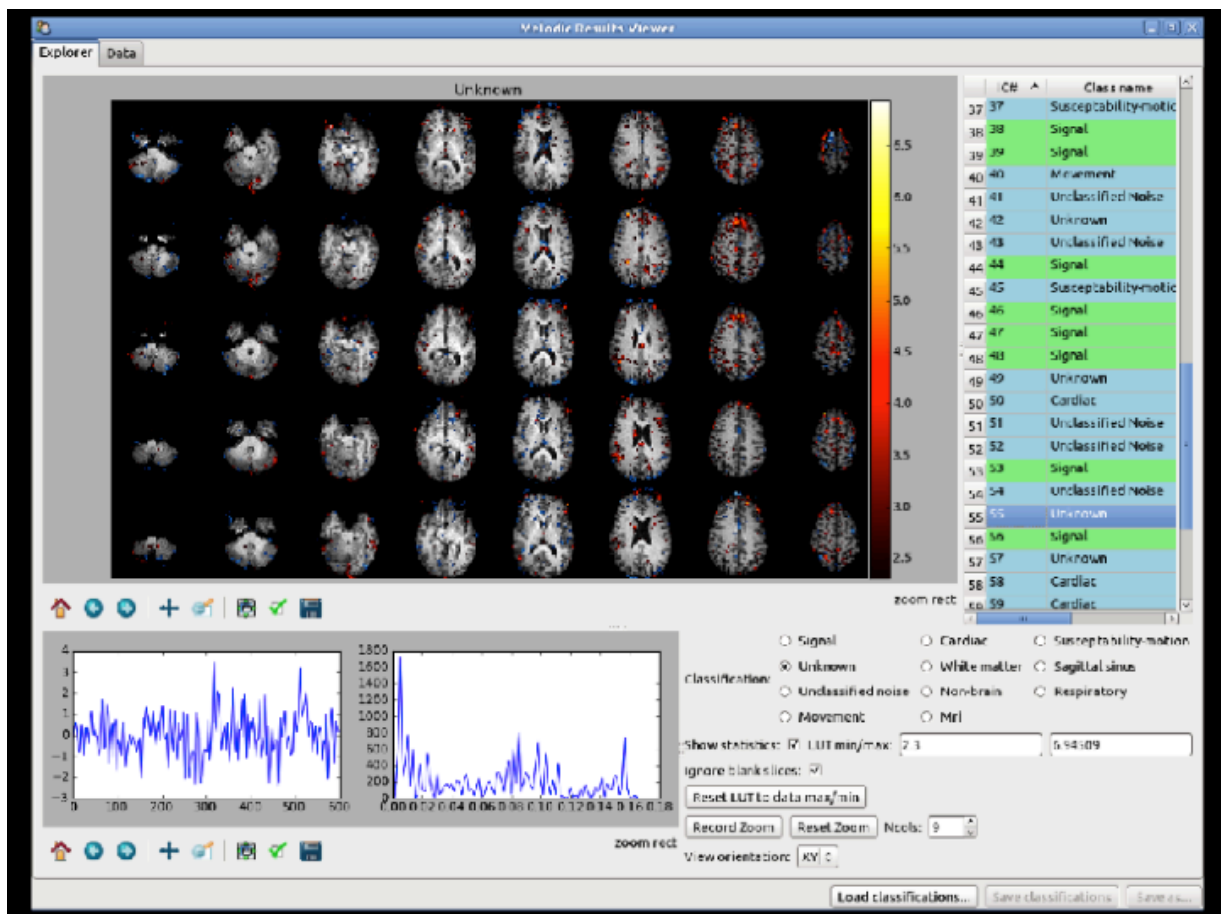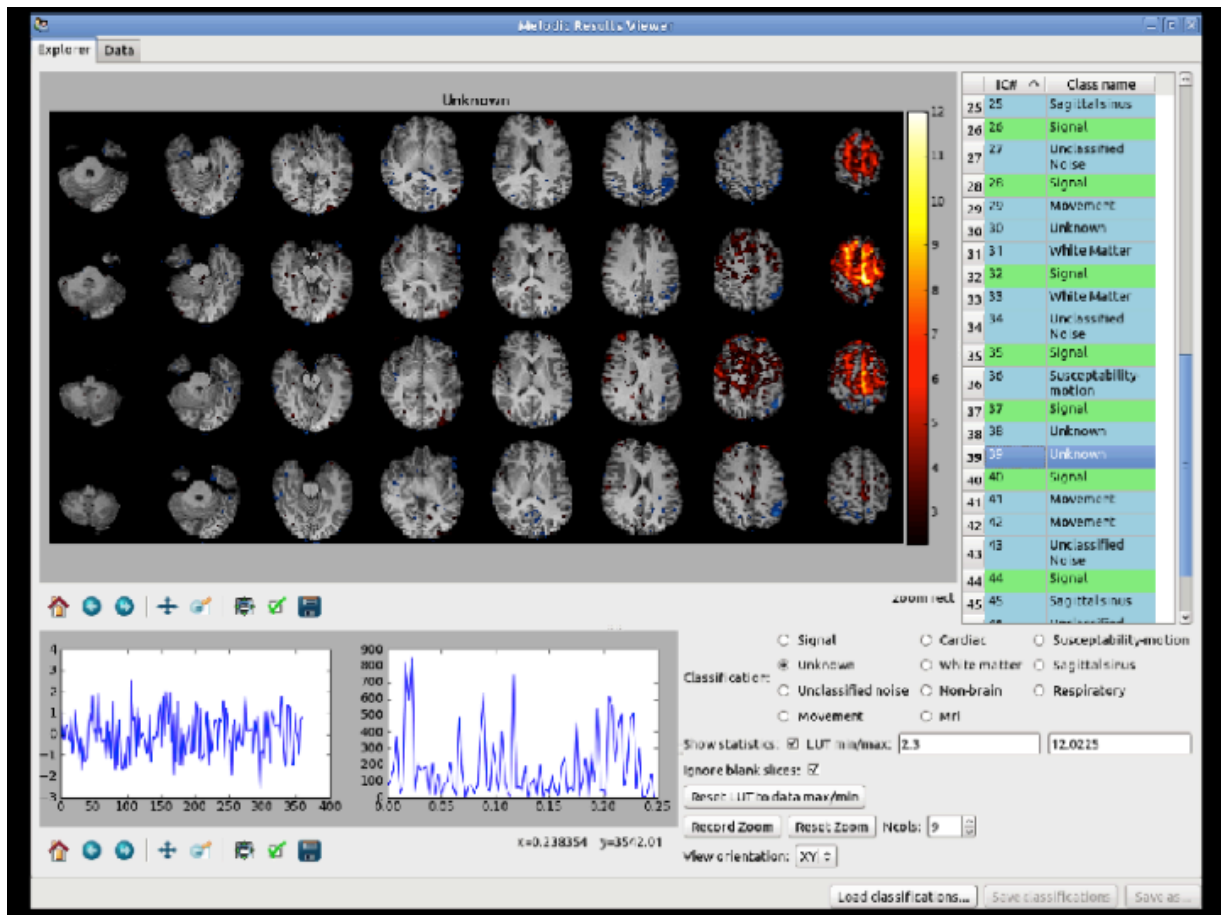
Figure 3.6. Two examples of "unknown" components

Features Extraction. On the basis of the characteristics described above for hand labelling, FIX extracts 178 features, capturing components spatial and temporal characteristics. The main subclasses of these features are summarised in table 3.1. For a complete description see Salimi-Khorshidi et al., (2014).

Table 3.1. Summary of the features classes and sub-classes used by FIX to discriminate signal and noise components.

Features' classes and subclasses	Main characteristic used to discriminate signal/noise	Signal characteristic	Noise characteristic
Spatiotemporal features (1-46)			
N = number of ICs determined by MELODIC	The presence and extent of various noise types affect the number of estimated components		
Temporal features			
Autoregressive properties	temporal smoothness estimated by fitting AR(n) models to a component's time series and temporal autocorrelation	high temporal autocorrelation	low temporal autocorrelation
Distributional properties	shape of the time series' distribution	fairly normal	bimodal or long-tailed
Jump amplitudes	Extent of jumps or sudden changes in time series' amplitude	fairly smooth time series	large jumps
Fourier transform	distribution of power in the frequency domain	low frequency	high frequency
Correlation	temporal correlation with other reference time series (GM, WM, CSF, head motion)	more GM correlated	more WM, CSF, motion correlated
Spatial features (47-178)			
Clusters' size and spatial distribution	Distribution of the activation and deactivation cluster-sizes	low number of large clusters	high number of small clusters
Voxels overlaying bright/dark raw data voxels	multiplication of ICA spatial maps by the mean fMRI image across time	more overlap with GM intensity	overlap with e.g. blood vessels
Percent of brain boundary	Overlap between spatial maps and brain bondaries	low overlap	motion related artefacts highly overlap with brain boundaries
Masked based features	Overlap between spatial maps and masks of GM, WM, CSF, vessels	overlap with GM mask	overlap with CSF, WM, vessels
other spatial features	…		

Features Selection. Feature selection attempts to automatically choose a subset of relevant features within the training dataset, for building robust learning models. FIX employs a combination of F-score, logistic regression and a linear support vector machine (SVM) for feature selection. Assuming L_F, L_{LR}, and L_{SVM} being the rankings resulting from F-score, logistic regression and linear SVM, respectively, FIX aggregates the top-ranking features from these three

rankings and decides on the final subset of features. If a feature is among the top 50% of at least one of the three rankings, then it will pass FIX's feature selection filter (see next paragraph)

Hierarchical classifier. In the N-dimensional feature space, signal and noise components are not simple clusters and hence not trivially separable. Moreover, when manually classifying the components, experts tend to consider the components spatial maps and time series separately, and then implicitly follow multiple if-then rules that determine the final label. In order to help mimic experts' decision process, while taking into account the components complex properties, FIX employs an ensemble learning (or classifier fusion) approach.

If D is defined as the set of all potentially useful features, then $D = D_T \cup D_S$, where D_T and D_S are the temporal and spatial feature sets. Let D_{sel} be the subset of selected features, also containing temporal and spatial feature sets, $D_{sel} = D_{T,sel} \cup D_{S,sel}$. As a result, the classifier must be trained on the 6 defined sets (D, D_{sel}, D_T, D_S, D_{T-sel} and D_{S-sel}).

As there is no absolute best classifier for the detection of signal/noise in a classification setting, FIX utilises an ensemble technique known as stacking (Wolpert, 1992), where outputs of individual classifiers (k-nearest neighbour algorithm (k-NN), support vector machine (SVM), and decision trees) become the inputs of a "higher-level" learner (in FIX's case, a decision tree) that works out the best way of combining them (see Figure 3.7).

Training the ensemble consists of extracting D, D_{sel}, D_T, D_S, D_{T-sel} and D_{S-sel}, training the k-NN, decision tree and SVMs, on each of the datasets, and training the fusion-layer decision tree using these classifiers outputs.

The inputs to the stacking classifier are the lower-level classifiers probabilistic outputs (Dzeroski and Zenko, 2004) and also the output of the fusion-layer decision tree (FIX's classification output) is a probability.
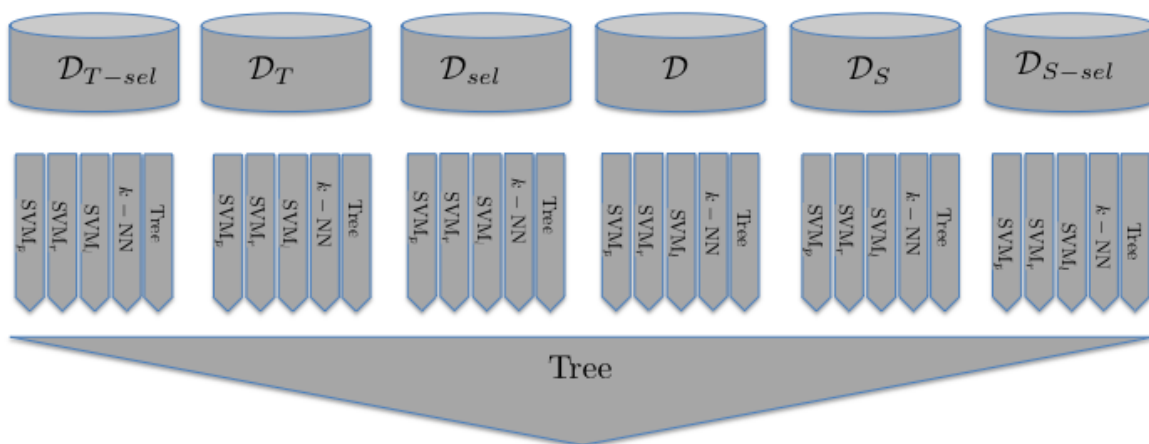
Figure 3.7. FIX's hierarchical classifier. In the data layer, full, feature-selected, temporal, spatial, temporal-feature-selected and spatial-feature-selected datasets (D, Dsel, D_T, D_S, D_T−sel and D_S−sel, respectively), are each classified by 5 classifiers. The result is a vector of 30 (5×6) probabilities (0 and 1 denoting perfect noise and perfect signal, respectively), which is the input to a fusion-layer decision tree, whose output is the probability of IC being signal/noise.

The decision tree at the fusion layer aims to generate a generalizable data-driven set of if-then rules. (adapted from Salimi-Khorshidi et al., 2014)

3.3. Methods

In the following paragraphs I will describe the analyses that I performed to test the classification accuracy of FIX, building three different training datasets and performing leave-one-out tests. The last step of FIX cleaning procedure, the denoising step, will be described in detail in chapter 4.

3.3.1. Subjects and MRI data acquisition

The accuracy tests on FIX performance were performed on the following datasets:

Dataset 1: 25 healthy subjects (age 70.6 ± 5.7 years, M/F = 18/7), participants in the Whitehall II MRI study (see details in par. 4.2.1.). Data have been previously acquired at FMRIB centre by the Neurobiology of Aging research group of the Psychiatry department (University of Oxford), using a 3T Siemens Verio MRI scanner with a 32-channel head coil. All subjects gave written informed consent to participate in the study. The images were acquired with a standard RS-fMRI sequence: single-shot EPI T2*-weighted images (TR = 3000 ms, TE = 30 ms, Flip Angle = 90°, voxel dimension = 3 mm isotropic, whole brain, acquisition time = 10 min for a total of 200 timepoints);

Dataset 2: The same 25 subjects of dataset 1 underwent a multi-band accelerated RS-fMRI sequence: single-shot EPI T2*-weighted images (TR = 1300 ms, multiband factor MB = 6, TE = 40 ms, Flip Angle = 66°, voxel dimension = 2 mm isotropic, whole brain, acquisition time = 10 min for a total of 460 timepoints), developed partly for the Human Connectome Project (Moeller et al., 2010; Feinberg et al., 2010; Setsompop et al. 2012);

In dataset 1 and dataset 2 the following sequences were also acquired:

- 3D high-resolution T1-weighted MR images were acquired using a MEMPRAGE sequence (TR = 2530 ms, TE = 1.79.3,65/5.51/7.37 ms, flip angle = 7°, field of view = 256 mm, voxel dimension = 1mm isotropic, acquisition time = ~6 min);

- Field maps were acquired to reduce MR distortion due to magnetic field inhomogeneities (TR = 400 ms, TE = 5.19/7.65 ms, flip angle = 60°, field of view = 258 mm, voxel dimension = 3 mm isotropic, acquisition time = ~1 min);

Dataset 3: 42 healthy subjects (age 35.7 ± 22.3 years, M/F = 19/23). The author was entitled to contribute to the MRI acquisitions that were performed in the Radiology Department of Fondazione don Carlo Gnocchi IRCCS in Milan, using a 1.5 T Siemens Magnetom Avanto (Erlangen, Germany) scanner with 8-channel head coil. RS-fMRI BOLD EPI images (TR/TE = 2500/30 ms; resolution = 3.1 x 3.1 x 2.5 mm^3; matrix size = 64 x 64; number of axial slices = 39;

number of volumes = 160) were collected at rest. T1-weighted 3D scans were also acquired (TR/TE = 1900/3.37 ms; resolution = 1 x 1 x 1 mm^3; matrix size = 192 x 256; number of axial slices = 176).

3.3.2. RS-fMRI data preprocessing and manual labelling of single-subject ICA components

The same preprocessing was performed for all datasets using FSL (Smith et al., 2004; Jenkinson et al., 2012). Each RS-fMRI dataset was corrected for head motion using MCFLIRT (Jenkinson et al., 2002) and corrected for EPI distortions using FMRIB's Utility for Geometrically Unwarping EPIs (FUGUE), which performs the unwarping of the EPI images based on fieldmap data. Non-brain tissue was removed with BET (Smith, 2002) and data was high-pass temporal filtered to remove slow drifts (cutoff period ~ 100.0 s). As the final aim of the study involving dataset 1 and dataset 2 was to compare the two sequences (see chapter 4), the data was not spatially smoothed, to retain the original information about spatial resolution; data belonging to dataset 3 was spatially smoothed with a 5mm (FWHM) Gaussian kernel.. Each 4D pre-processed dataset was then fed into MELODIC (Multivariate Exploratory Linear Optimised Decomposition of Independent Components – Beckmann and Smith, 2004) to perform single-subject spatial-ICA with automatic dimensionality estimation. Finally, the single-subject ICA components for each subject of each dataset were hand-labelled into "good" (predominantly signal) or "bad" (predominantly noise), on the basis of the criteria illustrated above (par 3.2).

3.3.3. Accuracy test and performance indices

The fundamental goal of machine learning is to generalise beyond the examples in the training set. In fact, performing well on the training set can be easy (the classifier can simply memorise the examples) and creates the illusion of success. Hence, when training and/or evaluating a learner algorithm, one must devise a strategy to minimise the risk of over-fitting (i.e., effectively memorising the examples).

In this study, FIX was tested using a leave-one-out (LOO) approach across sets of ICA output components. If the training data consists of n MELODIC outputs (e.g., one per imaged subject), each fold of the cross-validation uses n−1 datasets for training, and tests the learned decision boundary on the left-out dataset.

FIX's performance can be summarised by its accuracy in detecting signal and noise components in comparison with labels as provided by experts. We characterised the classification accuracy in terms of two measures of success: TPR ("true positive rate", meaning the percentage of true signal components correctly detected) and TNR ("true negative rate", meaning the percentage of true artefact components correctly detected).

Given that FIX's output (the output of the fusion-layer decision tree) is a probability, a threshold was applied to determine the binary classification of any given component. Changing the threshold shifts the balance between TPR and TNR; lowering it increases the TPR and decreases the TNR. For the LOO accuracy testing, therefore, we could evaluate several thresholds in order to show how the balance between TPR vs. TNR can be varied

As the desired final behaviour is generally to be conservative with respect to minimising the chance of incorrectly removing valid neuronal signal, when choosing the threshold to use we would recommend to prioritize high TPR, obviously at expenses of possible lower TNR.

Ideally, we would be interested in obtaining a TPR above 95% and TNR above 75%, but these values are only indicative and empirically obtained during the accuracy tests of FIX tool (see Salimi-Khorshidi et al., 2014), in order to give an indication of a good balance between noise removal and signal loss.

3.4. Results

The single-subject ICA decompositions found 71.60±15.59 components with the 3T Standard sequence data (*dataset 1*), 133.84±33.91 with 3T MB6 sequence data (*dataset 2*), and 18.76±5.96 with 1.5T standard EPI sequence (*dataset 3*), as judged by the MELODIC automatic dimensionality estimation. Of these, the noise components manually identified were: 63.40±16.84 (87.72±5.11 % of all components, corresponding to 69.33±11.61% of the total variance of the original data) for dataset 1; 119.40±36.74 (88.28±4.98 % of all components, 67.80±10.17% of the total variance) for dataset 2; 13.60±5.04 (71.96±10.02 % of all components, 30.60±12.89% of the total variance) for dataset 3.

The results of the LOO test are reported in Table 3.2, 3.3 and 3.4 for dataset 1, 2 and 3 Respectively and summarised in Figure 3.8 through the use of ROC curves. It can be noted that in all cases the optimal threshold (highlighted in bold) is an intermediate value among the tested thresholds (5 or 10).

Table 3.2. FIX classification accuracy for *dataset 1* (Standard EPI sequence, 3T scanner).

FIX threshold	1	2	**5**	10	20	30	40	50
TPR	97.8	97.8	**97.8**	96.3	94.6	93.0	92.0	90.8
FPR	91.9	91.9	**92.2**	94.7	96.1	97.3	97.3	97.6

TPR = True Positive Rate, i.e., the percentage of true signals correctly classified. TNR = True Negative Rate, i.e., the percentage of true artefacts correctly classified. As the FIX "threshold" is lowered, TPR is maximised at the expense of high TNR. The best threshold's results are highlighted in bold.

Table 3.3. FIX classification accuracy for *dataset 2* (Multiband accelerated EPI sequence, 3T scanner).

FIX threshold	1	2	5	**10**	**20**	30	40	50
TPR	97.2	97.0	96.5	**96.5**	**96.5**	96.0	96.0	95.5
FPR	92.2	93.0	95.2	**97.2**	**97.2**	97.3	97.3	97.3

TPR = True Positive Rate, i.e., the percentage of true signals correctly classified. TNR = True Negative Rate, i.e., the percentage of true artefacts correctly classified. As the FIX "threshold" is lowered, TPR is maximised at the expense of high TNR. The best threshold's results are highlighted in bold.

Table 3.4. FIX classification accuracy for *dataset 3* (Standard EPI sequence, 1.5T scanner).

FIX threshold	1	2	**5**	10	20	30	40	50
TPR	96.8	95.8	**95.8**	94.6	92.3	89.8	89.3	88.8
FPR	72.3	79.4	**79.4**	81.4	88.2	90.4	92.4	93.6

TPR = True Positive Rate, i.e., the percentage of true signals correctly classified. TNR = True Negative Rate, i.e., the percentage of true artefacts correctly classified. As the FIX "threshold" is lowered, TPR is maximised at the expense of high TNR. The best threshold's results are highlighted in bold.
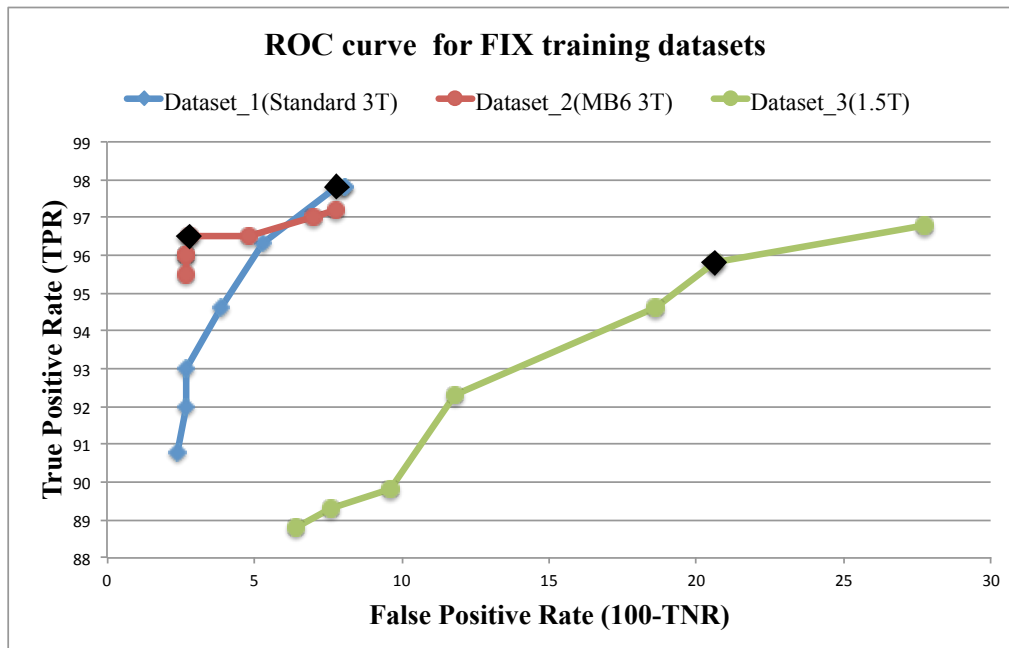
Fig. 3.8. ROC curves illustrating FIX performance as the threshold for the output of the fusion-layer decision tree varies. Threshold chosen for subsequent analyses are highlighted in black

3.5. Discussion and Conclusions

In this chapter I summarised the characteristics of a new tool for the automated denoising of artefacts in fMRI data, achieved by running independent component analysis, identifying which components correspond to artefactual processes in the data, and removing those from the data, developed at the Oxford University Centre for Functional MRI of the Brain (FMRIB). I described the analyses that I performed to test the classification accuracy of FIX, building three different training datasets and performing leave-one-out tests. The last step of FIX cleaning procedure, the denoising step (i.e. how to remove the artefactual components identified by the classificator), will be described in detail in Chapter 4.

From the training dataset building through manual labelling of the components, it emerged that the amount of noisy components is more than 70% of the estimated components for 1.5T images (which corresponds to the 30% of the total variance of the original data) and more than 85% (over 65% of the total variance) for 3T images. This highlights the importance to correctly identify and remove the artefacts from the data for a reliable analysis of RS-fMRI data, especially when increasing the static magnetic field strength.

FIX achieved, on the three datasets built by hand-labelling of the components, over 95% classification accuracy on all datasets. FIX therefore can be an effective tool for the identification of artefacts in fMRI data. Further analyses shown in (Salimi-Khorshidi et al., 2014), also evaluated the accuracy of FIX classification on the Human Connectome Project RS-fMRI data, showing over 99% accuracy, and on combined training datasets (using data acquired from different protocols), demonstrating that the accuracy is quite stable over protocols. However the performance is higher if study-specific training is carried out.

For all the accuracy evaluations performed in this study, FIX classification is compared to hand-labelled classification. It must be taken into account that manual labelling is likely to be not 100% accurate, as, although with guidelines and rules, it remains somehow subjective. However, it still represents the current gold standard method for signal and noise identification through the evaluation of different spatiotemporal characteristics, and therefore used in this study as a ground truth. We also tried to increase accuracy of hand labelling with a double-check/consensus by multiple experts (i.e. raters with a good knowledge of both BOLD signal characteristics and neuroanatomy to be able to classify the components into signal or noise by looking at their spatial and temporal features). If the raters were not in agreement on the classification of a component, it was labelled as "unknown" (not unambiguously identifiable as good or bad, and therefore treated by FIX as "good"). In pilot analyses (not shown in this thesis), FIX stability across multiple raters has

been shown to be good, although a systematic evaluation of inter-rater variability is certainly an interesting future development for this study.

The minimum number of subjects to create a reliable training dataset is variable, depending from the characteristics of the data (overall quality, different groups of subjects etc.). As an empirical indication, we would suggest to hand label at least 10 subjects ICA outputs, and quite possibly more than that (as empirically obtained during the different accuracy tests performed on FIX tool - data not shown).

FIX is now publicly available; the current version (v1.06) is available as a "plugin" for FSL (the FMRIB Software Library) at link www.fmrib.ox.ac.uk/fslwiki/fsl/FIX - it is not yet bundled as part of FSL, as it currently relies also on other software, in particular on Matlab (or Octave) and R. The FMRIB centre planned to recode a future version of FIX to remove these dependencies and release it as part of FSL. The FIX download includes training-weights files for "standard" fMRI acquisitions and for Human Connectome Project RS-fMRI data; the scripts supplied with fix make LOO evaluation very straightforward, and the value of adding further hand labelling can be established by noting whether the LOO result (as a function of number of datasets manually labelled) converges to a stable value.

Chapter 4 - ICA-based artefact removal and accelerated fMRI acquisition for improved Resting State Network imaging

This chapter covers the last step of the denoising procedure with FIX, introduced in chapter 3. Different options for the removal of the noisy components are tested with temporal, network and spatial maps analyses on the resting state networks extracted with low and high-dimensional group ICA. The optimized cleaning procedure is validated on standard and multiband slice accelerated EPI images, and a comparison of the results obtained with the two sequences is also discussed, highlighting the benefits of slice accelerated fMRI acquisition on resting state network analyses.

The preliminary results of this work are reported in a conference proceeding (Griffanti et al., OHBM 2013) and the final work was submitted for publication (Griffanti et al., under review). Partly due to the results obtained in this study, FIX is now in use as part of the default Human Connectome Project analysis pipeline (Smith et al., 2013), and FIX-cleaned data with the optimized options described in this chapter is the recommended version of the resting-state fMRI data that is publicly available.

4.1. Introduction

FMRIB's ICA-based X-noiseifier (FIX) tool is conceived to clean single-subject data before any further processing step (group-ICA, network analysis, or other approaches) exploiting a preliminary classification of single-subject independent components into signal or noise and regressing out the noise ones together with motion regressors. The last step of the denoising procedure with FIX tool is the removal of the nuisance components identified by the classifier (see Chapter 3 for further details), resulting in "cleaned" fMRI data. This is not trivial, as the noise components can share variance with components containing RSN signal. For this reason, the first aim of the present work was to compare several cleaning approaches and find a recommended procedure for noise removal, in order to clean the fMRI data of artefacts, while minimising the loss of signal.

We applied single-subject independent component analysis (ICA), followed by automatic component classification with FMRIB's ICA-based X-noiseifier (FIX) to identify artefactual components. We then compared two *first-level* (within-subject) cleaning approaches for removing

those artefacts and motion-related fluctuations from the data. The effectiveness of the cleaning procedures were assessed using time series (amplitude and spectra), network matrix and spatial map RSN analyses, feeding uncleaned and cleaned datasets into both low- and high-dimensional group-level ICA to identify resting-state networks (see sections 4.2.5 and 4.3 for details). For time series and network analyses we also tested the effect of a *second-level* cleaning, informed by group-level analysis (see sections 4.2.5).

Moreover, the cleaning procedure outcomes were used to quantify improvements yielded by a recent acquisition protocol named multiband (MB) or slice accelerated EPI vs. datasets obtained with standard EPI. MB EPI displays improved temporal and/or spatial resolution, leading to higher sensitivity in detecting RSNs (Moeller et al., 2010; Feinberg et al., 2010; Setsompop et al. 2012). Therefore, this technique is seeing rapid take-up in the imaging community, for example, in the Human Connectome Project (HCP) and the most recent Thousand Connectomes datasets from the Nathan Kline Institute. The second aim of this study was to further evaluate the potential of the multiband slice accelerated EPI sequence, and to investigate the effect of combining different acquisition pulse sequences with different artefact cleaning approaches (highlighting the different signal/noise content of the accelerated multiband acquisitions compared with standard EPI). Therefore, all evaluations were performed on two large datasets from the same group of subjects - a standard EPI sequence and an MB6 EPI sequence, demonstrating the efficacy of FIX cleaning on both sequences via investigation of RSN time series, correlation networks and spatial maps (see sections 4.2.5 and 4.3 for details). Partially due to the results obtained in this study, public releases of HCP RS-fMRI data are being cleaned using FIX using the "soft" clean-up approach described below (Smith et al., 2013).

4.2. Methods

4.2.1. Subjects and MRI data acquisition

Data from 76 healthy subjects, participants in the Whitehall II MRI study (ages 69.1 ± 5.8 years, M/F = 52/24), were acquired at FMRIB centre by the Neurobiology of Aging research group of the Psychiatry department (University of Oxford) (http://www.psych.ox.ac.uk/research/neurobiology-of-ageing/research-projects-1/whitehall-oxford) using a 3T Siemens Verio MRI scanner with a 32-channel head coil.

The Whitehall II study has examined 10,308 civil servants over the last 25 years at 5 yearly intervals, and has therefore information for risk factors, social background, exercise and mental activity. Combining long-term Whitehall II information from 800 people with MRI scanning will allow examining the connection between risk factors and protective factors and brain changes.

Furthermore, it will help establishing the effects of these brain changes on current mental state and performance, answering important questions about the natural history of depression and dementia.

All subjects gave written informed consent to participate in the study. The MRI protocol included:

- Standard RS-fMRI sequence: single-shot EPI T2*-weighted images (TR = 3000 ms, TE = 30 ms, Flip Angle = 90°, voxel dimension = 3 mm isotropic, whole brain, acquisition time = 10 min for a total of 200 timepoints);

- Multi-band slice accelerated RS-fMRI (MB) sequence: single-shot EPI T2*-weighted images (TR = 1300 ms, MB factor = 6 – MB6, TE = 40 ms, Flip Angle = 66°, voxel dimension = 2 mm isotropic, whole brain, acquisition time = 10 min for a total of 460 timepoints), developed partly for the Human Connectome Project (Moeller et al., 2010; Feinberg et al., 2010; Setsompop et al. 2012);

- 3D high-resolution T1-weighted MR images were acquired using a MEMPRAGE sequence (TR = 2530 ms, TE = 1.79/3.65/5.51/7.37 ms, flip angle = 7°, field of view = 256 mm, voxel dimension = 1mm isotropic, acquisition time = ~6 min);

- Field maps were acquired to reduce MR distortion due to magnetic field inhomogeneities (TR = 400 ms, TE = 5.19/7.65 ms, flip angle = 60°, field of view = 258 mm, voxel dimension = 3 mm isotropic, acquisition time = ~1 min).

4.2.2. RS-fMRI data preprocessing

The same preprocessing was performed on both Standard and MB6 RS-fMRI data using FSL (Smith et al., 2004; Jenkinson et al., 2012). Each RS-fMRI dataset was corrected for head motion using MCFLIRT (Jenkinson et al., 2002) and then corrected for EPI distortions using FMRIB's Utility for Geometrically Unwarping EPIs (FUGUE), which performs the unwarping of the EPI images based on fieldmap data. Non-brain tissue was removed with BET (Smith, 2002) and data were high-pass temporal filtered to remove slow drifts (cutoff period ~ 100.0 s). Data were not spatially smoothed, in order to make it easier to compare and interpret the effect of the different acquisition resolutions (e.g., on SNR and apparent spatial detail). Each 4D pre-processed dataset was then fed into MELODIC (Multivariate Exploratory Linear Optimised Decomposition of Independent Components – Beckmann and Smith, 2004) to perform within-subject spatial-ICA with automatic dimensionality estimation (we explain below how the ICA outputs were then used). The 76 subjects' datasets were then randomly split into two age-matched subsets: 23 subjects were used as the training dataset for FIX (dataset 1 and 2 described in Chapter 3), and 53 as the test dataset. The rationale beyond this group size difference is because we judged 23 subjects to be sufficient to train FIX well and provide robust group-level ICA decomposition for the templates (see section 4.2.3), reducing the manual intervention as much as possible. Moreover, many of the final

evaluations depend on cross-subject variance estimations, and hence the size of the second group is arguably more important to our quantifications than the size of the first. Subsequent analysis steps are summarized in Fig. 4.1.
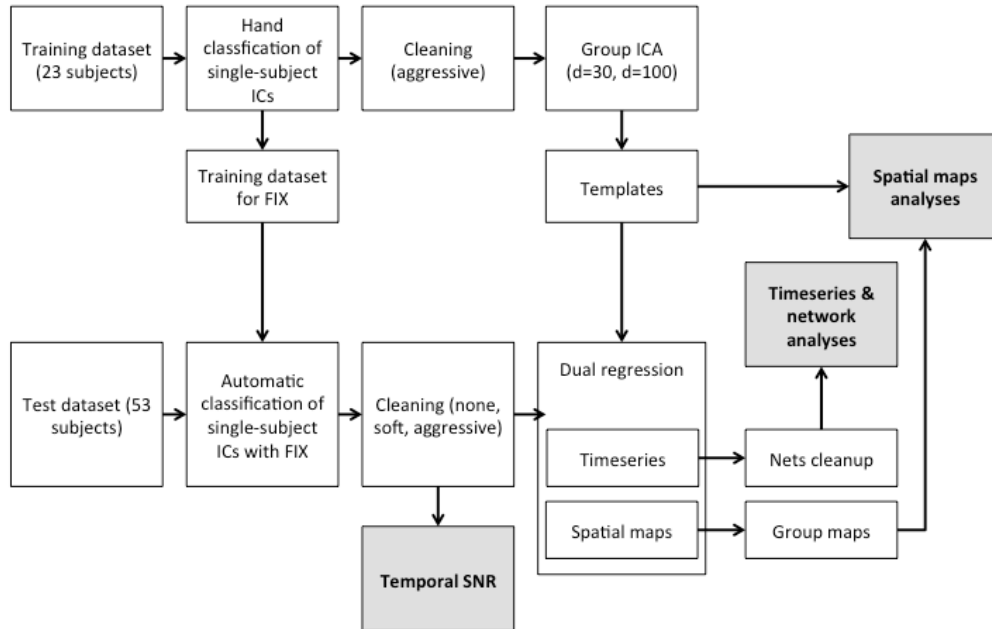
Fig. 4.1. Graphical illustration of overall evaluation.

4.2.3. Creation of group-ICA RSN templates

Next we applied ICA-based artefact removal for all single subject data in the training dataset. Each ICA component from every single-subject dataset (from both MB6 and Standard acquisitions) was hand-classified into signal or noise, on the basis of the temporal and/or spatial characteristics. See Chapter 3 for more detail regarding how hand-classification decisions were made. Next, the full space of all artefact time series and motion parameters (as opposed to the partial space, where the both artefact and non-artefact time series are included in the regression; see section 4.2.4 for further details) was regressed out of the 4D pre-processed data, to achieve a so called "aggressive" artefact removal. The rationale for applying a more aggressive artefact regression was that we wanted to obtain the cleanest possible group-level ICA maps from the training dataset, to be used as a reference of "true signal". The aggressive within-subject-cleaning approach maximizes the noise removal at the expense of a potential loss of some RSN-related signal in some subjects, which is compensated for by utilizing multiple subjects for the group-ICA-based template generation. We registered cleaned RS-fMRI 4D data from single subjects to their high-resolution structural image using FLIRT linear registration, enhanced with brain-boundary-registration (BBR – Greve and Fischl, 2009), and then to MNI152 standard space via the application of the nonlinear FNIRT tool

applied to the structural image (Andersson et al., 2007a,b). All 4D RS-fMRI datasets were resampled to $2 \times 2 \times 2$ mm^3 resolution in the final MNI152 space.

We then performed (separately for Standard and MB6 training datasets) group-ICA using MELODIC. The group ICA was performed at two dimensionalities (d): with 30 dimensions for a more "conventional" ICA analysis (i.e. using a number of components comparable to most of the RS-fMRI studies using group ICA – e.g. Beckmann et al., 2005; Filippini et al., 2009), and with 100 to achieve a more finely-detailed functional 70 parcellation of the data (this is useful for more detailed network analyses, if permitted by data quality). The four sets of group maps were used as reference templates in subsequent analyses performed on the test datasets, based on the assumption that ICA had extracted features common to the whole group (test and training data). The template components were manually classified as RSNs vs artefact based on previous knowledge of the RSNs patterns described in literature (Beckmann 2005; De Luca 2006; Rytty et al., 2013), and following the same rules used for single-subject manual labelling described in Chapter 3 (Salimi-Khorshidi et al., 2014; Smith, 2013), also including the study of the mean cross-subject temporal power spectrum of each component and double-checked by two further experts. (Although ICA-based clean-up was applied to each separate dataset, some artefactual components can still emerge at the group-level. For example, low-level artefactual processes that are too weak to be identified by single-session ICA may be consistent across subjects and hence be enhanced at the group level).

4.2.4. Automated classification and clean-up procedures with FIX

In addition to generating the group-ICA template maps, the hand-labelled components from the training dataset were also used to train the FIX (FMRIB's ICA-based X-noiseifier) component classifier (see chapter 3). We created one training dataset for the Standard data and extended a pre-existing training dataset for MB6 (though our classification accuracy results were extremely similar for MB6, if we only used this current study's MB6 training dataset). We evaluated FIX's classification accuracy via leave-one-out bootstrap testing (chapter 3).

The single-subject ICA components of the test dataset were then automatically classified into signal and noise using FIX. As the ground truth of signal and noise is unknown, from now on we will refer to "signal" and "noise" components according to FIX classification (purely for convenience of notation). For the clean-up procedure we used both the time series relative to noise components and 24 motion-estimation confound time series (the six rigid-body parameter time series, their backwards-looking temporal derivatives, and the squares of all twelve resulting regressors) (Satterthwaite et al., 2013). The 24 motion confound time series then had the same temporal highpass filtering applied to them that had been applied to the data.

We evaluated two different cleaning procedures: the "aggressive" clean-up, and a "soft" clean-up.

As previously introduced, the "aggressive" approach consisted of regression of the full space of all artefacts (noise components) and the motion confounds out of the 4D pre-processed data (Y), using:

$$Y_{clean} = Y - C \cdot (pinv(C) \cdot Y) \tag{4.1}$$

where C is the matrix of artefact and motion time series (C=[Cmotion ICA(bad)]) and pinv() is the matrix pseudo-inverse (for example, as estimated via pinv(C)=(C^{T}C)$^{-1}$C^T). With this method, the contribution of the motion and the artefacts is fully removed from the data. In general, the signal and noise ICA components are not completely orthogonal; this approach removes all shared variance between the two (hence the term "aggressive").

The "soft", less-aggressive, approach consisted of three steps. First, we regressed out the full space of the motion confounds (C$_{motion}$) from both the data and from all the ("good" and "bad") ICA component time series (ICA), in order to fully remove the effect of motion from the data (resulting in Ym) and the ICA time series (resulting in ICA$_m$):

$$Y_m = Y - C_{motion} \cdot (pinv(C_{motion}) \cdot Y) \tag{4.2}$$

$$ICA_m = ICA - C_{motion} \cdot (pinv(C_{motion}) \cdot ICA) \tag{4.3}$$

Second, we estimated the contribution of both good and bad components $(\widehat{\beta_{ICA}})$ via multiple regression of the data against all (motion-cleaned) ICA time series, in order to be able to identify the unique variance of the artefacts (Eq 4.4):

$$\widehat{\beta_{ICA}} = pinv(ICA_m) \cdot Y_m \tag{4.4}$$

Finally, using this, the unique contribution of the bad components was removed from the data, utilising only the bad ICA components' time series and the respective regression coefficients:

$$Y_{clean} = Y_m - ICA_m(bad) \cdot \widehat{\beta_{ICA}}(bad) \tag{4.5}$$

Hence we obtained 6 different test datasets (ordered by hypothetically decreasing noise):

- uncleaned Standard data
- uncleaned MB6 data
- softly-cleaned Standard data
- aggressively-cleaned Standard data
- softly-cleaned MB6 data
- aggressively-cleaned MB6 data

For each dataset, the raw temporal signal-to-noise ratio (temporal-SNR) image was formed for each subject, eroded to exclude brain-edge effects, and the median SNR value was calculated as a first measure of the cleaning effect (note that the temporal "noise" in the SNR here includes

valid RSN-related fluctuations). All subjects' RS-fMRI test data were then resampled into 2 mm MNI152 space, as carried out on the training datasets.

4.2.5. Dual regression and analyses

In order to evaluate sensitivity and consistency of RSNs estimated from the test datasets, we applied dual-regression (described below) of the training-dataset group-level template spatial maps into each test dataset. This resulted in test-dataset subject-specific spatial maps corresponding to the template maps, and associated subject-specific time series (Filippini et al., 2009).

For each version of each single-subject RS-fMRI *test* dataset (created as described above), the full set of *d* template spatial maps was regressed into the single-subject data (as a spatial regression), the output being *d* single-subject time series (separately for each subject in the test dataset). These *d* subject-level time series (from each of the 53 test dataset subjects) were then used to perform *time series* (temporal standard deviation to represent the time series amplitude, and temporal power spectra to analyse the frequency content) and correlation-based *network* analyses (see section 4.3.4-4.3.6 for details).

Four different analyses were carried out by separately applying the four sets of group-ICA templates previously defined in the first stage of dual regression as sets of spatial regressors.

As the group ICA contained some artefactual components, only for time series and network analyses we introduced a further second-level clean-up ("Nets clean-up"), where the time series corresponding to the artefactual group-level components manually identified in the templates (see section 4.2.3) were regressed out of the remaining RSNs time series using Eq.4.6:

$$\text{ICA}_{\text{clean}} = \text{ICA}(\text{good}) - \text{ICA}(\text{bad}) \cdot (\text{pinv}(\text{ICA}(\text{bad})) \cdot \text{ICA}(\text{good})) \tag{4.6}$$

In the case of unknown group-level components (not artefacts but also not clearly RSNs), these were simply discarded for the purposes of the Nets clean-up evaluations, and not regressed out of the good components. Time series and network analyses were evaluated only using time series derived from good template components, with 6 different combinations of first-level (no cleaning, soft, aggressive) and time series (with vs. without Nets) cleaning. For the temporal analyses we calculated the mean amplitude of the time series for each component (section 4.3.4) and the mean power spectrum across subjects and components (section 4.3.5). For the network analysis, *d* x *d* full correlation, partial correlation and L1-norm regularised partial correlation matrices (Smith et al., 2011) were estimated using the set of RSN time series (section 4.3.6). The temporal characteristics and network matrices were estimated separately for each subject.

Finally, the second stage of dual regression was carried out for each subject, resulting in subject-specific spatial maps corresponding to the template maps. This was achieved by regressing the subject-specific RS-fMRI datasets against the set of *d* subject-specific time series as estimated in

the first stage. We calculated two sets of test-dataset cross-subject group-level maps (one using mixed-effects (ME) statistics and one using approximate fixed-effects (FE) statistics), and compared them against the template maps, under the assumption that the more a group RSN map reflects the corresponding template map, the more the cleaning approach (or the acquisition sequence) correctly identifies the true signal. To do this, we calculated the spatial correlation coefficients between the group maps and the templates, which were compared between different cleaning procedures and acquisitions. All *d* components were used in the two dual-regression stages, but only the non-artefactual components were then used when comparing the test-dataset maps against the training-dataset template maps (see section 4.3.7 for details).

In the following section we describe in more detail the different comparison analyses, and present the comparison results. Section 4.4 then includes a broader discussion of the results

4.3. Results

4.3.1. Single-subject independent component classification

The single-subject ICA decompositions, performed on all 76 subjects, found 69.8 ±14.9 components (per dataset) with the Standard sequence data, and 124.9 ± 25. 7 with MB6 sequence data, as judged by the MELODIC automatic dimensionality estimation (Beckmann et al., 2004). Of these, the artefact components (which were manually identified on the 23-subject training/template dataset) were more than 85% of all components (60.9 ± 14.9, i.e., 87.7%, for Standard and 111.5 ± 24.0, i.e., 88%, for MB6). On the remaining 53 subjects, FIX automatically identified 57.4 ± 15.8 (82%) artefactual components on Standard data and 108.1 ± 29.8 (87%) on MB6 data, in line with the proportion of artefacts found with hand labelling of the training dataset. FIX performed with higher classification accuracy on MB6 data, with an overall accuracy of 98% for MB6 and 95% for Standard (see Chapter 3 for details).

4.3.2. Temporal SNR results

Based on the expectation that the cleaning procedure should decrease fluctuation of the signal around its mean, we first compared the temporal SNR for each clean-up and sequence. For each RS-fMRI run (both for Standard and MB6 sequences), a temporal-SNR image was generated after motion correction and highpass filtering; the "noise" here includes RSN-related fluctuations, which therefore places an upper limit on the possible SNR. The SNR image was eroded by 3 voxels at the brain edge to avoid edge effects, and the median SNR value across voxels was computed. This process was repeated after soft and aggressive clean-up. The results were then compared across cleaning approaches and between sequences by means of two-tailed paired t-tests.

The boxplots in Fig. 4.2 show the distributions of the median (across space) SNR value over the 53 subjects for the two acquisitions with different cleaning options. The raw SNR results (Fig. 4.2.A) show that the cleaning procedure significantly increases the SNR (p<0.01), while, when comparing the two sequences, the combined decrease in voxel volume and the EPI acceleration in MB6 results in significant lower SNR (p<0.01) (mainly due to the former, Smith et al., 2013). However, if the increased number of time points is taken into account (Fig 4.2.B), the statistical power for simple analyses applied to MB6 data is seen to be comparable to those from the Standard acquisition. This is of great value because it means that the increase in statistical power due to the acceleration counteracts the loss in SNR caused by the increase in spatial resolution. Of course, these SNR results do have somewhat limited meaningfulness, because the "noise" in the "SNR" includes both interesting signal fluctuations as well as various sources of noise.
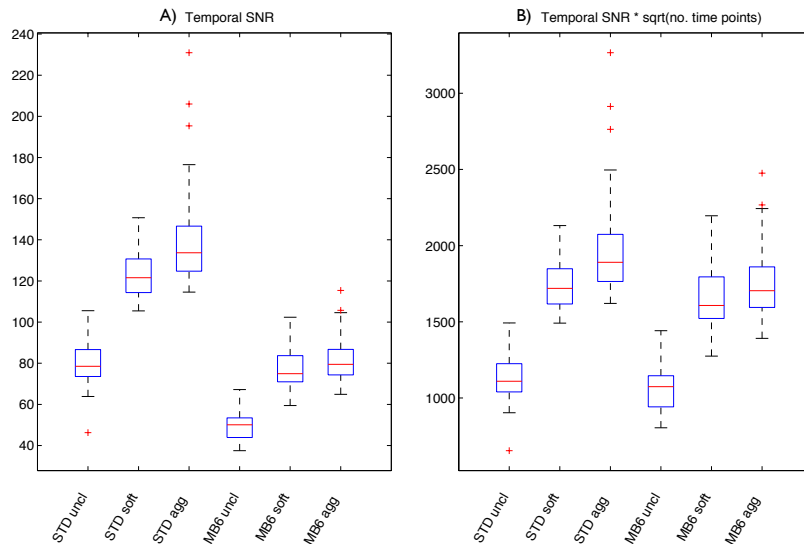
Fig. 4.2. Temporal SNR estimation for various cleaning procedures and acquisition protocols. The boxplots show the distribution across 53 test subjects. From the raw SNR results (A), it is clear that the cleaning procedure increases the SNR, while the reduced voxel volume and EPI acceleration decreases it. However, taking into account the increased number of time points (B), the statistical power for simple analyses applied to MB6 data is seen to be comparable to those from the standard acquisition. This is of great value because it means that the increase in statistical power due to the acceleration counters the loss in SNR caused by the increase in spatial resolution.

4.3.3. Group ICA components and dual regression - summary

As described above, group ICA was performed at two dimensionalities (d=30 and d=100). Based on visual inspection (agreement of 3 experts) of each component spatial map and (mean cross-subject) temporal power spectrum, 28/30 and 58/100 group-ICA components were judged to be non-artefactual in the MB6 templates, while 19/30 and 43/100 in the Standard ones. We identified 1/30 and 7/100 components as unknown (i.e., components which could not be unambiguously identified as good or bad) in the MB6 templates and 1/30 and 17/100 in the Standard ones. For each

dimensionality, the difference in these proportions between the two sequences was tested with a binomial test. We found that the proportion of good components found in the templates was significantly higher for MB6 ($p < 0.05$), and the proportion of unknown components significantly lower (except for the case of only having 1/30 unknown component for both acquisitions with the d=30 analyses). These results clearly suggest that MB6 data can be more effectively cleaned of artefacts by FIX, both at low and high group-ICA dimensionality.

As we were interested in comparing both different cleaning procedures and the two acquisitions, we performed 12 sets of dual regressions (two sequences × two dimensionalities × three cleanings). However, noise removal and high dimensional dual-regression was fully possible with MB6 only, while, with Standard data, the temporal degrees of freedom after the cleaning procedure were not sufficient to perform the full dual-regression with d=100. For this reason, subsequent comparisons among different cleaning approaches were performed on Standard d=30, MB6 d=30 and MB6 d=100, while the comparisons between the two acquisitions was performed at d=30. Where possible and meaningful we included and discussed the results obtained on Standard d=100. For each dataset, we obtained subject-level time series (first stage of dual regression) and spatial maps (second stage), which were analysed to test the effect of the different cleaning procedures and the differences between the two acquisitions. More specifically, the output of the first stage of dual regression (subject-level time series of the 53 test subjects) was used to perform time series (amplitude and power spectra) and network analyses, while the output of the second stage was entered into spatial map analyses.

4.3.4. Time series amplitude analysis

Given the hypothesis that the cleaning procedure should decrease the fluctuation of the subject-level time series with respect to the uncleaned data, we compared the time series amplitude across cleanings and sequences. This measure was obtained by scaling each time series standard deviation (for each subject and component) by the standard deviation of the corresponding uncleaned time series. The ratio between the amplitude of cleaned vs. uncleaned data yielded the normalized amplitude (hereon, amplitude) considered in statistical analyses. We directly compared the amplitudes obtained with different cleaning approaches through two-tailed paired t-tests and the results obtained with the two sequences using two-tailed independent t-tests, and the results are shown in Fig. 4.3 and Table 4.1. The boxplots show the distribution of amplitudes across components (with the scaled amplitude for a given component averaged across subjects). With all protocols, each cleaning step (both at 1st and 2nd level) significantly reduced the time series amplitude ($p < 0.01$). Regarding 1st level clean-up, the largest difference was observed between uncleaned and cleaned data (almost 50% amplitude reduction), while the difference between soft

and aggressive approach was less strong, although statistically significant (p<0.01). Nets clean-up significantly reduced the amplitude, especially if the data had not been cleaned at 1st level. On MB6 d=30 data the effect of Nets clean-up was statistically significant but limited in effect size, because only one artefactual component was removed.

As with the SNR results, these results have limited interpretability because it is not known what the balance is between remaining noise and signal contributions to the amplitudes; nevertheless, the results are useful indicators of how much variance is being removed in the various cases. For example, if there was almost no variance being removed by a given method, further investigations would be rather pointless.
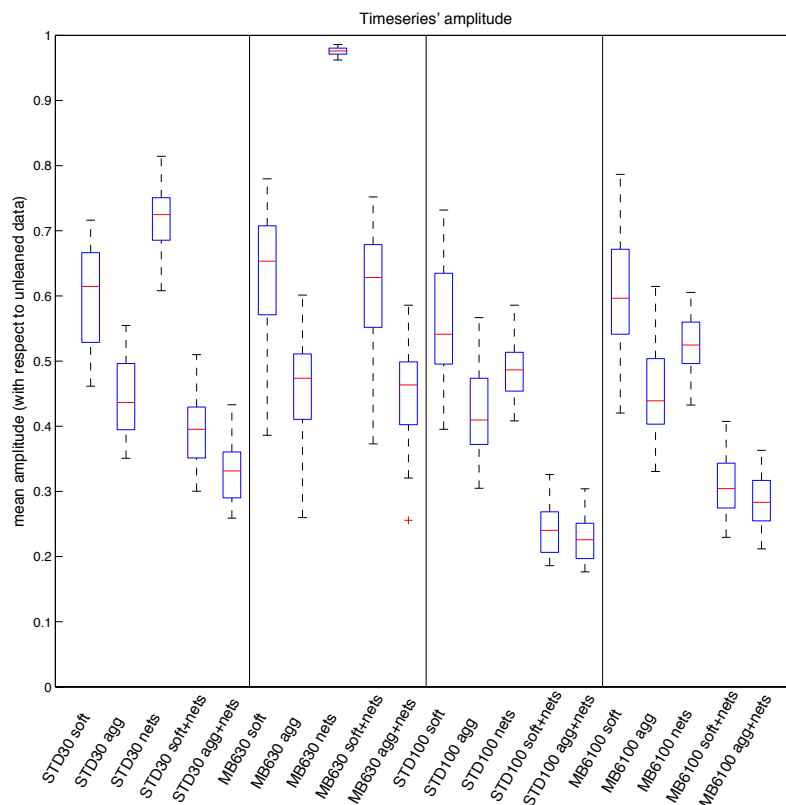
Fig. 4.3. Time series amplitudes. This measure was obtained by scaling (the standard deviation of the) single-subject time series associated with each group-level map by the standard deviation of the corresponding uncleaned time series. The boxplots show the distribution of amplitudes across components (each component is first averaged across subjects). All clean-up approaches decrease the amplitude; the amplitude is higher with MB6 sequence than with Standard. STD=Standard sequence; uncl=uncleaned; soft=FIX soft cleaning; agg=FIX aggressive cleaning; nets=Nets cleaning.

Table 4.1. Time series Amplitude. Comparison among cleaning approaches (paired t-test).

Time series amplitude. Comparison across cleanings	Standard d=30 t-value	MB6 d=30 t-value	Standard d=100 t-value	MB6 d=100 t-value
uncleaned - soft	**21.52**	**19.59**	**32.83**	**32.62**
uncleaned - aggressive	**37.54**	**34.82**	**58.04**	**59.39**
uncleaned - nets	**25.01**	**22.91**	**81.98**	**82.60**
uncleaned - soft+nets	**44.89**	**21.58**	**150.43**	**114.60**
uncleaned - agg+nets	**59.58**	**36.58**	**168.27**	**133.79**
soft - aggressive	**30.83**	**30.89**	**31.90**	**38.41**
soft - nets	**-8.39**	**-18.82**	**6.99**	**8.76**
soft - soft+nets	**23.59**	**26.04**	**31.85**	**38.01**
soft - agg+nets	**28.06**	**32.17**	**32.00**	**38.55**
aggressive - nets	**-24.20**	**-34.18**	**-8.91**	**-10.91**
aggressive - soft+nets	**7.97**	**-28.30**	**28.65**	**27.79**
aggressive - agg+nets	**18.77**	**15.17**	**29.27**	**30.83**
nets - soft+nets	**39.38**	**20.84**	**101.86**	**84.86**
nets - agg+nets	**51.69**	**35.97**	**96.85**	**99.49**
soft+nets - agg+nets	**23.46**	**30.19**	**24.64**	**25.65**

Significant results ($p<0.01$) are highlighted in bold.

Regarding the comparison between the two sequences (see Table 4.2), amplitude with MB6 was always higher than Standard: this difference was significant only on Nets clean-up results at low dimensionality, and for all cleaning options at high dimensionality. This means that a slightly smaller fraction of the temporal variance is removed by the cleaning of the MB6 data.

Table 4.2. Time series Amplitude. Comparison between sequences (unpaired t-test).

Time series' amplitude. Comparison between sequences	soft	aggressive	nets	soft+nets	aggressive+nets
standard d=30 - MB6 d=30 (t-value)	-1.23	-0.88	**-27.56**	-8.76	-5.90
standard d=100 - MB6 d=100 (t-value)	**-2.75**	**-2.44**	**-4.77**	**-8.30**	**-7.93**

Significant results ($p<0.01$) are highlighted in bold.

4.3.5. *Time series power spectra*

Time series power spectra (from scaled time series) were also generated in order to evaluate the impact of the cleaning procedures at different frequencies. The mean spectra were obtained by averaging the spectra across subjects and calculating the median across components. With this qualitative analysis we compared: no cleaning, soft clean-up and aggressive clean-up for first-level (FIX) cleaning; no cleaning, Nets clean-up and global signal removal, for second-level ("Nets" time series) cleaning. As global signal removal is frequently used in the literature (Fox et al., 2009), we included this option when comparing our different cleaning approaches, calculating the global

signal as the mean time series across all components (good and bad) for each subject. Fig. 4.4 (panel A) shows the power spectra at each cleaning step for the MB6 sequence at high dimensionality (results were similar for other protocols, results not shown). As expected, uncleaned data have the highest power both at low frequency (LF, mainly signal) and at high frequency (HF, mainly noise, as the content of thermal noise and structured artefacts should strongly dominate over neural-related signal). After soft clean-up the power is more reduced at HF than at LF, while aggressive clean-up causes the largest power reduction both at LF and HF. Regarding the effect of second-level cleaning, there is negligible additional reduction after the removal of the global signal (slightly lower power both at LF and HF), while Nets clean-up caused a large additional reduction.

In order to obtain a different measure of contrast-to-noise ratio (CNR), we scaled each power spectrum (Fig. 4.4 panel B) according to the amount of thermal noise. We assumed as index of thermal noise level the mean value of the power spectra at the highest frequencies (last 10 bins of the spectrum), where the spectral curve has (or nearly has) asymptoted, and where the content of thermal noise is higher than the content in signal (Cordes et al., 2002; Triantafyllou et al., 2005). Clearly, after this normalisation, the highest CNR was obtained with soft cleaning (green line). This cleaning approach is also the one most affected by Nets clean-up, probably because Nets clean-up is not effective if the first-level cleaning has not been performed (red dotted line); conversely, data cleaned with aggressive clean-up are less affected, since most of the noise has already been removed (blue line).
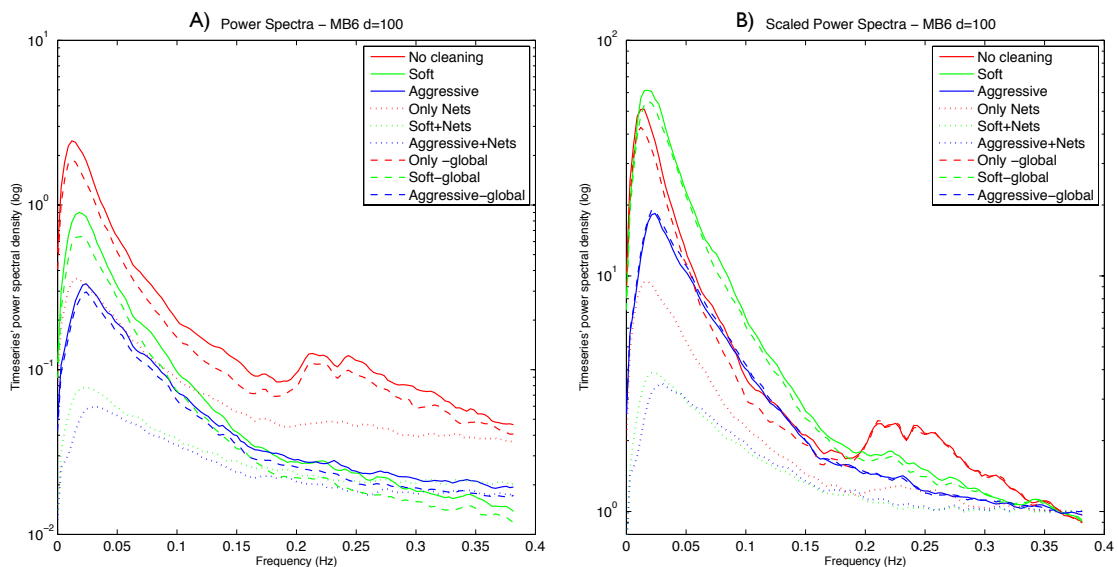
Fig. 4.4. Temporal power spectra (panel A) for different cleaning approaches, obtained from scaled time series (i.e., each normalised by the amplitude of the corresponding uncleaned time series), averaging the spectra across subjects and then calculating median spectra across components. Uncleaned data have the highest power both at low and high frequency; however, after normalising for power at the highest frequencies (last 10 bins of the spectrum, where the content of thermal noise is higher than the content in signal) (panel B), it is clear that with soft clean-up we obtained the highest contrast-to-noise ratio. Results are shown for MB6 data, at d=100 (y axis in logarithmic scale).

In Fig. 4.5 we present similar comparisons, but addressing the comparison of the power spectra across the different protocols and processed with the different cleaning options. The clear artefact peak that was seen in non-cleaned MB6 data at ~0.25 Hz is not apparent in Standard data power spectra because of temporal aliasing of physiological artefacts; the lower temporal resolution (TR=3s) does not allow the capturing of such fluctuations cleanly, so the effect of physiological artefacts is mixed in with the true underlying fluctuations at other frequencies. At d=30, the LF peak (dominated by RSN signal) is always higher for MB6 than Standard, and the difference is increased at both first and second level cleaning. The large differences between MB6 d=30 and d=100 after Nets clean-up arise because of the different number of bad components removed from each dataset (1 bad component for MB6 d=30 and 35 bad components for MB6 d=100). From these figures we can also observe that Nets clean-up is not as effective as FIX: in fact, comparing the spectra obtained with the two methods (Fig. 5 B vs 5 D), we can see that the HF peak is always lower using FIX. Regarding the effect on LF, for MB6 d=100 data the LF peak is higher with FIX, suggesting that FIX retains more RSNs-related signal than Nets cleaning. On the contrary, for MB6 d=30 the LF peak is higher with Nets cleaning. However, it must be taken into account that, as only one component is removed with Nets clean-up, the spectra is almost identical to the one from uncleaned data (Fig. 5 A), indicating that FIX still offers the best balance between noise removal and signal loss. No significant differences at LF peak were observable on Standard d=30.
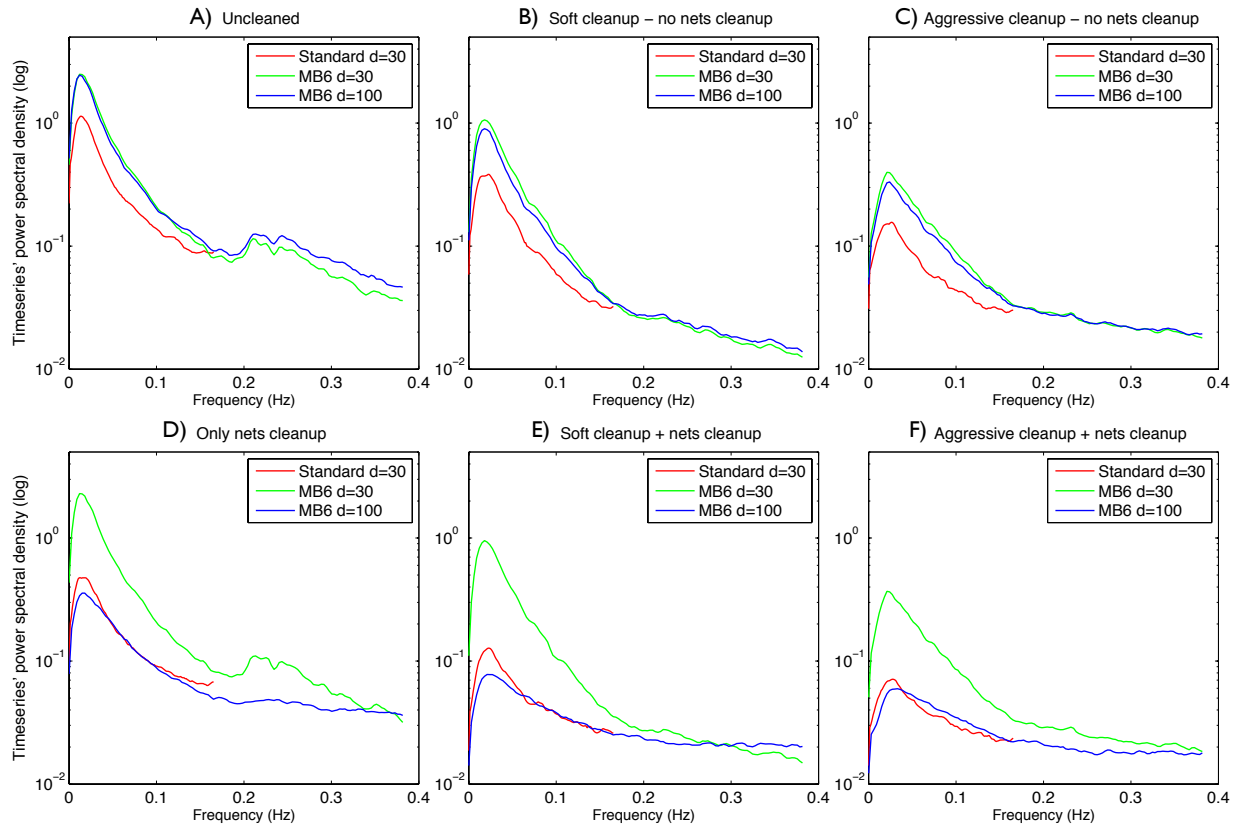
Fig. 4.5. Temporal power spectra of the different protocols for each cleaning option. The spectra were obtained by averaging the single subjects' spectra (from time series scaled using the amplitude of uncleaned data) and calculating median spectra across components, without normalisation for high frequency power. Y axis in logarithmic scale.

4.3.6. Network analyses

Network analysis was performed by estimating correlations between all pairs of time series (good components only). Full correlation, partial correlation, and L1-norm regularised partial correlation ("ICOV" - obtained by regularising the inverse of the covariance matrix) were used for the computation of network matrices. Full correlation directly evaluates the similarity between two time series and reflects both direct and indirect functional connections; conversely partial correlation evaluates the similarity between two time series after regressing out all other time series, thus emphasizing direct functional connections, cancelling the indirect ones (Marrelec et al., 2006; Smith et al., 2011; Smith, 2012). The L1-norm regularised partial correlation (regularised ICOV) shrinks entries that are close to zero more than those that are not (Friedman et al., 2008). In our analyses we used a regularisation-controlling parameter lambda=0.1. In this way we were able to estimate regularised partial correlation network matrices also for Standard data at high dimensionality d=100, for which the degrees of freedom were not sufficient to estimate unregularised partial correlation. Correlation matrices were transformed into z-scores using the Fisher transform (including an empirical correction for temporal autocorrelation using FSLNets (http://fsl.fmrib.ox.ac.uk/fsl/fslwiki/FSLNets) to improve normality.

The effect of the different cleaning approaches was evaluated by comparing how similar the network matrices are across subjects. In a homogeneous group of healthy controls, effective cleaning should increase the networks consistency (similarity) across subjects (Smith et al., 2005). This analysis was performed by calculating the correlation coefficient between the two network matrices (unwrapped into long vectors for the purpose of correlating the networks against each other) for each pair of subjects, giving a global index of network similarity across subjects; see Fig. 4.6. These values were then compared across sequences with two-tailed paired t-tests, and the results are shown in Table 4.3 and Table 4.4.

It can be observed that FIX clean-up (either soft or aggressive) significantly improved the similarity across subjects in almost all cases. Aggressive cleaning generally led to higher similarity than soft, when considering full correlation. As full correlation is more influenced by the presence of any shared signal or noise, it benefits from the aggressive noise removal. The improvement is lower for partial correlation and regularised ICOV, particularly for the more detailed network modelling (d=100) (which is probably the set of results likely to be of highest general interest). In this case almost all improvement in similarity is already achieved with soft cleaning. Nets clean-up is not needed for partial correlation by definition, while it increases the similarity assessed by full correlation at d=100, when not combined with 1st level cleaning. However, it must be taken into account that the results shown in this study were obtained removing the contribution of the template bad components, that were obtained with aggressively FIX-cleaned training data (as they were used as the reference of "true signal" and "true noise"). In this case the good and bad group components were clearly identifiable in the templates. However, if FIX clean-up was not performed, the group ICA results themselves would have been less clean, and this would have affected the results of Nets clean-up, making this approach certainly less effective.

Comparing the two sequences (d=30), with MB6 data we obtained higher similarity than with Standard data, especially with partial correlation and regularised ICOV. However, when moving to higher parcellation (d=100) the superiority of MB6 was evident also in full correlation results. The degrees of freedom in Standard data were not sufficient to achieve successful clean-up and (regularised or unregularised) partial correlation network modelling, even if the regularisation allowed the estimation of the network matrix.
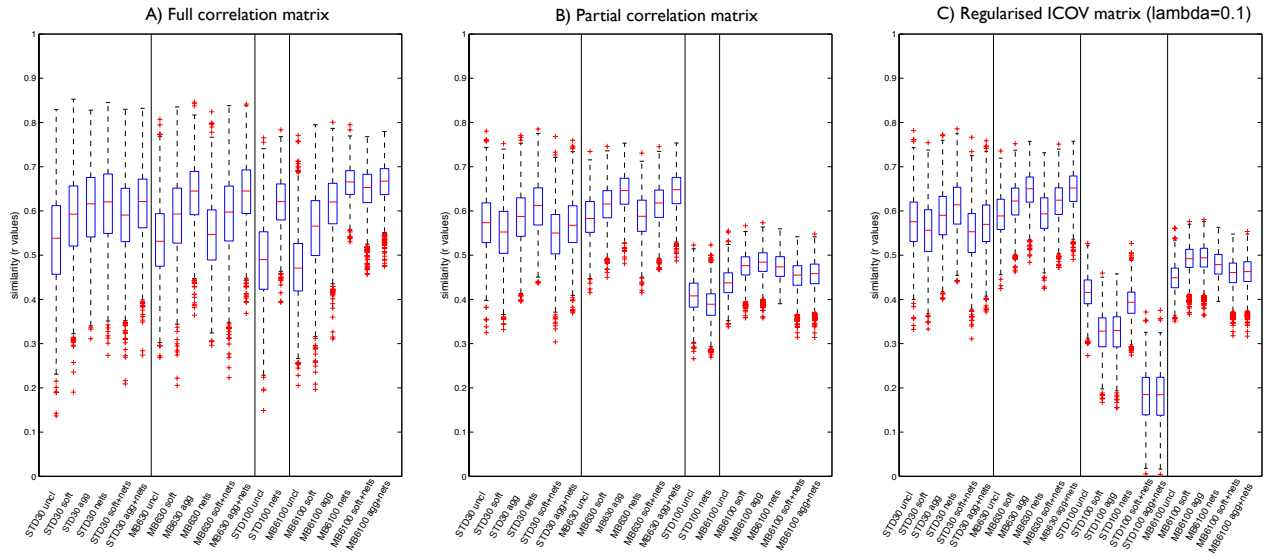
Fig. 4.6. Networks' similarity across subjects. The boxplots show the correlation coefficients (full correlation, partial correlation, and regularised ICOV) between network matrices (unwrapped into a vector of network matrix edges) for all pairs of subjects, with different cleaning steps and for different protocols. ICOV= L1-regularised partial correlation; STD=Standard sequence; uncl=uncleaned; soft=FIX soft cleaning; agg=FIX aggressive cleaning; nets=Nets cleaning.

Table 4.3. Network Similarity across subjects. Comparison among cleaning approaches (paired t-test).

Similarity across subjects comparison across cleanings (paired t-test)	Standard d=30		MB6 d=30		Standard d=100		MB6 d=100	
	mean delta r	t-value	mean delta r	t-value	mean delta r	t-value	mean delta r	t-value
FULL CORRELATION								
uncleaned - soft	-0.050	**-18.00**	-0.052	**-20.72**	-0.038	**-15.21**	-0.085	**-36.91**
uncleaned - aggressive	-0.072	**-23.54**	-0.104	**-41.36**	-0.075	**-28.33**	-0.140	**-60.87**
uncleaned - nets	-0.080	**-34.51**	-0.012	**-19.53**	-0.130	**-54.90**	-0.191	**-94.14**
uncleaned - soft+nets	-0.050	**-15.53**	-0.057	**-21.96**	-0.028	**-10.47**	-0.174	**-76.95**
uncleaned - agg+nets	-0.079	**-24.52**	-0.106	**-41.90**	-0.041	**-15.35**	-0.189	**-85.80**
soft - aggressive	-0.022	**-12.89**	-0.052	**-29.44**	-0.037	**-25.74**	-0.056	**-35.45**
soft - nets	-0.030	**-11.06**	0.041	**16.13**	-0.093	**-39.14**	-0.106	**-49.45**
soft - soft+nets	0.000	-0.07	-0.005	**-6.27**	0.010	**4.61**	-0.089	**-45.75**
soft - agg+nets	-0.029	**-13.08**	-0.053	**-30.44**	-0.003	-1.45	-0.104	**-53.11**
aggressive - nets	-0.008	**-2.64**	0.092	**37.06**	-0.056	**-25.52**	-0.050	**-29.06**
aggressive - soft+nets	0.022	**9.24**	0.047	**26.47**	0.047	**24.45**	-0.033	**-22.96**
aggressive - agg+nets	-0.006	**-3.22**	-0.002	**-4.00**	0.034	**19.33**	-0.049	**-37.27**
nets - soft+nets	0.030	**11.49**	-0.046	**-17.82**	0.102	**54.67**	0.017	**13.75**
nets - agg+nets	0.001	0.48	-0.094	**-37.83**	0.090	**49.85**	0.002	1.54
soft+nets - agg+nets	-0.028	**-24.59**	-0.049	**-29.58**	-0.012	**-34.78**	-0.015	**-36.00**
PARTIAL CORRELATION								
uncleaned - soft	0.023	**10.23**	-0.030	**-18.21**	-	-	-0.036	**-40.47**
uncleaned - aggressive	-0.013	**-6.09**	-0.059	**-38.76**	-	-	-0.044	**-49.72**
uncleaned - nets	-0.039	**-27.36**	-0.003	**-11.25**	0.020	**20.77**	-0.037	**-67.57**
uncleaned - soft+nets	0.027	**11.25**	-0.031	**-19.25**	-	-	-0.014	**-14.34**

93

uncleaned - agg+nets	0.005	**2.01**	-0.060	**-39.33**	-	-	-0.017	**-17.88**
soft - aggressive	-0.036	**-52.61**	-0.030	**-81.27**	-	-	-0.008	**-60.77**
soft - nets	-0.062	**-29.76**	0.027	**16.60**	-	-	0.000	-0.31
soft - soft+nets	0.004	**3.21**	-0.002	**-13.50**	-	-	0.023	**60.04**
soft - agg+nets	-0.019	**-15.38**	-0.031	**-80.85**	-	-	0.019	**47.34**
aggressive - nets	-0.026	**-13.15**	0.057	**37.23**	-	-	0.008	**9.55**
aggressive - soft+nets	0.040	**32.81**	0.028	**76.41**	-	-	0.031	**88.12**
aggressive - agg+nets	0.018	**16.91**	-0.001	**-10.14**	-	-	0.027	**76.82**
nets - soft+nets	0.066	**31.23**	-0.029	**-17.68**	-	-	0.023	**26.68**
nets - agg+nets	0.044	**21.80**	-0.058	**-37.87**	-	-	0.019	**22.56**
soft+nets - agg+nets	-0.022	**-42.02**	-0.029	**-83.65**	-	-	-0.003	**-47.17**
REGULARISED ICOV								
uncleaned - soft	0.021	**9.66**	-0.030	**-19.16**	0.091	**67.52**	-0.041	**-47.28**
uncleaned - aggressive	-0.013	**-6.31**	-0.058	**-38.61**	0.090	**65.61**	-0.043	**-49.15**
uncleaned - nets	-0.038	**-27.19**	-0.003	**-11.18**	0.023	**25.22**	-0.030	**-56.96**
uncleaned - soft+nets	0.027	**11.35**	-0.031	**-19.95**	0.235	**139.90**	-0.008	**-8.86**
uncleaned - agg+nets	0.005	**2.24**	-0.058	**-39.09**	0.235	**139.14**	-0.011	**-11.70**
soft - aggressive	-0.035	**-50.96**	-0.027	**-75.78**	-0.001	**-2.29**	-0.002	**-10.04**
soft - nets	-0.060	**-29.18**	0.028	**17.58**	-0.067	**-52.17**	0.011	**13.25**
soft - soft+nets	0.005	**4.63**	-0.001	**-10.27**	0.144	**120.39**	0.033	**87.71**
soft - agg+nets	-0.016	**-13.74**	-0.028	**-75.49**	0.145	**119.79**	0.030	**74.46**
aggressive - nets	-0.025	**-12.81**	0.055	**37.10**	-0.067	**-50.31**	0.012	**15.42**
aggressive - soft+nets	0.040	**33.41**	0.026	**72.28**	0.144	**125.29**	0.034	**103.02**
aggressive - agg+nets	0.018	**17.81**	-0.001	**-8.97**	0.145	**124.89**	0.032	**93.42**
nets - soft+nets	0.065	**31.33**	-0.029	**-18.39**	0.211	**130.57**	0.022	**26.17**
nets - agg+nets	0.043	**21.94**	-0.056	**-37.65**	0.212	**129.67**	0.019	**22.83**
soft+nets - agg+nets	-0.022	**-41.77**	-0.027	**-79.04**	0.001	**11.08**	-0.003	**-36.57**

Significant results (p<0.01) are highlighted in bold.

Table 4.4. Network Similarity across subjects. Comparison between sequences (paired t-test).

Similarity across subjects between-sequence comparison (paired t-test)	uncleaned	soft	aggressive	nets	soft+nets	aggressive+ nets
FULL CORRELATION						
standard d=30 - MB6 d=30 (mean delta r)	0.000	-0.002	-0.032	0.068	-0.007	-0.027
t-value	-0.04	-0.71	**-11.17**	**22.27**	**-2.19**	**-10.36**
standard d=100 - MB6 d=100 (mean delta r)	0.014	-0.033	-0.052	-0.047	-0.132	-0.135
t-value	**4.87**	**-12.30**	**-23.35**	**-28.39**	**-64.51**	**-70.14**
PARTIAL CORRELATION						
standard d=30 - MB6 d=30 (mean delta r)	-0.012	-0.065	-0.059	0.024	-0.071	-0.077
t-value	**-6.20**	**-31.41**	**-29.92**	**13.08**	**-33.86**	**-38.91**
standard d=100 - MB6 d=100 (mean delta r)	-0.030	-	-	-0.086	-	-
t-value	**-24.25**	-	-	**-71.48**	-	-

REGULARISED ICOV						
standard d=30 - MB6 d=30 (mean delta r)	-0.016	-0.068	-0.060	0.020	-0.074	-0.079
t-value	**-8.06**	**-33.21**	**-30.98**	**11.05**	**-36.24**	**-40.42**
standard d=100 - MB6 d=100 (mean delta r)	-0.033	-0.165	-0.166	-0.087	-0.276	-0.280
t-value	**-27.55**	**-138.87**	**-132.80**	**-72.97**	**-196.12**	**-196.38**

Significant results (p<0.01) are highlighted in bold.

Finally, as the cleaning procedure should enhance not only the consistency across subjects but also the discriminability regarding classifications of interest, we tested if it was possible to predict the subjects' age from the network matrices using multiple regression. We used the correlation values between pairs of nodes for each subjects as design matrix columns (features), pre-selecting the strongest features (the 25% of the total number of correlations with higher correlation values), and performed leave-one-out and permutation testing using FSLNets. As shown in Table 4.5, the predicted age was significantly correlated ($p_{corr}<0.05$) with the real age only with MB6 and soft clean-up on high dimensional (d=100) partial correlation and regularised ICOV matrices.

Table 4.5. Prediction of subjects' age with multiple regression.

Protocol	correlation matrix	p value					
		uncleaned	FIXsoft	FIXagg	Nets	FIXsoft+ Nets	FIXagg+ Nets
MB6 d=100	full	0.180	0.953	0.974	0.114	0.833	0.835
	partial	0.739	**0.048**	0.076	0.111	0.342	0.272
	ICOV 0.1	0.767	**0.046**	0.052	0.128	0.362	0.258
Standard d=100	full	0.091	0.163	0.295	0.108	0.398	0.616
	partial	0.928	-	-	0.115	-	-
	ICOV 0.1	0.936	0.259	0.075	0.097	0.273	0.300
MB6 d=30	full	0.252	0.301	0.709	0.144	0.484	0.774
	partial	0.543	0.215	0.368	0.415	0.305	0.423
	ICOV 0.1	0.520	0.286	0.419	0.408	0.322	0.483
Standard d=30	full	0.660	0.342	0.515	0.298	0.340	0.408
	partial	0.350	0.248	0.673	0.399	0.637	0.536
	ICOV 0.1	0.357	0.328	0.708	0.412	0.660	0.521

Significant results ($p_{corr}<0.05$) are highlighted in bold.

To summarise the main results from these tests: networks are more reproducible across subjects when using the MB acquisition. In this case, when carrying out more detailed network modelling (higher dimensionality) with partial correlation, both soft and aggressive clean-up gave good (and similar) results, while Nets clean-up was not useful. We emphasize here the importance of higher dimensional network modelling using partial correlation because we consider this to be the most interesting and useful general approach for network modelling (compared with the other analyses tested above).

4.3.7. Spatial maps analysis

The output of the second stage of dual regression (subject-level RSN spatial maps for the 53 test dataset subjects) was used for spatial map analyses. For mixed effect (ME) cross-subject analysis, group maps were obtained by performing a one-sample t-test on all subjects' spatial maps, for each component, calculating the corresponding z-statistic map and applying a mixture model correction to ensure comparable null distributions in different tests (Beckmann et al., 2004). For fixed effects (FE) analysis the single subject, z maps were mixture model corrected, averaged, and multiplied by the square root of $N_{subjects}$ to obtain valid z-statistics.

In Fig. 4.7 we show sample group maps derived from the Standard data, 30-dimensional group ICA, MB6 d=30, and MB6 d=100 using the corresponding training-dataset templates for dual regression (dual regression stage 2 could not be run at high dimensionality for the cleaned Standard data, because it did not have enough time points). The displayed components (sensory-motor and lateral visual networks, left and right panel respectively) are shown without, with soft, and with aggressive clean-up. The effects of the clean-up are quite strong in these components and the cortical signal is more focal in the cleaned data. At low dimensionality, these RSNs show similar spatial patterns in Standard and MB6 data, but the signal is stronger with MB6 (especially in the right sensory-motor network). With high dimensionality group ICA decomposition, these RSNs are split into multiple components, allowing a more detailed analysis of network connectivity.
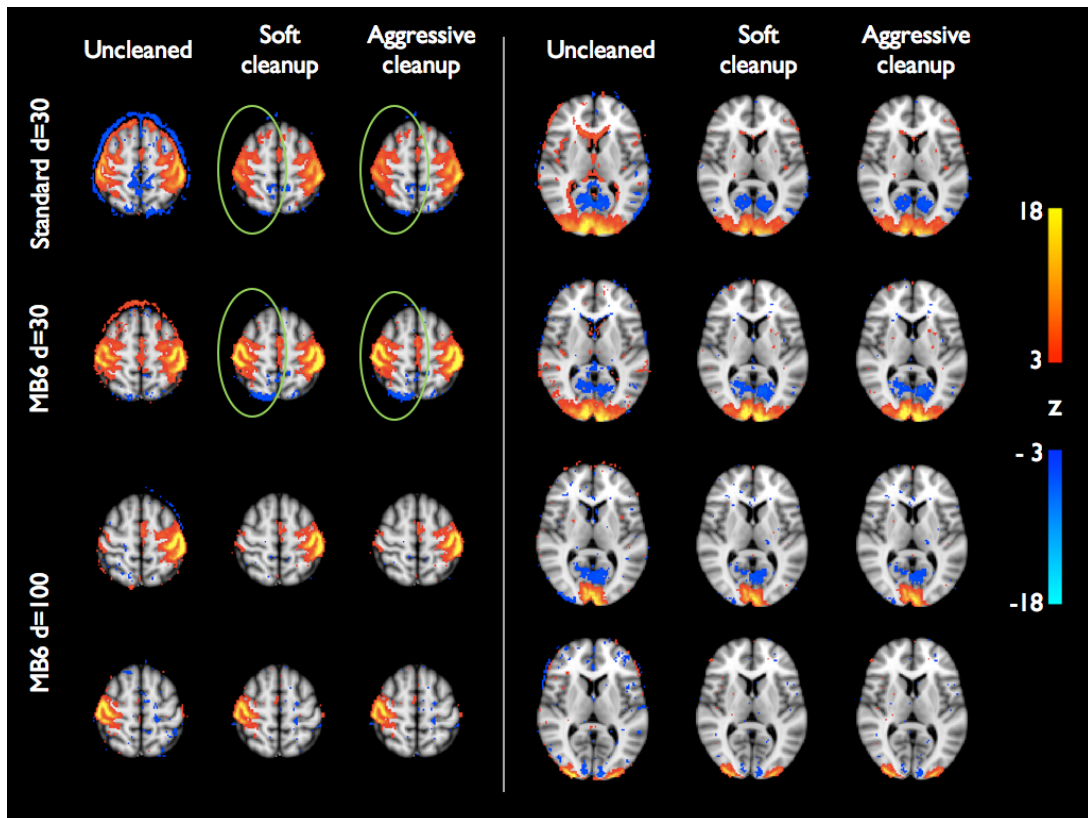
Fig. 4.7. Group-level z-statistic maps of two RSNs (sensory-motor network, left panel, and visual network, right panel), derived from Standard (d=30) and MB6 (d=30 and d=100) datasets using the corresponding training data templates, without and with soft or aggressive FIX clean-up. Individual subjects' z-statistic maps were mixture model corrected and combined using fixed-effects averaging. Group maps are thresholded at abs(z)>3 (red-yellow colour coding for positive z values, blue-light blue for negative ones). The effect of the cleaning is quite strong in terms of noise removal and more focal signal (as highlighted with the ring around the right sensory-motor network). With high dimensionality the RSNs are split into multiple components, allowing a more detailed analysis of network connectivity.

Under the hypothesis that similarity between a group map and the corresponding template map reflects the ability of the clean-up (or acquisition method) to improve correct identification of the true signal, we calculated the spatial correlation between the group maps (ME and FE) and the templates, as a quantitative measure to describe the ability of the cleaning approach and/or the acquisition to correctly detect RSNs. We then compared the correlation values across cleanings with two-tailed paired t-tests and across sequences with two-tailed unpaired t-tests.

The results reported in Figure 4.8 and Tables 4.5 and 4.6 show that cleaning significantly increases the similarity between the group maps and the template. Soft and aggressive clean-up are quite similar to each other with a difference in mean correlation as low as 0.01, though statistically significant. When comparing the two acquisition methods on uncleaned data, the correlation values obtained with Standard data are higher than MB6. This is mainly due to the lower spatial resolution (and higher SNR) of the standard sequence; Feinberg et al (2010) already demonstrated that EPI acceleration, while keeping spatial resolution fixed, *increases* the z-statistics of the RSN spatial maps. After cleaning, the difference between MB6 and standard sequence ME maps at d=30 is no

longer statistically significant, demonstrating the additional benefit of the combination of acceleration and cleaning, besides the feasibility of high dimensionality ICA analyses.
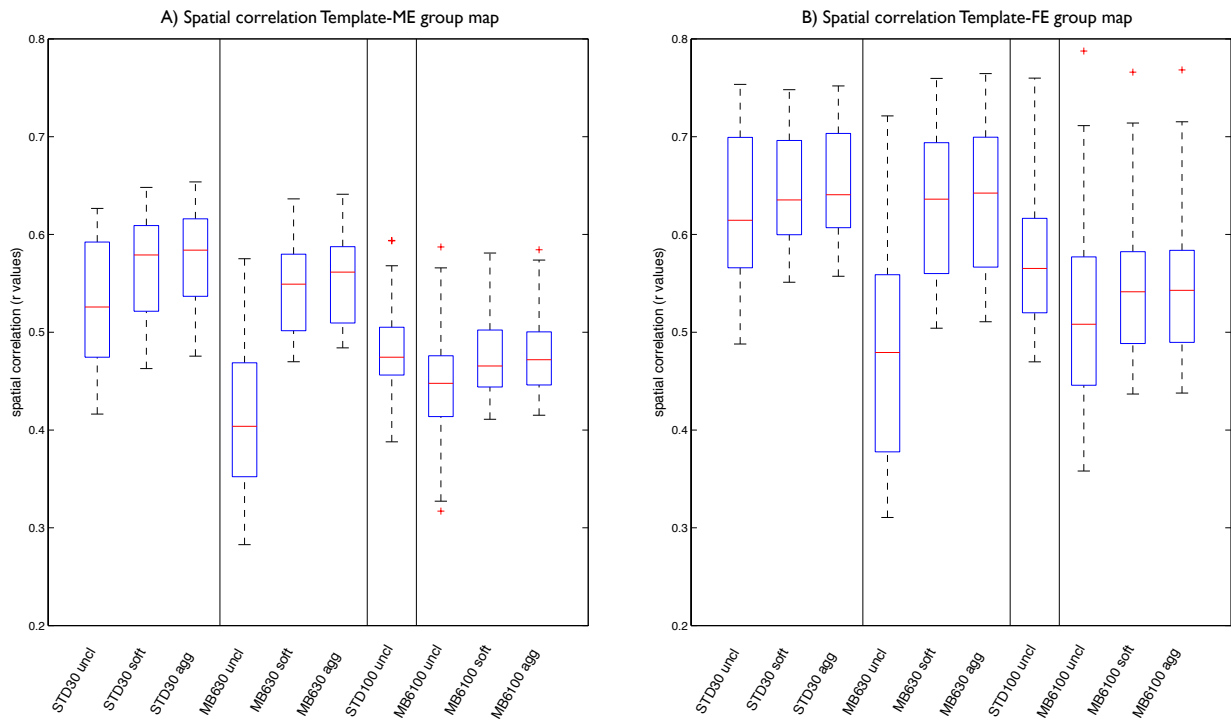
Fig. 4.8. Spatial correlations. The boxplots show the distributions across components of the correlation coefficients between the group maps (obtained with ME and FE statistics) and the corresponding templates, for different cleaning approaches and for different acquisition protocols. STD=Standard sequence; uncl=uncleaned; soft=FIX soft cleaning; agg=FIX aggressive cleaning.

Table 4.5. Spatial correlation between template and group maps. Comparison among cleaning approaches (paired t-test).

Spatial correlation between template and group maps. Comparison across cleanings.	Standard d=30		MB6 d=30		MB6 d=100	
	mean delta r	t-value	mean delta r	t-value	mean delta r	t-value
MIXED EFFECTS GROUP MAP						
Uncleaned-soft	-0.042	**-5.98**	-0.130	**-13.72**	-0.027	**-8.47**
Uncleaned - aggressive	-0.051	**-7.09**	-0.139	**-14.48**	-0.030	**-9.86**
Soft - Aggressive	-0.009	**-10.39**	-0.009	**-10.36**	-0.004	**-9.06**
FIXED EFFECTS GROUP MAP						
Uncleaned-soft	-0.022	**-3.30**	-0.149	**-13.24**	-0.028	**-7.83**
Uncleaned - aggressive	-0.028	**-4.19**	-0.156	**-13.72**	-0.029	**-8.22**
Soft - Aggressive	-0.006	**-20.62**	-0.007	**-28.49**	-0.001	**-35.68**

Significant results (p<0.01) are highlighted in bold.

Table 4.6. Spatial correlation between template and group maps. Comparison between sequences (unpaired t-test).

Spatial correlation between template and group maps. Comparison between sequences.	uncleaned	soft	aggressive
MIXED EFFECTS GROUP MAP			
mean(r standard d=30) - mean(r MB6 d=30)	0.1106	0.0224	0.023
t-value	**4.88**	1.46	1.59
mean(r standard d=100) - mean(r MB6 d=100)	0.039		
t-value	**3.72**	_	_
FIXED EFFECTS GROUP MAP			
mean(r standard d=30) - mean(r MB6 d=30)	0.143	0.015	0.014
t-value	**4.70**	0.74	0.70
mean(r standard d=100) - mean(r MB6 d=100)	0.053		
t-value	**3.30**	_	_

Significant results (p<0.01) are highlighted in bold.

4.4. Discussion

FMRIB's ICA-based Xnoisefier (FIX) is a fully automatic solution (once trained) for cleaning fMRI data of various types of noise. The cleaning procedure with FIX consists of four major operations: spatial ICA, classifier training, component classification (noise detection), and denoising. The first three steps are extensively described in Salimi-Khorshidi et al., (2014) and summarised in chapter 3, demonstrating FIX's ability to classify the independent components into signal or noise with high accuracy. Here we investigated the final stage of the cleaning procedure by carrying out detailed spatial and temporal analysis in order to successfully remove the noise components while preserving as much signal as possible.

In this study we evaluated the efficacy of FIX's automatic denoising step, testing two different *first-level* (single subject) cleaning approaches (*aggressive* and *soft*) for removing the artefactual components from the fMRI time series data, previously identified in the classification step. We compared their effect on both temporal and spatial RS-fMRI analyses: RSNs time series (amplitude and power spectra), network matrices (full correlation, partial correlation and L1-norm regularised partial correlation) and spatial maps. In this way we were able to investigate the trade-off between artefact removal and the partial loss of significant signal. All these evaluations were performed on two datasets from the same set of 76 subjects: a Standard EPI acquisition and a MB EPI acquisition (MB6) (Moeller et al. 2010, Feinberg et al., 2010) developed partly for the Human Connectome Project.

Our results showed the efficacy of artefact removal, which proved to be important for reliable temporal and spatial RS-fMRI analyses. If an artefact is not cleaned at the single subject level and its spatial pattern is partially overlapped to one of the RSNs, it will in general influence the single-

subject RSNs time series, i.e. the output of the first stage of dual regression. Consequently, the non-cleaned time series will have higher amplitude with respect to the cleaned data, often with high frequency confounds visible in the power spectra. The presence of shared noise, in general, will also produce less consistent network matrices across subjects. During the second step of dual regression, the noise contained in the time series corrupts the RSN maps. This leads to noisy subject-level z-maps, and affects any following group-level analyses, reducing the ability to detect specific activation patterns within the RSNs (resulting here in lower spatial correlation with the training data templates). Most likely, this problem does not only affect the group-ICA analyses followed by dual-regression addressed in this work, but would also affect other methods as "back-projection" ICA and seed-based resting-state correlation maps, for similar reasons.

Concerning the comparison of the two cleaning approaches (*soft* vs *aggressive*), we obtained similar results for spatial correlation measures within spatial maps. Also the network analysis results were generally comparable, especially at high dimensionality. However, by way of mean amplitudes and power spectra analyses we observed that the reduction in the mean standard deviation (time series amplitude) after soft cleaning was caused by a more selective removal of the noise related high frequency power, which increases the contrast-to-noise ratio. With aggressive cleaning, the significant reduction in mean amplitude, strongly affects the low frequency peak, causing a significant signal loss. For this reason we would in general suggest the use of the soft cleaning approach, which consists of: 1) removing the full space of the 24 motion parameters (Satterthwaite et al., 2013) from the data and the ICA time series; 2) estimating the contribution (spatial regression coefficients) of both good and bad components, in order to identify the unique variance of the artefacts; 3) subtracting the contribution of the bad components from the data (i.e., the sum of the outer product of each noise time series by its spatial regression coefficient). In this way a good balance between noise removal and signal loss was achieved. The overall level of artefact removal is significant, as shown in Figs 4.3-4.5.

We also tested the effect of *Nets clean-up*, a cleaning option for time series and network analyses, applied within-subject to the output of dual-regression stage 1, which yields a time series for each group-ICA component. Instead of simply discarding noise components, Nets performs a regression of each signal time series against all noise time series and uses the residual as cleaned signal. However, despite the improvement observed on amplitude and network similarity results, this approach proved to be quite aggressive and to significantly decrease the signal, as the amplitude reduction after Nets clean-up was localized both at low and high frequencies, not selectively at high frequency as FIX-based clean-up does, as demonstrated with the power spectra analysis. Moreover, if FIX clean-up was not performed prior to group ICA, the latter would have been less powerful,

making the Nets clean-up to be performed next even less effective than seen in this study. For these reasons the use of Nets clean-up is probably not advisable, especially when a large number of noise components are identified in the group-ICA.

A detailed analysis of the effects of global signal regression was beyond the scope of this work, as resting-state research is increasingly focusing on network matrices estimated with methods related to partial correlation, and spatial maps derived from multiple temporal regression. Indeed, standard partial correlation analyses cannot be carried out after global signal regression, as the correlation matrix is no longer full rank and it is not possible to invert it. Similarly, the generation of RSN spatial maps via dual regression (i.e., against RSN time series) is a multiple regression, so global signal regression is largely irrelevant. However, we believe it was an interesting result that global signal removal has almost no effect on power spectra because it equally affects both LF and HF, resulting in a non-specific amplitude loss, and on its own provides a poor level of clean-up.

The results discussed so far (the relative merits of different clean-up options) were similar for both the Standard and MB6 data, demonstrating the efficacy of the cleaning procedure on two quite different EPI acquisitions. The only cleaning-approach-specific adjustment to the two datasets was the training dataset used for the FIX classification, which was tailored to each pulse sequence type. The use of a good (i.e., sequence-specific) training dataset is important because it allows FIX to optimize the classification training for the kind of data from a specific study.

Once successfully cleaned, the second aim of this work was to directly compare the data from the Standard and MB6 sequences using the same sets of analysis. As MB-EPI has proven to be powerful for obtaining sub-second (or close) whole brain images, reducing the acquisition time and/or increasing spatial resolution (Moeller et al., 2010; Feinberg et al., 2010), we wanted to further investigate the potential of this sequence for identifying the activation patterns of RSNs and detecting their functional connectivity.

The results suggest MB-EPI as advantageous for RS-fMRI analysis for several reasons. First, the increased temporal and spatial resolution yielded a better FIX classification accuracy (98% for MB6 versus 95% for Standard, with leave-one-out testing). We obtained, on average, 8.6 good single-subject independent components for the Standard sequence and 15.2 for MB6. Thus, per subject, on average, 0.43 good components are misclassified as bad in Standard data, compared to 0.3 only in MB6 (i.e., one subject out of three has a single good component misclassified, and the other two subjects have none). Second, a considerably higher proportion of non-artefactual group-ICA components was identified in the MB6 dataset, thus suggesting more successful ICA-based clean-up of MB data (even when driven by hand-labelling of the ICA components). Third, the MB data allowed a more detailed time series and network analyses through higher dimensionality

decomposition (d=100), which was not achievable with the Standard sequence because of its lower temporal degrees of freedom. Fourth, despite comparable mean amplitudes of the time series, the spectra after cleaning showed considerably less structured artefacts (i.e., deviation from the expected clean 1/f-like spectrum). Fifth, networks were more reproducible across subjects with MB6. Finally, the results of spatial map analyses (spatial correlation) were similar between the two sequences, notwithstanding much higher static image SNR in the lower-resolution Standard data. Arguably, a limitation of this study is the lack of a direct comparison between the two sequences at the same resolution, to test the pure effect of acceleration. However, this has already been evaluated by Feinberg et al (2010), showing significant statistical advantages of EPI acceleration (with a up to 60% increase in z statistics), with all acquisitions held at 3x3x3mm. Hence, in our study, given what is already known from the Feinberg results, we wanted to make a targeted comparison addressing a large number of combinations of various clean-up approaches with the two acquisition types.

Our results have been already effective for analysis developments in the Human Connectome Project: RS-fMRI are acquired with the same spatial resolution as in our MB6 data, and with even greater temporal resolution (MB8, 2x2x2mm, 0.72s; Smith et al., 2013); FIX is now in use as part of the default HCP analysis pipeline, and FIX-cleaned data is the recommended version of the resting-state fMRI data that is publicly available – already over 200 subjects' worth of hour-long datasets having been released to date.

In this work we used a dataset of healthy (albeit older) controls in order to evaluate the effect of cleaning and acquisition protocols on the identification of RSNs; we also demonstrated that the combination of the accelerated acquisition and the optimized cleaning (FIX soft) enhance not only the consistency across subjects but also the discriminability with respect to a variable of interest (subjects' age). An interesting future development could be the study of the impact of the cleaning procedure in enhancing the between-group discriminability regarding other classifications of interest (controls vs patients, or correlation with behavioural or cognitive indices etc.) (Tian et al., 2013). We will describe an application to Alzheimer's disease in Chapter 5.

4.5. Conclusion

In conclusion, we have demonstrated that, by combining an accurate ICA component classifier with an effective approach for noise removal, we were able to remove artefacts automatically and with confidence and that we were not removing significant amounts of non-artefactual signal. Moreover, with MB sequences and effective cleaning, we can perform higher dimensionality decompositions and more detailed RSN analyses than with a standard EPI acquisition.

Chapter 5 - The impact of data-driven cleaning procedures for resting state fMRI on the detection of DMN functional connectivity alterations in Alzheimer's disease

In this chapter, the ICA-based cleaning method (FIX), developed and tested in Chapters 3 and 4, is applied in a pathological condition (i.e. Alzheimer's disease) and compared to other two commonly used data-driven cleaning procedures. The different denoising approaches are compared in terms of within-group consistency across subjects and of ability to detect the functional connectivity alteration of the default mode network typically observed in patients with Alzheimer's disease.

The preliminary results are presented in an abstract (Griffanti et al.,) accepted as PowerPoster at ISMRM 2014 and a full paper is in preparation.

5.1. Introduction

The cleaning of RS-fMRI data from artefacts is an essential step for a better identification of the resting state networks (RSNs) (see Chapter 3.1 and 4). Studies evaluating the efficacy of cleaning procedures for fMRI data are usually performed on one group of healthy controls (Marx et al., 2013; Bright and Murphy 2013; Tohka et al., 2008; Weissenbacher et al., 2009) or on two groups of healthy subjects differing for the amount of a specific artefact, typically head motion (Van Dijk et al., 2012; Satterthwaite et al., 2013). The performance of the clean-up is generally tested in terms of increased within-group consistency of activations and functional connectivity (FC) maps, reduction of correlation with noise, and decrease of between-group differences. However, it is more difficult to evaluate the success of cleaning when multiple sources of artefacts (not only motion) are removed. Moreover, it is important for a cleaning procedure that only the inter-subject variability due to the artefacts is removed, preserving valuable individual differences. In fact, the ability to capture between subjects variability in FC is very important in clinical applications, in order to discriminate different pathologies and monitor their evolution and staging.

In Alzheimer's disease (AD) a decreased FC is mainly observed in the posterior cingulate cortex (PCC) within the default mode network (DMN), and this is becoming a possible new biomarker for this pathology (see chapter 1.4; Greicius 2004; Li et al., 2011; Gili et al., 2011). In this framework, an effective preprocessing of RS-fMRI data is crucial, allowing the correct identification of this FC alteration.

The aim of this study was to compare four data-driven cleaning procedures (i.e. without the need of external recordings of physiological signals) on data relative to elderly healthy subjects and AD patients in a mild to moderate stage of the disease, and to evaluate the impact of the cleaning step on the ability to detect the typical DMN functional connectivity alterations in AD. In particular, the first two cleaning approaches are commonly used in the preprocessing of RS-fMRI data: the regression of motion parameters (Satterthwaite et al., 2013) and the regression of motion parameters, mean white matter (WM) signal and mean cerebrospinal fluid (CSF) signal (Satterthwaite et al., 2013; Fox et al., 2005), while the other two are the *soft* and *aggressive* options of the previously described FMRIB's ICA-based Xnoiseifier (FIX) (see Chapter 3 and 4), based on single-subject ICA decomposition followed by automatic classification and removal of the motion parameters and the full (in aggressive option) or unique (in soft option) variance of the noise components.

The denoising procedures were firstly compared, separately for the HC and AD groups, in terms of temporal SNR and BOLD signal fluctuation reductions with respect to the uncleaned data. With the datasets obtained with the different cleaning options, we then performed a FC analysis of the DMN with two methods: seed-based correlation and template-based dual regression (Khalili-Mahani et al., 2012; 2013). Finally, we compared the FC results in terms of within-group consistency across subjects and pattern of between-group differences, hypothesizing that a more effective cleaning approach would lead to more consistent FC results and would allow a better identification of the well-known pattern of DMN FC alterations in AD patients.

5.2. Materials and methods

5.2.1. Subjects and MRI data acquisition

Data from 41 subjects (20 healthy controls, HC and 21 AD patients) were acquired at Don Gnocchi Foundation, IRCCS Santa Maria Nascente, in Milan, and their characteristics are reported in Table 5.1. AD patients were recruited from the Memory Clinic of Don Gnocchi Foundation, with a diagnosis of probable AD dementia according to the revised NINCDS-ADRDA criteria (Mc Khann et al., 2011) in a mild to moderate stage (Clinical Dementia Rateing Scale, CDR≤2). The twenty age-matched HC (Mini-Mental State Examination, MMSE ≥ 26) had no history of

neurological, cardiovascular or metabolic disorders and voluntarily participated in the study. All subjects and/or their caregivers provided written informed consent to participate in the study according to the recommendations of the declaration of Helsinki for investigations on human subjects.

Table 5.1. Subjects' characteristics

	Healthy Controls (HC)	AD patients	Group comparison (p-value)[#]
N	20	21	
Age (years)	71.05 ± 3.66	73.62±5.22	p=0.08
Gender (F:M)	13:7	13:8	p=0.21
MMSE	29.55±0.69	21.62±2.71	p<0.01
motion during fMRI acquisistion (*)	0.07±0.04	0.09±0.06	p=0.27

MMSE=Mini Mental State Examination; (*) mean relative displacement in mm as calculated during the preprocessing with MELODIC FSL tool. [#] calculated with two-sample independent t-test or Fisher's exact test, as appropriate.

MRI acquisitions were performed using a 1.5T Siemens Magnetom Avanto (Erlangen, Germany) scanner with 8-channel head coil. Resting state fMRI (RS-fMRI), BOLD EPI images (TR/TE = 2500/30 ms; resolution = 3.1 x 3.1 x 2.5 mm^3; matrix size = 64 x 64; number of axial slices = 39; number of volumes = 160; acquisition time 6 min and 40 s) were collected at rest. Subjects were instructed to keep their eyes closed, not to think about anything in particular, and not to fall asleep. T1-weighted 3D scans were also acquired (TR/TE = 1900/3.37 ms; resolution = 1 x 1 x 1 mm^3; matrix size= 192 x 256; number of axial slices = 176) and used as anatomical references for fMRI analysis and for voxel-based morphometry (VBM) analysis.

5.2.2. Voxel-based morphometry (VBM) analysis

In order to verify the typical pattern of atrophy in AD patients, we evaluated grey matter (GM) volume differences between HC and AD. Structural data were analysed with FSL-VBM (Douaud et al., 2007), an optimised VBM protocol (Good et al., 2001) carried out with FSL. First, structural images were brain-extracted and grey matter-segmented before being registered to the MNI 152 standard space using non-linear registration (Andersson et al., 2007a). The resulting images were averaged and flipped along the x-axis to create a left-right symmetric, study-specific grey matter template. Second, all native grey matter images were non-linearly registered to this study-specific template and "modulated" to correct for local expansion (or contraction) due to the non-linear component of the spatial transformation. The modulated grey matter images were then smoothed

with an isotropic Gaussian kernel with a sigma of 3 mm. Finally, voxel-wise GLM was applied using permutation-based non-parametric testing, correcting for multiple comparisons across space.

5.2.3. RS-fMRI data preprocessing and cleaning approaches

The individual common preprocessing steps for the analysis of RS-fMRI data were carried out using FSL (Smith et al., 2004; Jenkinson et al., 2012). Firstly, images were motion corrected with MCFLIRT (Jenkinson et al., 2002); from this operation the six rigid-body parameter time series were extracted for each subject (to be used for subsequent cleaning) and the mean relative displacement was calculated to ensure that the two groups were matched in terms of average amount of head motion (see Table 5.1). Non-brain tissues were removed with brain extraction tool (BET) (Smith, 2002), data were spatially smoothed with a 5 mm full width at half maximum (FWHM) Gaussian kernel, and high-pass temporal filtering was applied with a cut-off frequency of 0.01 Hz to remove slow drifts.

Five datasets were obtained with the following data-driven cleaning approaches:

1) Uncleaned data: only common preprocessing;

2) MOTreg (Satterthwaite et al., 2013): a regression of 24 motion parameters. (the six rigid-body parameter time series, their backward-looking temporal derivatives, and the squares of all twelve resulting regressors);

3) MWCreg (Satterthwaite et al., 2013; Fox et al., 2005): regression of 24 motion parameters, WM mean signal and CSF mean signal. (The WM and CSF mean signal was extracted as the mean time series from each 4D pre-processed dataset within a ventricular region of interest and a region centered in the white matter identified in the MNI space and registered to each subject's individual space);

4) FIXsoft (see section 4.2.4): single-subject spatial ICA with MELODIC (Beckmann and Smith, 2004) with automatic dimensionality estimation followed by ICA-based automatic denoising using FMRIB's ICA-based Xnoiseifier (FIX) removing the full variance of the 24 motion parameters, but only the unique variance of the noisy components (*soft clean-up*);

5) FIXagg (see section 4.2.4): single-subject spatial ICA with MELODIC (Beckmann and Smith, 2004) with automatic dimensionality estimation followed by ICA-based automatic denoising using FIX removing the full variance of both the 24 motion parameters and of the noisy components (*aggressive clean-up*).

The training dataset used to clean the data was the same for both groups and it was built with data from healthy controls (dataset 3 described in chapter 3). Due to the modest number of subjects, we were able to manually check the classification results on AD patients and we found a good accuracy.

5.2.4. Measures of BOLD signal variation

To test how the different cleaning approaches affect the BOLD signal variation in the two groups, we calculated the following measures: 1) a global measure of signal to noise ratio (raw temporal-SNR) and 2) a voxel-wise measure (%ΔSTD map) to examine the regional impact of each correction method on the BOLD signal (Khalili-Mahani et al., 2013).

1) For each dataset, a raw temporal-SNR image was formed dividing the mean image across time by the standard deviation image over time (STDimg). The temporal-SNR image was then eroded to exclude brain-edge effects, and the median SNR value was calculated and compared between the two groups at each cleaning step and within groups among different clean-ups.

2) The %ΔSTD map was defined by Khalili-Mahani et al., (2013) as the percentage of the voxel-wise temporal fluctuation amplitude (STDimg) of the uncleaned data that is suppressed by the cleaning. This map was calculated for each subject as the difference between the STDimg of the cleaned datasets and the STDimg of the uncleaned data, with respect to the STDimg of the uncleaned data (Eq. 5.1):

$$\%\Delta STD_{map} = \frac{STD(img_{uncl} - img_{clean})}{STD(img_{uncl})} \cdot 100 \ \% \tag{5.1}$$

The %ΔSTD map of all subjects were then registered to the individual's structural scan using Brain-Boundary Registration (BBR - Greve and Fischl, 2009) and to the 2 mm MNI152 standard space using non linear registration (FNIRT - Andersson et al., 2007a,b), and used to build, for each group, a probability map of areas where %ΔSTD>25% across subjects.

5.2.5. Functional connectivity analyses

After the cleaning procedures each single subject 4D pre-processed dataset was coregistered to the individual's structural scan using BBR and to standard space using FNIRT, and resampled to $2 \times 2 \times 2$ mm^3 resolution in the MNI152 space. We then computed DMN functional connectivity analyses with two methods.

<u>Seed-based correlation</u>: a region of interest (ROI) in the PCC was selected in the MNI152 template (6-mm radius sphere, centred in x=0; y=-26; z=52) according to previous studies (Van Dijk et al., 2010; Andrews-Hanna et al., 2007), and the corresponding mean time series was extracted from each 4D pre-processed dataset. Seed-based voxel-wise FC maps were then obtained by computing the linear correlation between the PCC-time series and the time series of all acquired voxels (REST toolbox; Song et al., 2011). Correlation maps were then converted to z-maps using Fisher's r-to-z transformation before entering the statistical analysis.

Template-based dual regression (Khalili-Mahani et al., 2012,2013): in order to be able to compare the five datasets, functional connectivity was defined in terms of fitting the BOLD fluctuations at each voxel with respect to the dominant fluctuation within ten major RSNs (Smith et al., 2009), which are frequently detected in resting-state functional connectivity analyses. Therefore, the ten-RSNs template was used in the first stage of dual regression (Filippini et al., 2009) as set of spatial regressors to generate individual temporal dynamics and spatial maps of the RSNs of the five datasets. The component corresponding to the DMN of each subject entered the statistical analysis.

5.2.6. Statistical analysis

In absence of a ground-truth of the neural signal, the cleaning of the data should both enhance reproducibility (stability of the functional connectivity measures across subjects) and also discriminability regarding classifications of interest (in this case healthy subjects versus AD patients). For this reason we tested, for each cleaning procedure, both within-group consistency across subjects of the FC measures and between group differences.

The within-group consistency of the DMN connectivity for each voxel was measured as the standard deviation of the z-maps (obtained with seed-based correlation or template-based ICA) across subjects, separately for HC and AD groups. The standard deviation maps (unwrapped into long vectors for the purpose of comparing them against each other) were then compared voxel-by-voxel within the brain with a paired t-test, both across cleanings and between groups.

The comparison between the two groups for the different cleaning approaches was performed on the z-maps obtained with the two methods through voxel-wise statistics using non-parametric permutation test ("randomise"). Normalised grey matter volume was included as a covariate to control for the effect of atrophy. Results were considered significant at $p < 0.05$. Full multiple comparison correction was applied after initial cluster-forming threshold of $p_{uncorr} < 0.05$, within a mean mask created by averaging the grey matter segmentations obtained from each subject's T1-weighted images with FSL-FAST (Zhang et al., 2001)

5.3. Results

5.3.1. VBM results

Figure 5.1 shows the results of the VBM analysis on structural MRI data. Patients with AD were significantly more atrophic than controls in the medial temporal lobe structures (bilateral hippocampus and parahippocampus), and in several other brain regions including medial, anterior and postero-inferior regions of temporal lobes bilaterally, precuneus/posterior cingulate, thalamus,

basal ganglia (putamen and caudate nuclei), and frontal lobes. These results are consistent with the well-known pattern of grey matter atrophy typical of AD, as described in several previous publications (Busatto et al., 2008; Zamboni et al., 2013).
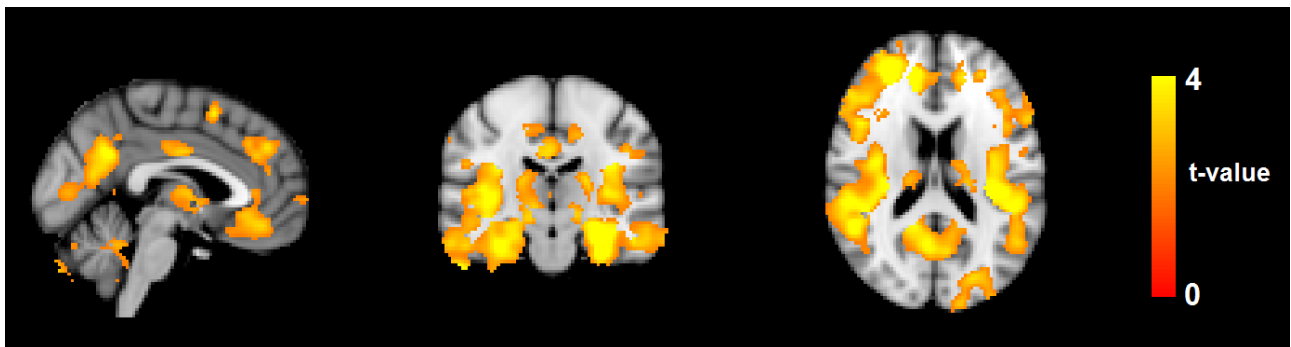

Fig. 5.1. VBM results from group comparison. Results are shown using a significance threshold of p<0.005 fully-corrected for multiple comparisons using threshold free cluster enhancement. Images are shown in radiological convention.

5.3.2. Effect of cleaning on BOLD signal variation

The temporal SNR values for the two groups with different cleaning options are reported in Figure 5.2 and the results of the comparisons across cleanings are shown in Table 5.2. Within-group analyses revealed that SNR was significantly higher after cleaning (uncleaned < motion reg < MWCreg < FIX soft < FIX aggressive; p<0.01 at paired t-test). The temporal SNR was not statistically different between the two groups, except for aggressive FIX clean-up (AD>HC, p=0.044; independent two sample t-test).
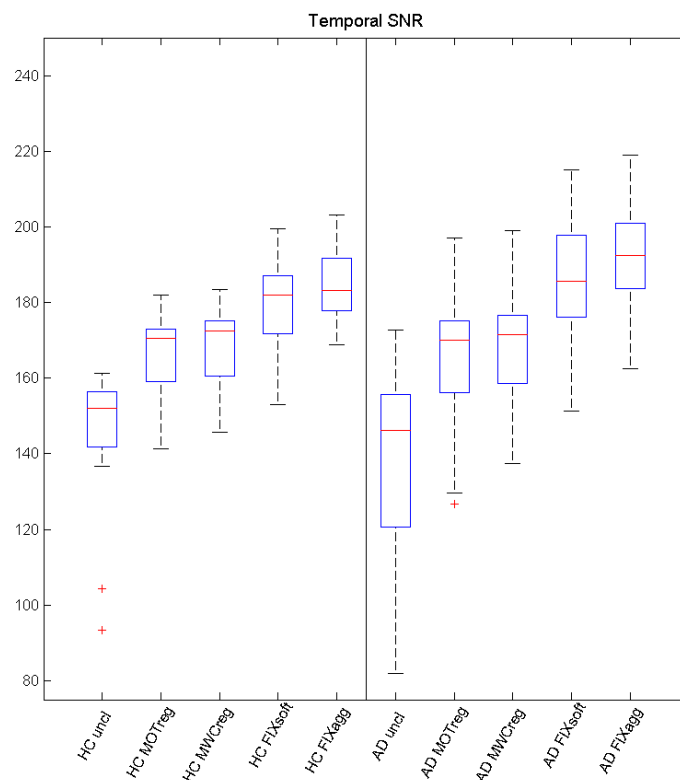

Fig. 5.2. Temporal SNR estimation for various cleaning procedures in the two groups.

Table 5.2. Temporal SNR. Comparisons among different cleaning approaches (paired t-test)

	HC (t-values)	AD (t-values)
Uncleaned-MOTreg	-9.80	-10.55
Uncleaned-MWCreg	-9.51	-10.30
Uncleaned-FIXsoft	-12.86	-10.27
Uncleaned-FIXagg	-10.00	-9.66
MOTreg-MWCreg	-7.21	-5.48
MOTreg-FIXsoft	-11.38	-7.86
MOTreg-FIXagg	-9.26	-8.30
MWCreg-FIXsoft	-10.14	-7.94
MWCreg-FIXagg	-9.38	-8.45
FIXsoft-FIXagg	-3.62	-3.31

All comparisons were statistically significant (p<0.01).

Figure 5.3 shows the probability maps of the spatial distribution of BOLD fluctuation reduction (%ΔSTD>25%) across subjects in the two groups. After regressing out the contribution of motion parameters, the highest reduction of BOLD fluctuation was localised at brain boundaries, while the inclusion of WM and CSF regressors led to a small further decrease also in correspondence of the ventricles and the WM, especially in the AD group. After FIX clean-up (both soft and aggressive), the highest reduction of BOLD fluctuation with respect to uncleaned data was more pronounced at brain boundaries and within ventricles, but also involved the lateral sulcus and areas in correspondence of blood vessels, mainly the sagittal sinus and straight sinus veins, the posterior cerebral artery and the middle cerebral branches. These effects were always higher in AD patients than HC.
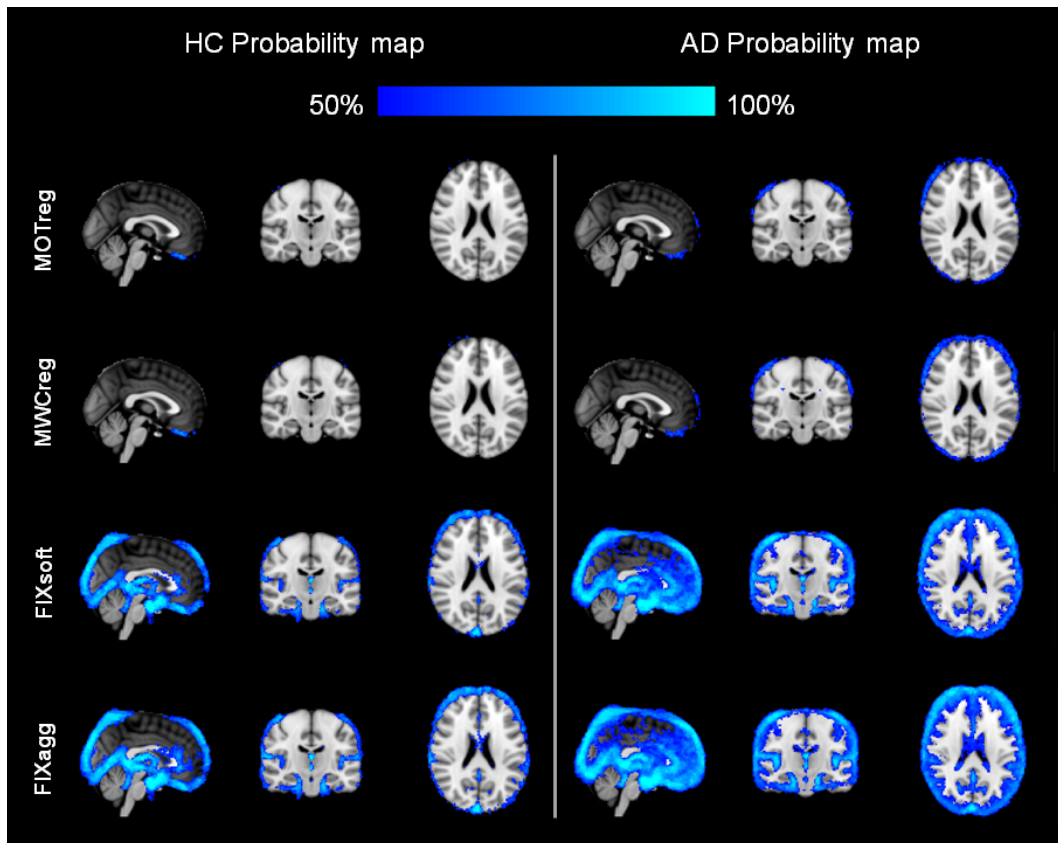
Fig. 5.3. Spatial pattern of changes in BOLD signal standard deviation: probability map of areas where %ΔSTD>25% across all HC (left) or AD patients (right). Images are shown in radiological convention.

5.3.3. Within-group consistency results

The within-group consistency map (standard deviation across subjects of the z-maps obtained with seed-based correlation or template-based dual regression) for the two groups with different cleaning approaches is shown in figures 5.4 and 5.5 (the relative mean maps across subjects are also reported). The standard deviation z-values across space are showed in the boxplots in Figure 5.6 and the results of the statistical comparisons across cleanings are reported in Table 5.3. In both groups the consistency increased significantly after cleaning (lower standard deviation) and the lowest standard deviation values were obtained after MWCreg and FIXagg. The standard deviation was, in general, lower (i.e. higher consistency) within the HC group ($p<0.01$ at paired t-test) with respect to the AD group (except for seed based FC on FIXagg data and template-based dual regression MWCreg data, where the standard deviation was higher in HC than AD). Comparing the results across the FC analysis methods, the seed-based FC results showed a lower variability across subjects with respect to template-based dual regression, but also the mean z-statistics of the FC maps were much lower.
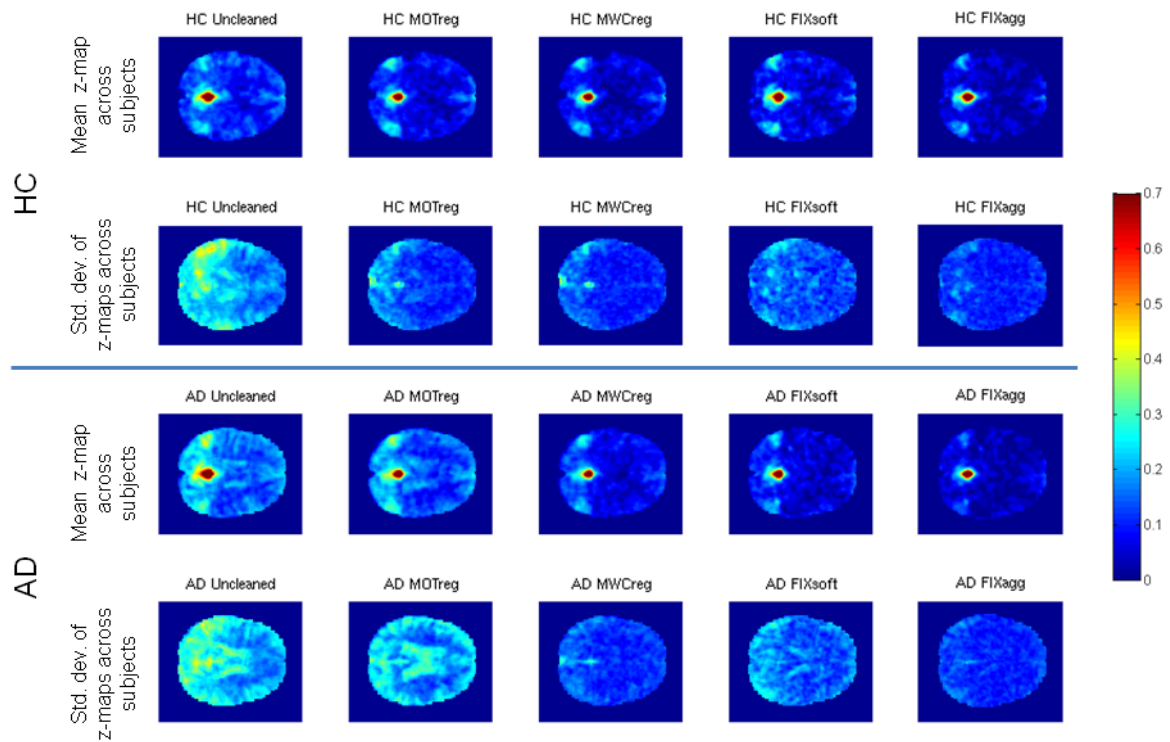
Fig. 5.4. Within-group consistency of PCC seed-based FC. A representative slice o the mean z-map (first and third row) and the standard deviation of z-maps (second and fourth row) across subjects is reported for HC (first and second row) and AD group (third and fourth row) after the different cleaning procedures.

Fig. 5.5. Within-group consistency of the DMN component obtained with Template-based dual regression. A representative slice o the mean z-map (first and third row) and the standard deviation of z-maps (second and fourth row) across subjects is reported for HC (first and second row) and AD group (third and fourth row) after the different cleaning procedures.
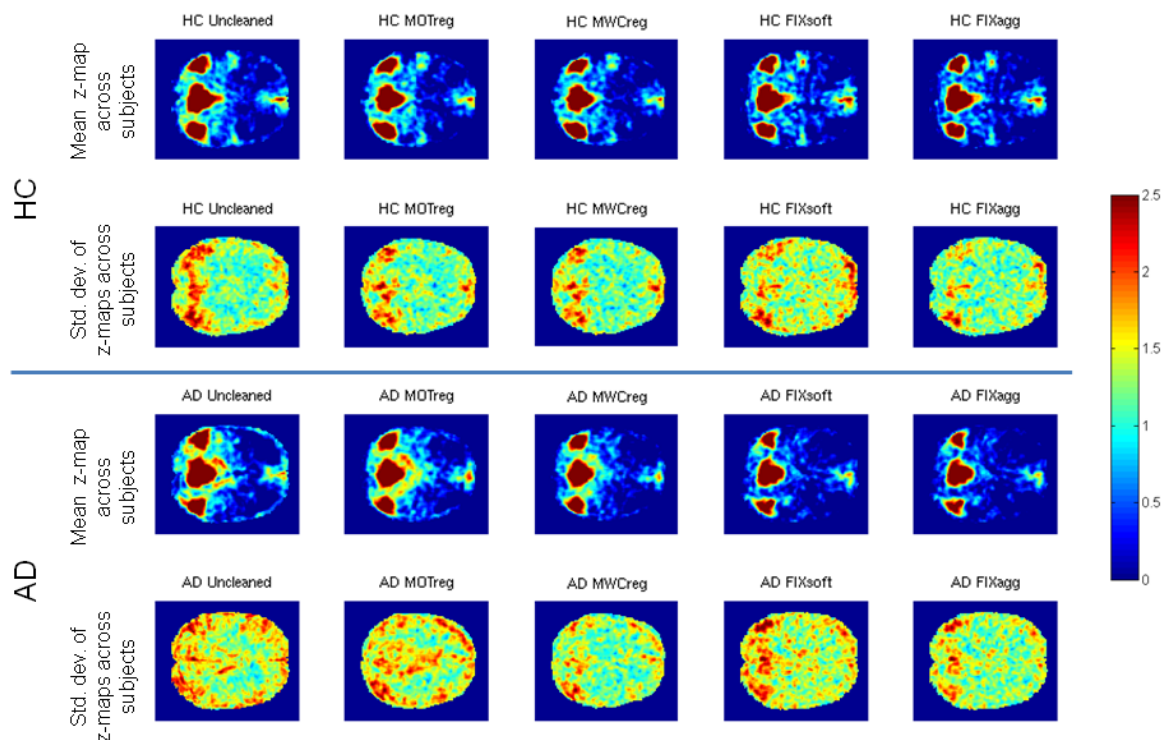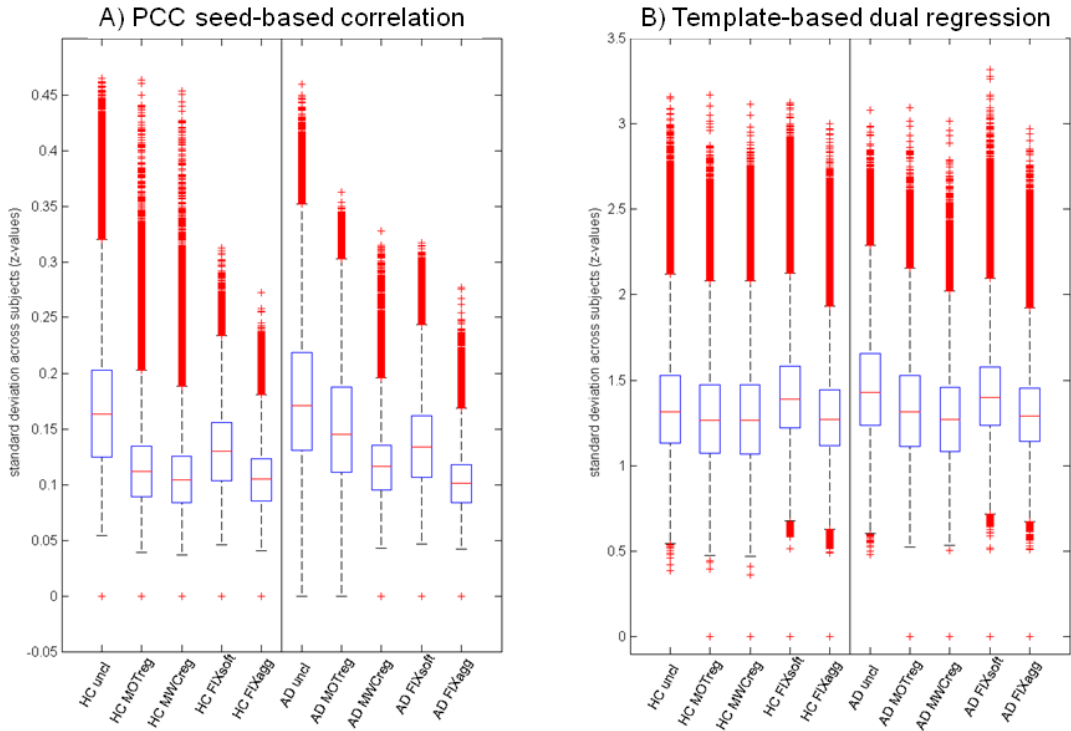
Fig. 5.6. Variability of DMN functional connectivity across subjects. Standard deviation of z-values across space obtained with seed-based correlation (A) or template-based dual regression (B) on data cleaned with different cleaning procedures for the two groups (HC and AD).

Table 5.3. Across-subjects standard deviation. Comparison among different cleaning approaches in the two groups (paired t-test on the z-values of the standard deviation maps).

	PCC seed		template-based dual regression	
	HC (t-values)	AD (t-values)	HC (t-values)	AD (t-values)
Uncleaned-MOTreg	511.3588	260.2754	137.3739	171.8571
Uncleaned-MWCreg	520.7048	478.4355	135.653	221.4
Uncleaned-FIXsoft	363.0041	363.8185	-94.8889	53.7983
Uncleaned-FIXagg	524.6706	559.3019	98.5434	210.6886
MOTreg-MWCreg	276.2291	393.0219	-3.4958	164.191
MOTreg-FIXsoft	-191.9647	178.8484	-194.3158	-154.9582
MOTreg-FIXagg	147.2746	463.0707	-81.4483	-55.2723
MWCreg-FIXsoft	-292.9114	-264.4339	-192.9672	-210.0587
MWCreg-FIXagg	38.3945	249.9889	-80.7162	-107.1374
FIXsoft-FIXagg	502.2432	602.6446	638.9623	721.0622

All comparisons were statistically significant (p<0.01).

5.3.4. Between-group differences in FC analysis

We observed no between group differences at a corrected threshold (not masked for main effect) with uncleaned data, MOTreg, MWCreg, and FIXsoft data with both seed-based FC and template-based dual regression.

Only after FIXagg a decreased FC in the AD group with respect to HC was observable (see Figure 5.7). In particular, with seed-based correlation AD group showed lower FC in PCC, precuneus, left middle and inferior temporal gyri, and left medial temporal lobe structures. With template-based dual regression the FC decrease in AD was localised in the PCC, precuneus, and left superior and inferior parietal lobule.
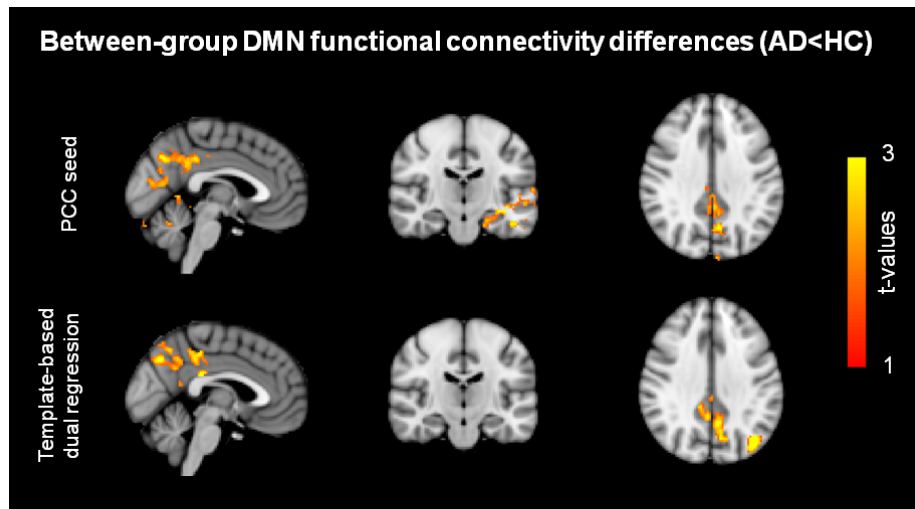

Fig. 5.7. Between-group differences in functional connectivity results using a seed in the PCC (top) or DMN template-based dual regression on data cleaned with FIX aggressive clean-up. Images are shown in radiological convention.

5.4. Discussion

In this work we compared different approaches for the cleaning of RS-fMRI data in a group of elderly healthy controls (HC) and a group of AD patients in mild to moderate stage of the disease in order to evaluate the impact of noise removal in within-group and between-group analyses.

Firstly, we evaluated the impact of the different cleaning approaches on the BOLD signal variation in terms of temporal SNR and of % reduction of cleaned signal STD with respect to the uncleaned data (%ΔSTD). The results showed an increase of SNR after each cleaning step and a localization of the reduction in BOLD signal fluctuation (%ΔSTD) in line with the well-known spatial characteristics of the artefacts being removed. In particular, the higher probability of BOLD fluctuation reduction after MOTreg is clearly observable at brain boundaries, where the motion-related artefacts are usually localised. This effect is more pronounced in the AD group, which showed higher mean relative displacement than the HC group, although not statistically significant. When FIX clean-up is performed, a consistent reduction of BOLD fluctuation is also localised in correspondence of blood vessels and CSF. This suggests that this data-driven method is able to capture and remove also the physiological noise (vascular and CSF pulsation artefacts) in absence of external recordings. The higher reduction of BOLD fluctuations observed in AD patients with

114

respect to HC is mainly localized in the perivetricular areas and cortical sulci, regions that are more extended in AD, due to atrophy, as confirmed by the VBM analysis.

Regarding the FC results, we observed that after all the clean-up procedures we obtained higher within-group consistency across subjects both for seed-based and for template-based dual regression results, but only after FIXagg the FC alteration in DMN of AD vs HC were observable.

Conversely, after MOTreg no differences in FC were detected with both seed-based correlation and template-based dual regression. This demonstrates that the removal of only the motion parameters is not necessarily sufficient to perform an effective FC analysis.

The lowest standard deviation values across subjects were obtained after MWCreg and FIXagg and the consistency pattern was very similar. However, only after FIXagg the DMN alterations in AD patients were detectable. Although both remove the full variance of the artefacts and make the data more consistent across subjects, the removed signal is very different: the WM and CSF components identified and removed by FIXagg are subject-specific and obtained from ICA decomposition, while the WM and CSF regressors removed in MWCreg are derived from anatomical basis and might be affected by registration errors. It is also an open issue where the ROIs should be located to reliably represent the WM and CSF (Chao-Gan and Yu-Feng, 2010). Therefore, they might contain some useful signal that is removed with the clean-up. Moreover, FIXagg also removes other important confounds like vascular and susceptibility artefacts. These results demonstrate that a single measure of within-group consistency is not always sufficient to have a reliable measure of effectiveness of a cleaning procedure, because it is possible that useful across-subject variability, necessary to discriminate the two groups, is removed with the cleaning or that the cleaning is not effective enough to capture the between-group differences. In fact, from the within-group consistency results we observed a significant reduction of the across-subjects standard deviation, but from this analysis it was not possible to evaluate if the removed variability was due to noise or to neural-related signal.

Compared to the most commonly used approaches for confounds removal, we showed that FIX was more effective in removing multiple sources of artefacts, and allowed the detection of pathological FC alterations. Surprisingly, the FC results were not significant at a corrected threshold with FIXsoft, while the FC alteration was detectable with FIXagg. The soft and aggressive FIX options remove the same number of single-subject ICs, but with FIXagg also the shared variance between the good and the noisy components is removed. We therefore hypothesize that this amount of variance could contain more artefacts, probably related to morphological changes due to atrophy, and its removal in this specific target population is particularly beneficial. As these data were acquired with a clinical scanner (1.5T) and a standard EPI protocol, this

hypothesis should be confirmed with future studies on the same population on images with higher spatial and temporal resolution, for which FIXsoft was the recommended option on healthy subjects (see Chapter 4; Smith et al., 2013).

It must be taken into account that, even if FIX approach was demonstrated to be the best one to detect FC alterations in AD, a loss of meaningful and disease-specific information cannot be excluded. For example, there could be loss of neural-related signal that correlates with motion and with the vascular components (certainly different between groups). While no way for distinguishing neural-related signal correlating with motion parameters from real motion artifacts is known, so far, and we must consider this possible loss as part of the optimized trade-off between noise removal and signal loss, interesting future development would be the specific study of the cardiovascular components in HC and AD and what is the clinical value of their neural and/or vascular related information.

Moreover, we based our evaluation of FIX efficacy in AD on the assumption that FC in the DMN is significantly altered in AD with respect to HC, which has been demonstrated with MRI and other imaging modalities (see par 1.4). It would be undoubtedly a corroboration of our findings to be able to replicate the differences we observed across cleaning modalities in a different population, with a different well-documented functional alteration.

The FC results obtained (on FIXagg cleaned data) with seed-based correlation and template-based dual regression are consistent, but not identical, as the FC was measured in different ways: the seed-based connectivity results are relative only to the correlation of the mean signal within the PCC and the other brain voxels, while the template-based dual regression approach evaluates the whole DMN connectivity pattern. Both methods were able to correctly detect the typical DMN alteration in AD patients, which involves the PCC and the precuneus (Binnewijzend et al., 2012; Greicius et al., 2004; Zhang et al., 2009; Gili et al., 2011; Wang et al., 2007), extending towards the parietal cortex (Wang et al., 2007; Greicius et al., 2004) especially in template-based dual regression results. For this reason they both showed to be reliable techniques for the evaluation of this candidate biomarker for AD. However, only with seed-based correlation we observed other damaged areas in the middle and inferior temporal cortex and the medial temporal lobe structures (Zhang et al., 2009; Greicius et al., 2004). This higher sensitivity is probably due to the fact that with seed-based correlation we were investigating the FC of a more localized area, as we wanted to answer a specific question, arising from previous literature evidence. As already pointed out by Cole and colleagues (2010), it is advisable to use seed-based FC methods only under precise *a priori* hypothesis (e.g. in this case the PCC connectivity alteration), to ask a straightforward question about the FC of a specific area with the rest of the brain, and receiving a direct answer. On

the other hand, a data-driven approach, like ICA or template-based dual regression, allows an overall view of the FC of the whole network of interest and allows the study of more than one RSN at the same time. Thus this option is more advisable in absence of a precise hypothesis to test.

5.5. Conclusion

In this work we compared on elderly healthy controls and people with Alzheimer's disease four data-driven cleaning approaches (two commonly used in the preprocessing of RS-fMRI data and two options of the recently developed ICA-based denoising method, FIX). We demonstrated the importance of an effective cleaning of RS-fMRI data from different sources of artefacts, in order to correctly detect FC alterations in pathology, in this case the DMN alterations of the PCC in Alzheimer's disease patients. These are promising results towards the definition of a reliable non-invasive biomarker for AD.

Chapter 6 – Future developments: towards a detailed parcellation of the brain for the detection of functional connectivity alterations

In the preliminary study described in this chapter, high-dimensional ICA, introduced in Chapter 4, is applied to a population affected by Alzheimer's disease. Promising results of this pilot study obtained with spatial and temporal (amplitude and network) analyses and describing the functional disconnections due to this neurodegenerative disease will be discussed. Future developments in this direction will be described, towards a detailed parcellation of brain functional networks and an enhanced analysis of the temporal information for the detection of functional connectivity alterations in pathological conditions.

The preliminary results of this study are described in an abstract (Griffanti, Di Pasquale et al.,) submitted to the annual meeting of the International Society for Magnetic Resonance in Medicine (ISMRM 2014).

6.1. Introduction

In Chapter 4 we introduced the use of group-level high-dimensional independent component analysis (ICA), through which the resting state networks (RSNs) are decomposed in sub-networks to obtain more detailed and informative network analyses with respect to the more common low-dimensional approach. The components split by the high-dimensional group-ICA could be the result of a differential functionality of sub-networks forming the larger networks obtained with the low dimensional analysis (Smith et al., 2009; Abou Elseoud et al., 2010). In applications to pathological conditions, this differential functionality of sub-networks could be due to the specific set of subjects (Abou Elseoud et al., 2010; Damoiseaux et al., 2012) and driven by the pathology itself, allowing a more disease-specific FC analysis. Moreover, Abou Elseoud and colleagues (Abou Elseoud et al., 2010) showed that ICA analyses results are affected by model order selection and demonstrated on patients with seasonal affected disorder (Abou Elseoud et al., 2011) that the between-group differences measured with ICA increase with model order (reaching a maximum around 70 components on data acquired with Standard EPI sequence), thus suggesting multilevel ICA

exploration of FC to optimize sensitivity to brain disorders. We therefore hypothesize that the analysis of high dimensional independent components could give further insight also into the description of the pathological alterations in Alzheimer's disease (AD).

We also investigated (Chapter 4) the potential of the temporal information obtained by ICA (at low and high dimensionality) from RS-fMRI data in the study of brain function from a complementary perspective to the information provided by spatial maps. This was also confirmed by Tian and colleagues (Tian et al., 2013) in a recent study conducted on healthy subjects investigating spatial and temporal features of RS-fMRI related to behaviour, where they highlighted the benefit of the temporal analysis of RSNs.

In this study we applied these innovative analyses in AD, in order to assess whether spatial and temporal analyses at low and high ICA dimensionality can give further insight also into the understanding of the FC pattern of this pathology, and its differences with respect to the physiological condition. For this purpose, we analysed the RS-fMRI data used in the study presented in Chapter 5 with two ICA model orders. Firstly, we aimed at developing suitable criteria for automatically classifying each high-dimensional component as belonging to a low-dimensional one, either classified according to the RSNs described in literature, or as residual noise. Our second aim was then to explore the functional connectivity in AD patients and HC within two resting state networks (RSNs) (the DMN, primarily altered in AD, and the sensory-motor network - SMN, not primarily altered in this pathology) with low- (i.e., 25 components) and high-dimensional analysis (i.e., 70 components). To this end, a low-dimensional spatial map analysis was used to verify that the results of our study were in line with previous literature (Binnewijzend et al., 2012; Greicius et al., 2004; Zhang et al., 2009; Hafkemeijer et al., 2012). We then performed temporal (amplitude and network) analysis at low dimensionality, and spatial and temporal analyses at high-dimensionality, aiming at investigating in more detail the functional connectivity of the selected RSNs and their sub-networks revealed at high dimensionality.

6.2. Materials and methods

6.2.1. Subjects, MRI data acquisition and Preprocessing

The details of subjects (20 healthy controls – HC- and 21 AD patients) and MRI acquisitions (RS-fMRI EPI and T1-weighted 3D images) are described in Chapter 5 (par. 5.2.1).

After initial standard preprocessing with FSL (motion correction, non-brain tissue removal, spatial smoothing with 5mm FWHM Gaussian kernel, temporal filtering with a cutoff frequency of 0.01 Hz), data were cleaned with FIX using the aggressive option (see Chapters 4 and 5), and registered to MNI standard space. RS-fMRI data of all the subjects were temporally concatenated

across subjects to create a space × time data matrix and group-ICA was performed with MELODIC (Beckmann and Smith, 2004). The group-ICA was performed at two dimensionalities (*d*): with 25 independent components (ICs) for the low-dimensional ICA, and with 70 for the high-dimensional ICA as suggested in (Abou Elseoud et al., 2010,2011) and judged to be compatible with the temporal degrees of freedom of the cleaned data. As the low-dimensional group independent components (ICs) were used as reference template for the classification of the high-dimensional ICs, they were manually classified as RSNs or artefact based on previous knowledge of the RSNs patterns described in literature (Beckmann 2005; De Luca 2006; Rytty et al., 2013), following the same rules used for single-subject manual labelling described in Chapter 3, and double-checked by a second expert.

6.2.2. Low-dimensional ICA analysis

Subject-specific time series and spatial maps from the 25 group ICA components were obtained with dual regression (Filippini et al., 2009). Among the components that were functionally interpretable (judged not to be purely associated with artefact sources), we focused on those attributable to the DMN and the SMN.

Using the subject-specific time series, output of the first stage of dual regression, we calculated the amplitude of the selected RSNs as the standard deviation of the time series. Low-dimensional network analysis was also performed by estimating full correlation values between all pairs of time series of the selected components. Significant differences in amplitude and correlations between HC and AD patients were then assessed with a two sample t-test.

The spatial maps derived from the second stage of dual regression were compared between the two groups through voxel-wise statistics using a non-parametric permutation test. Results were considered significant at $p < 0.05$, fully corrected for multiple comparisons, after initial cluster-forming threshold of $p_{uncorr} < 0.05$.

6.2.3. High-dimensional ICA analysis

Also in this case, dual regression was used to obtain for each of the 70 ICs, the time series and spatial maps for each subject. In order to correctly label a high-dimensional component as part of a specific RSN identified with low-dimensional ICA, we developed an automatic labelling algorithm.

Three criteria were experimented for labelling: space-based, correlation-based or spatiotemporal labelling.

Space-based labelling: a high dimensional component i is labelled as part of the low-dimensional component j with which it has the highest spatial overlap calculated with Dice coefficient (DC_{ij}) on the group maps. If DC_{ij} is lower than a threshold T_{DC}, the component is classified as noise.

Correlation-based labelling: a high dimensional component *i* is labelled as part of the low-dimensional component *j* according to the subject specific (i.e., computed after dual regression) temporal correlation (TC_{ij}) and maximal average score across subjects. Max<TC_{ij}>, which must be also higher than a threshold T_{TC}, otherwise the component is classified as noise. (It is worth to recall that component ordering derives from group ICA and is shared across subjects).

Spatiotemporal labelling: a high dimensional component *i* is labelled as part of the low-dimensional component *j* with which it has the highest Dice coefficient *and* the highest temporal correlation. If component *i* has DC_{ij} *or* TC_{ij} under the thresholds T_{DC} and T_{TC}, it is classified as residual noise. When the spatial and temporal matching results disagree, the component is classified as "unknown".

A manual labelling was used as gold standard firstly to assess the best performing thresholds for the spatial and temporal criterion separately, and then to compare the three criteria. In particular we tested two T_{DC} (0.1 and 0.4) and two T_{TC} thresholds (0.4 and 0.55) and the comparison between the three criteria was performed using the optimised thresholds.

The labels provided by the best performing algorithm were used to select the high dimensional components relevant to the RSNs selected for this study (DMN and SMN). The calculation of amplitude values and temporal correlations among these components was analysed as described above for low dimensional analysis and the results were compared between the two groups (HC vs AD, two sample t-test). Similarly, the spatial maps analyses of the components of interest were compared between AD and HC through voxel-wise statistics using a non-parametric permutation test. Results were considered significant at $p<0.05$, fully corrected for multiple comparisons, after initial cluster-forming threshold of $p_{uncorr}<0.05$.

6.3. Results

6.3.1. Low dimensional ICA results

<u>Components of interest</u>. Out of the 25 components detected by low-dimensional ICA, we identified 9 RNSs and focused our analysis on the following three (see Figure 6.1):

1) the posterior portion of the DMN: it included the posterior cingulate cortex (PCC), the inferior parietal lobule and part of the frontal lobe. Hereon we will refer to this component as the *PCC component*;

2) the anterior part of the DMN: mainly the medial prefrontal cortex (mPFC);
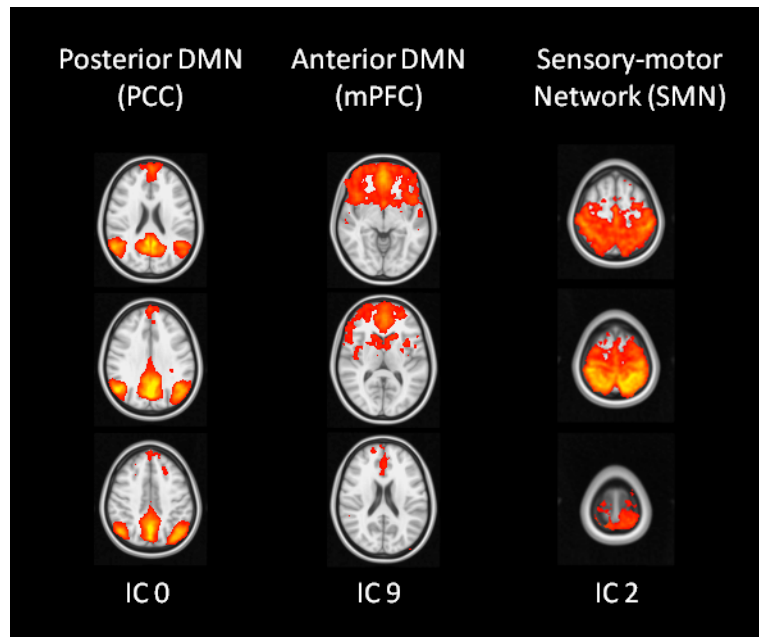
3) the sensory-motor network (SMN).

Fig. 6.1 Low-dimensional components relative to the neworks of interest selected for this study: the default mode network in its posterior and anterior portion, respectively the posterior cingulate cortex (PCC) and the medial prefrontal cortex (mPFC), and the sensory-motor network (SMN). The number of each component was based on the ranking of variance explained by the component.

<u>Time series amplitude.</u> From the time series analysis, we observed that in all the three components AD patients showed significantly decreased amplitude values (p<0.05, Figure 6.2).
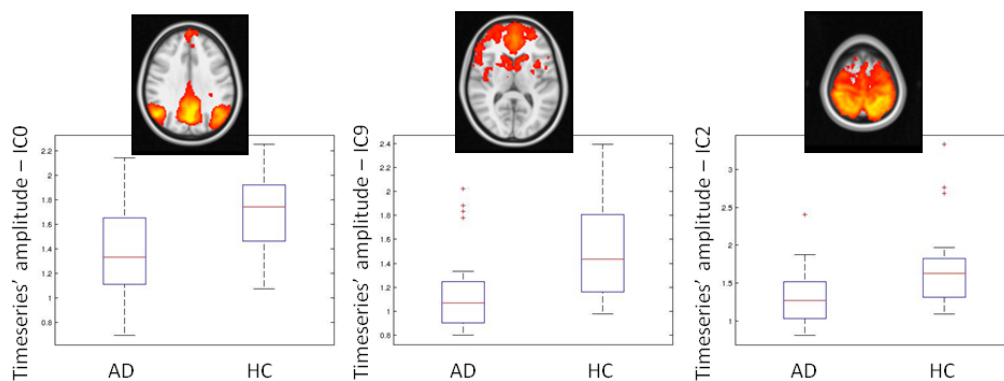

Fig. 6.2. Low-dimensional components (IC0,PCC; IC9, mPFC; IC2,SMN) showing decreased amplitude values in AD patients compared to HC (p<0.05).

<u>Network analysis (full correlation)</u>. Only the correlation between PCC and mPFC was significantly different between the two groups (p < 0.05, AD<HC; Figure 6.3).
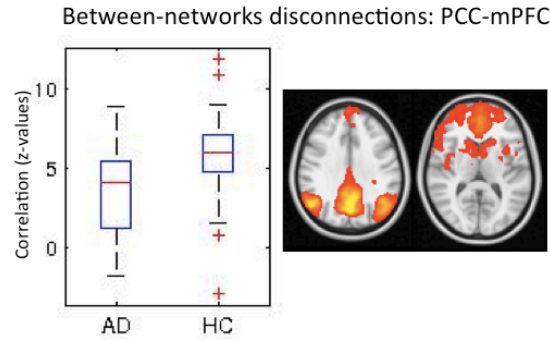
Figure 6.3. Between-networks disconnections (p<0.05; AD<HC) identified with low-dimensional ICA analysis.

Spatial maps analysis. Significantly smaller activation areas were found in AD patients only in the posterior portion of the DMN, the PCC component, mainly localised in the PCC, the precuneus, and the left superior and inferior parietal lobule (Figure 6.4).
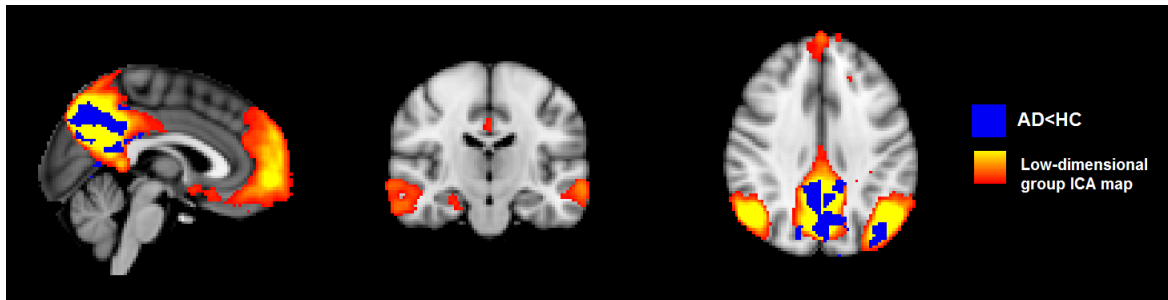
Fig. 6.4. Between-group differences (AD<HC) in functional connectivity in the posterior part of the DMN (PCC component identified with low-dimensional ICA). Images are shown in radiological convention.

6.3.2. High dimensional ICA results

Labelling algorithm for the selection of the components of interest. The optimal spatial and correlation threshold for the labelling algorithm were found to be $T_{DC} = 0.1$ and $T_{TC} = 0.4$, respectively.

The spatiotemporal criterion showed the best accuracy (95.7%) in signal vs noise classification, compared to correlation-based and the space-based ones (89% and 85%, respectively). The high-dimensional components labelled as part of the selected RSNs are shown in figure 6.5 (their automatic classification was in concordance with the manual labelling): the posterior default mode network (PCC) was identified in two components, the mPFC in three components, and five components were labelled as belonging to the SMN.
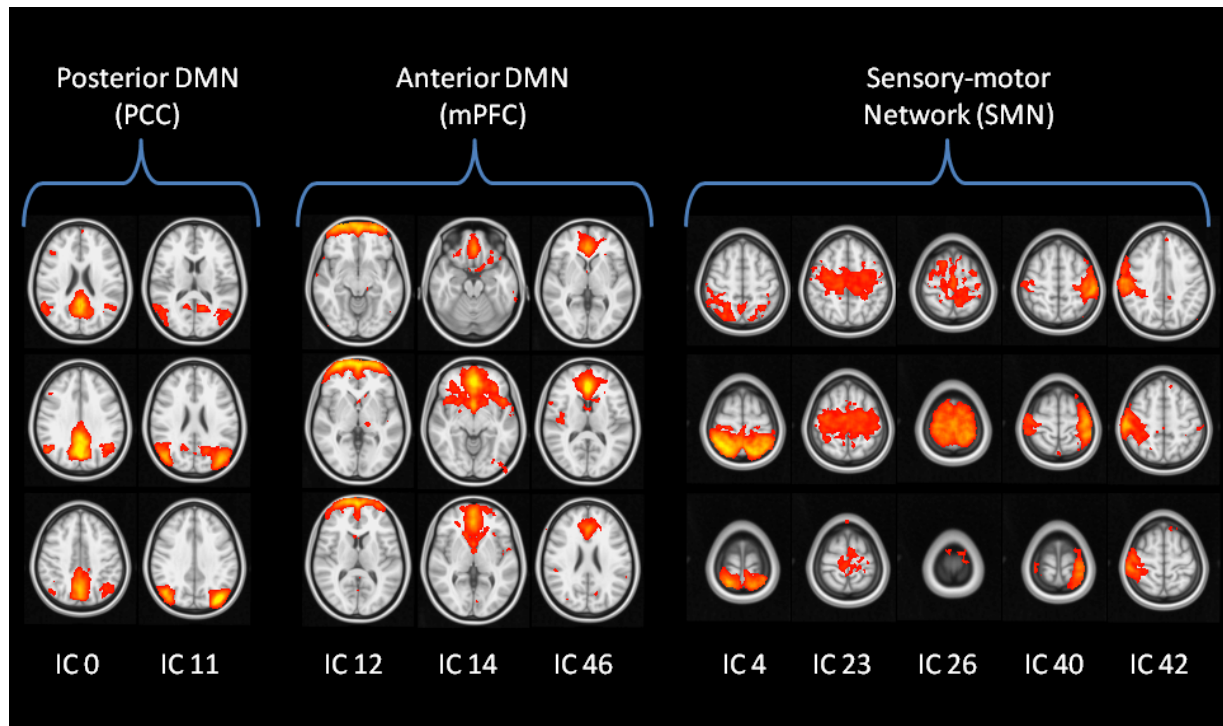
Fig. 6.5. High-dimensional components relative to the neworks of interest automatically selected by the labelling algorithm with the spatiotemporal-based criteria: the posterior default mode network (PCC) was identified in two components, the medial prefrontal cortex (mPFC) in three, and five components were labelled as belonging to the sensory-motor network (SMN). The number of each component was based on the ranking of variance explained by the component.

Time series amplitude. The time series amplitude analysis performed on these components revealed a significantly decreased amplitude ($p<0.05$) in AD patients in both PCC sub-networks (PCC_0, PCC_{11}), but only in one component within the mPFC (the ventral mPFC, $mPFC_{14}$) and one in the SMN (precentral gyrus, SMN_{23}) (Figure 6.6).

Fig. 6.6. High-dimensional components (from top-left to bottom-right: PCC_0, PCC_{11}, $mPFC_{14}$, SMN_{23}) showing decreased amplitude values in AD patients compared to HC ($p<0.05$).

Network analysis (full correlation). From the network analysis we observed the presence of disconnections both within-network (i.e., the connectivity between sub-networks belonging to the same RSN) and between-network (i.e., the connectivity between either RSNs or sub-networks belonging to different RSNs) in AD patients.
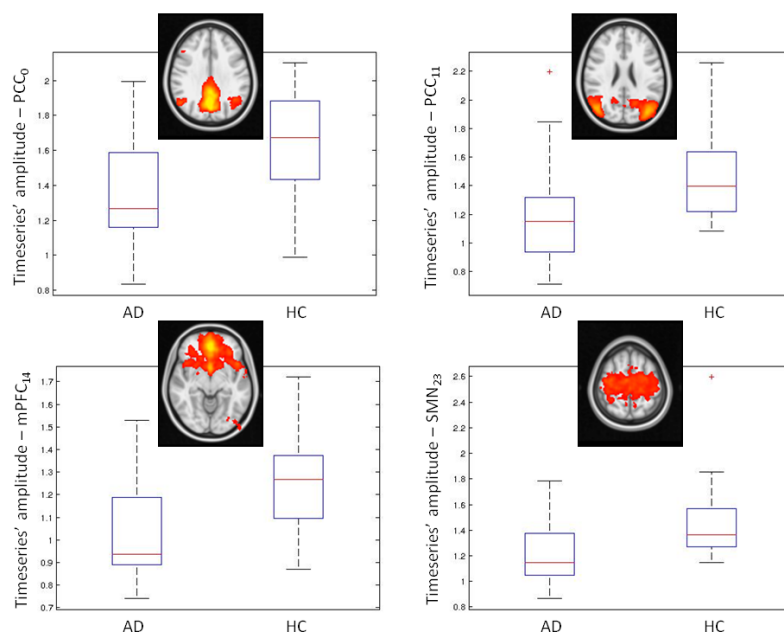
Regarding the DMN, the within-network connectivity was not different in the PCC, while a FC alterations in AD ($p<0.05$; AD<HC) was detected among two of the three connections in the mPFC network, namely those involving the ventral mPFC ($mPFC_{12}$- $mPFC_{14}$; $mPFC_{14}$- $mPFC_{46}$, Figure 6.7, A), in which we previously observed the amplitude's decrease. As regards the between-network connectivity, the anterior-posterior disconnection in AD patients observed between PCC and mPFC at low dimensionality was also detectable at high dimensionality among two PCC components and two mPFC components (PCC_0-$mPFC_{12}$, PCC_0-$mPFC_{14}$, PCC_{11}-$mPFC_{12}$, PCC_{11}-$mPFC_{14}$, Figure 6.7, B).
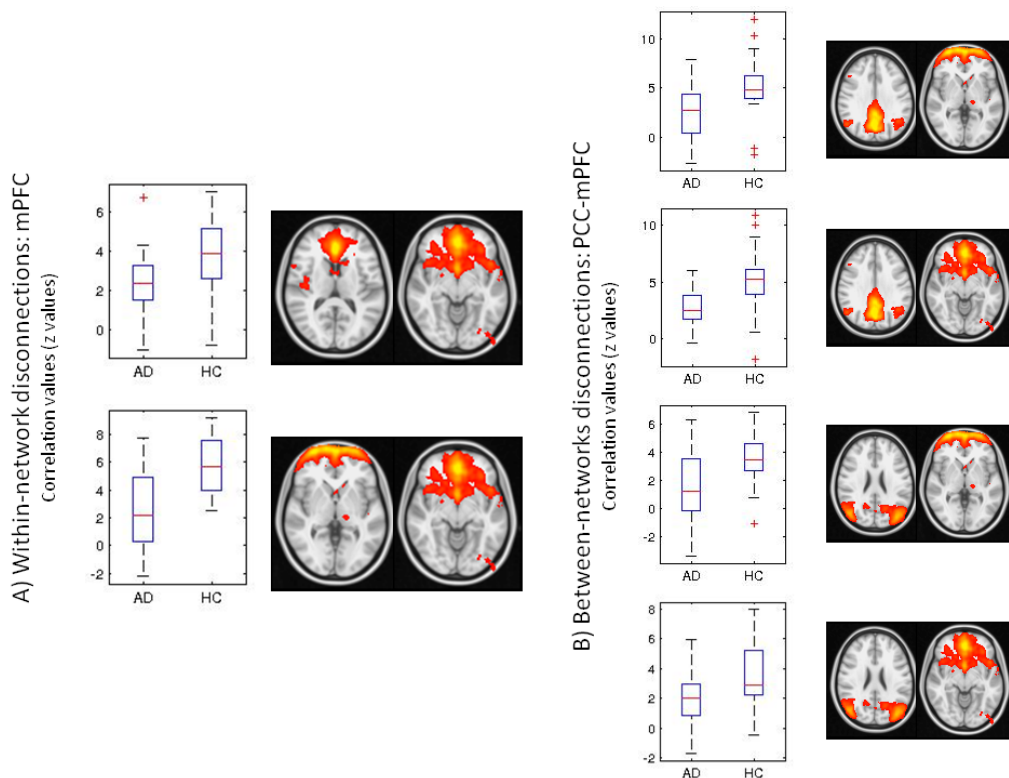
Figure 6.7. High-dimensional ICA network analysis of the DMN. A) Within-network disconnections ($p<0.05$; AD<HC) in the mPFC and B) between-networks disconnections ($p<0.05$; AD<HC) between the anterior and posterior DMN sub-components.

The same analysis in the SMN resulted in a decreased within-network connectivity among all the subnetworks belonging to the SMN (Figure 6.8, A), and one altered between-network connection between SMN and DMN (PCC_0-SMN_{26}) (Figure 6.8, B)
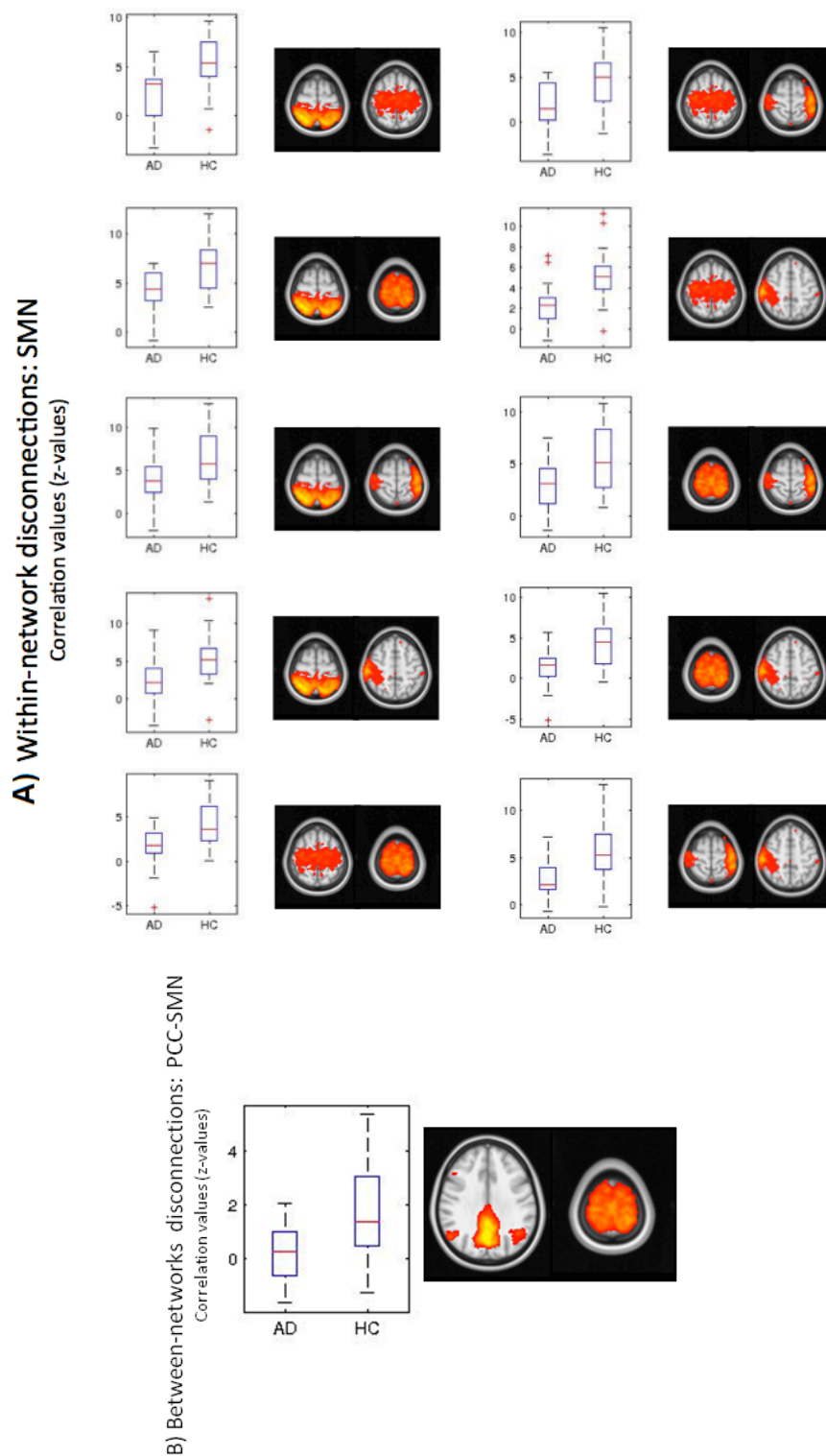
Figure 6.8. High-dimensional ICA network analysis of the SMN. A) Within-network disconnections ($p<0.05$; AD<HC) in the SMN and B) between-networks disconnections ($p<0.05$; AD<HC) between the DMN and SMN sub-components.

Spatial maps analysis. Significantly lower activation was found in AD patients in three high-dimensional components (PCC_0, $mPFC_{14}$, SMN_{23}). In the PCC sub-network (PCC_0), the decreased activation was localised in the PCC and the precuneus; the alteration in the mPFC ($mPFC_{14}$) involved the ventral mPFC, while a decreased activation in the SMN was localised in the precentral gyrus (see Figure 6.9).
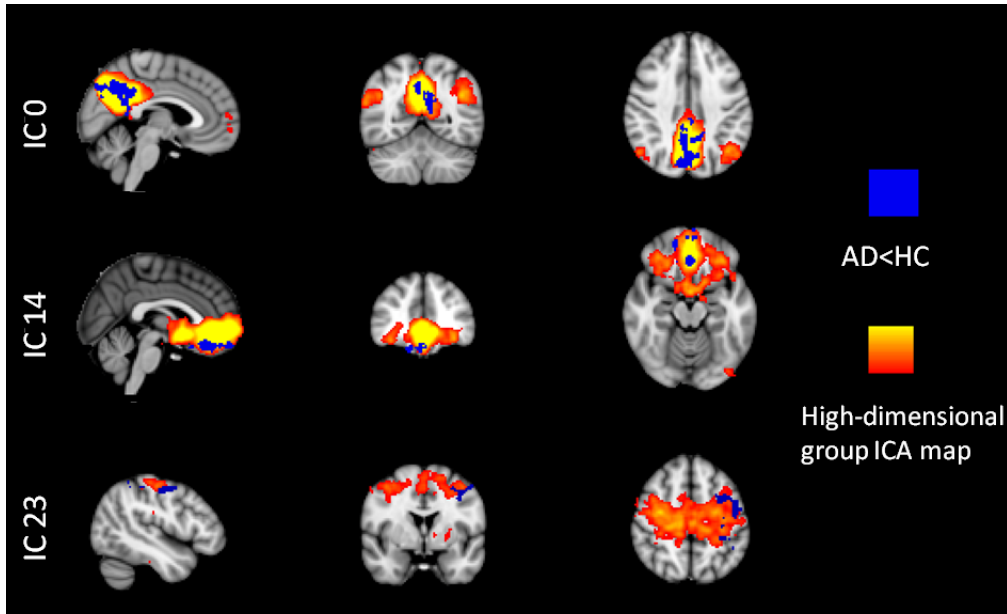
Fig. 6.9. High-dimensional spatial maps analysis. Between-group differences (AD<HC) were detected in one PCC component, one mPFC component and one SMN component. Images are shown in radiological convention.

6.4. Discussion

In this work we applied low- and high-dimensional group ICA on RS-fMRI data of a group of elderly healthy controls (HC) and a group of AD patients in mild to moderate stage of the disease in order to investigate the effect of the dimensionality of group ICA decomposition in the detection of FC damage using spatial and temporal (amplitude and network) analysis.

The creation of an automatic labelling algorithm allowed to automatically identify the sub-networks of interest with an objective and quantitative criterion and to perform a high-dimensional analysis that was a complementary approach to the low-dimensional one. A future improvement of the algorithm could be the use of standard templates, avoiding the time consuming labelling phase, or a customization of the classifier used by FIX for the automated labelling of group-level components at low and high dimensionality.

In our application to AD patients we focused on two RSNs: the DMN (divided in its posterior and anterior portions), as the most damaged by AD, and the SMN, for which the role of the pathology is still unclear and under debate.

As regards the posterior part of the default mode network (the PCC), through the low-dimensional spatial map analysis we verified the loss of activation in the PCC typical of AD patients and extensively supported by literature (Binnewijzend et al., 2012; Greicius et al., 2004; Zhang et al., 2009; Gili et al., 2011). The same analysis at higher dimensionality better localised the altered activation in the PCC. Considering the time series amplitude of low- and high-

dimensional PCC components, a significant decrease was always observable in AD patients, probably because the two PCC sub-components are equally (and fully) altered in terms of activation with respect to the HC. This is confirmed by the results of the within-network connectivity at high dimensionality, where no differences were found in the correlation values.

At low dimensionality, no differences in the spatial maps between HC and AD were found in the mPFC component, the anterior part of the DMN. However, the ventral mPFC sub-network showed a reduced activation in AD with high-dimensional spatial maps analysis. This is an interesting result in the light of the time series analyses, that showed: i) decreased amplitude in AD at low-dimensionality; ii) decreased amplitude in the ventral mPFC component; iii) decreased within-network connectivity between the ventral mPFC component and the other two. The alteration in the anterior part of the DMN in AD is also described in literature (Greicius et al., 2004; Zhang et al., 2009; Gili et al., 2011), but more at an advanced stage of the disease (Brier et al., 2012; Zhang et al., 2010; Damoiseaux et al., 2012), probably due to the progression of the structural changes of the pathology (Buckner et al., 2005; Minoshima et al., 1997). We hypothesize that in our sample this alteration was not severe enough to be detectable on the low-dimensional spatial maps (Abou Elseoud et al., 2011). Moreover, the analysis of the temporal information showed to be more sensitive with respect to the spatial information, as between-group differences were detected both at low and high dimensionality (Tian et al., 2013).

This innovative temporal analysis at low and high dimensionality was also useful to better explain the FC between the anterior and posterior DMN previously described in literature (Gili et al., 2011; Wang et al., 2007). In fact, although this alteration was already detectable at low dimensionality, it was better localised at high dimensionality, where it emerged that one of the three mPFC sub-networks still preserved its FC with the PCC, probably due to the fact that the AD patients were in mild to moderate stage of the disease.

The SMN confirmed to be less altered in AD patients with respect to the DMN. No differences were found between the two groups in the low-dimensional spatial maps, and a decreased activation in only one of the five sub-networks was detectable at high dimensionality. Alterations in the time series amplitude were observable in the low dimensionality component and in one high-dimensional sub-network. Interestingly, despite the amplitude alteration in only one SMN sub-network, all the within-network correlations were significantly lower in AD patients. We therefore hypothesize that the connectivity damage in AD could be not confined into the DMN, but could extend to other areas as the sensory-motor regions (in line with recent findings by Damoiseaux et al., 2012), manifesting, in the initial stage of the disease, more as a loss of within-network

connectivity than a decreased activation. Of course this speculation needs further research to be confirmed.

A wider analysis using different ICA dimensionalities would also be useful to define the most suitable model order for the detection of AD alterations. As already pointed out by Abou Elseoud and co-workers (2011), the higher model order provides higher sensitivity, but also increases the risk of false positives and advanced statistical methods applied at the level of RSNs would be beneficial in order to correct for type I errors.

Certainly, future studies including subjects in the prodromal stage of AD (Mild Cognitive Impairment) and moderate to severe AD patients, or longitudinal studies on AD patients would better clarify if the changes we observed with the temporal analyses in mild to moderate AD were early signs that anticipate future changes in the spatial maps.

6.5. Conclusion

In this work we showed that high-dimensional ICA, supported by a component classification based on low-dimensional ICA, can be applied in RS-fMRI to gain additional knowledge regarding brain functional connectivity also in applications to diseased populations. A detailed parcellation of the brain and the analysis of the temporal information (e.g. amplitude and network) could give further insight into the detection of functional connectivity alterations in pathological conditions and their monitoring at different stages. This promising, albeit preliminary, results obtained in describing the functional disconnections due to this neurodegenerative disease, support future developments in this direction.

Chapter 7 – Discussion and conclusion

The functional organization of the human brain and its changes in clinical conditions still present several unclear and unexplored characteristics that have to be investigated. Advanced fMRI techniques have shown invaluable capacity of non-invasively investigating *in vivo* brain activity, thus opening a window on overall cerebral organization and its pathological alterations. Namely, functional connectivity (FC) analyses of resting-state fMRI (RS-fMRI) data allow describing the relationship between spontaneous neuronal activation patterns involving anatomically separated brain regions and reflecting the level of functional communication between regions. With RS-fMRI different characteristics (spatial, temporal, network properties) of the so-called resting state networks (RSNs) can be studied, evaluating different functions disentangled out of a single acquisition, with an easy and standard acquisition protocol also applicable in cases where the subject active interaction is impaired.

However, the correct separation of noise from the neural-related signal from the RSNs is particularly challenging in RS-fMRI data, due to the lack of prior knowledge about the temporal signal of interest and of any external reference timing. In fact, several sources of noise are present in the data, many of which display some spatial or spectral overlap with RSNs. Spatially extended artefacts can be caused by the scanner (e.g., hardware instabilities) or, more frequently, they are caused by non-neuronal though physiological mechanisms (head motion, cardiac and respiratory cycles) (Murphy et al., 2013). Their correct identification and removal is therefore crucial for reliable FC analyses in healthy subjects and in clinical applications. In fact, FC analyses of the RSNs are currently used to study a wide range of neurological and psychiatric disorders (Cole et al., 2010), and the ultimate goal of the optimization of FC analysis methods is certainly the quantitative evaluation of FC changes in pathological condition, and their monitoring at different stages.

In Alzheimer's disease (AD) it has been consistently demonstrated by RS-fMRI a decreased functional connectivity of the default mode network (DMN), and this is considered a possible new biomarker for AD (Li et al., 2011; Greicius et al., 2004; Gili et al., 2011). Therefore an early detection and a detailed characterization of this alteration are crucial to clinical diagnosis, staging, and monitoring of AD.

In this work objective methods for RSNs identification and noise separation in RS-fMRI were introduced and validated in healthy subjects and patients with Alzheimer's disease. In particular,

once quantified the amount of FC estimation errors in seed-based FC analyses (chapter 2), this work faced the wider problem of artefact removal from the raw data in order to optimize via ICA any further FC analysis, whether based on ICA or other approaches. Therefore, an automated denoising method (FMRIB's ICA-based X-noisefier – FIX) was developed (chapter 3 and 4) in collaboration with the FMRIB (Functional Magnetic Resonance Imaging of the Brain) Centre (University of Oxford, UK), and was tested on different acquisition sequences (standard and multi-band accelerated EPI, chapter 4), increasing network dimensionalities (obtained with low- and high-dimensional group ICA, chapter 4), and different populations (healthy controls, HC, and AD patients, chapter 5). Finally, we obtained promising results for a better localisation and quantification of FC alterations in AD, through the combination of an effective cleaning procedure and high-dimensional RSNs analysis (chapter 6).

From the preliminary estimation of errors in the single-subject seed-based FC maps we observed a homogeneous distribution of random error within the brain, which suggests that this kind of error, although always present, is independent from the resting state activity itself. The proposed thresholding methods are promising for a better identification of the RSNs at single-subject level and in future studies they could be applied in a clinical setting to quantify the FC alterations with respect to a seed ROI through the definition of specific FC measures. Indeed, the availability of a reliable single-subject FC analysis could be particularly useful for rare case studies (when a group study is not feasible) and for the longitudinal evaluation of a single patient's disease progression or response to treatment or rehabilitation.

The developed tool (FMRIB's ICA-based Xnoisefier - FIX) for the identification and removal of noise, further improved the reliability of FC estimation as, through the cleaning of the single-subject raw data, can be applied to any FC analysis. FIX is a fully automatic solution (once trained) for cleaning fMRI data of various noise types, and it consists of four major operations: spatial ICA, classifier training, component classification (noise detection), and denoising.

Regarding the ability to classify the independent components into signal or noise, FIX achieved over 95% classification accuracy on the three training datasets built by hand-labelling of the components, demonstrating to be a very valuable tool for the identification of artefacts in RS-fMRI data.

As regards to the final stage of the cleaning procedure, i.e. the removal of the artefactual components from the RS-fMRI data, we aimed at successfully remove the noise components while preserving as much signal as possible. Our results on the denoising efficacy showed that FIX cleaning is useful to obtain reliable temporal and spatial RS-fMRI analyses: if an artefact is not

cleaned at the single-subject level and its spatial pattern is overlapping one of the RSNs, it will in general influence both the single-subject RSNs time series, (i.e. the output of the first stage of dual regression) and the RSN spatial maps (obtained from the second step of dual regression). In fact, the non-cleaned time series will have higher amplitude with respect to the cleaned data, often with high frequency confounds visible in the power spectra, and the presence of shared noise will in general produce less consistent network connection matrices across subjects. Noise would also lead to altered subject-level z-maps, thus affecting any following group-level analyses, reducing the ability to detect specific activation patterns within the RSNs, and obscuring pathological alterations. This problem also affects seed-based resting-state correlation maps for similar reasons, as also demonstrated in the application on AD patients.

The efficacy of the cleaning procedure was demonstrated on two quite different EPI acquisitions (standard EPI and multiband accelerated EPI), obtaining similar results on the relative merits of different clean-up options. The only difference in the cleaning approach for the two datasets was the training dataset used for the FIX classification, which was tailored to each specific pulse sequence. The use of a sequence-specific training dataset is important because it allows FIX to optimize the classification training for the kind of data from a specific study. An interesting future development would be to investigate whether and how the different preprocessing steps can influence the training phase, the cleaning of the data, and consequently the final results, depending on the scan hardware and the sequence features.

Compared to most of the currently available ICA-based approaches (see introduction Chapter 3), FIX approach can be considered a development/improvement of those methods, as it takes into account and merges information regarding spatial characteristics (as used in Perlbarg et al., 2007), temporal characteristics (Beall and Lowe, 2007), and spectral characteristics (Thomas et al., 2000) of the components. It is also an extension of methods that already combined multiple features (Tohka et al., 2008; De Martino et al., 2007). Moreover, the use of a hierarchical fusion of classifiers provides high classification accuracy. Conversely, the multi-echo method proposed by Kundu and colleagues (2012) relies on a totally different and original approach characterizing neurally-related BOLD signals in terms of changes in R_2* (inverse of the relaxation time T_2*) and initial signal intensity (S_0), based on the analysis of TE dependence. As a direct comparison between the two methods was not feasible in this study, due to the lack of data acquired with multi-echo EPI, a detailed comparison of FIX vs multi-echo method is provided in Table 7.1.

Table 7.1. Main characteristics comparison of two denoising approaches.

	Multi-echo method (Kundu et al., 2012)	FIX
Acquisition sequence	Requires a specific acquisition sequence with different TEs.	Applicable to any RS-fMRI dataset. No specific sequence required.
Priors	Theoretical reference functions (models for R_2^* and initial intensity S_0 changes to fit signal changes)	Individual T1 image and standard vessels masks required
Features	Two features related to R_2^* (modulated by changes in field homogeneity) and S_0 (modulated by changes in T1): κ (high κ in BOLD-like components) and ρ (high ρ in non BOLD-like components)	More than 180 features related to spatial, temporal, spectral characteristics of the components.
Component classification	Automatic classification of BOLD-like components as the ones for which the associated κ is over a threshold and ρ is under a threshold.	Training dataset required, built by hand labelling of components (requires expertise about signal and noise characteristics); automatic classification in signal, noise, unknown components.
Unknown components	If a component is not classified as purely signal is removed. (Possible loss of meaningful information).	If a component is classified as pure noise is removed. (Conservative approach).
Components removal	Subtraction of the partial fit of the nuisance regressors (the non BOLD-like components)	Subtraction of the contribution of the noisy components to the data. Two options for noise removal (soft and aggressive)

From this summary it clearly emerges that both methods have different advantages and limitations and a future development comparing them on the same dataset would undoubtedly be interesting.

When comparing two different acquisition sequences it emerged that the use of multiband (MB) accelerated EPI is advantageous for RS-fMRI analysis for several reasons: i) the increased temporal and spatial resolution yielded a better FIX classification accuracy (98% for MB6 versus 95% for Standard, with leave-one-out testing); ii) a considerably higher proportion of non-artefactual group-ICA components was identified in the MB6 dataset, thus suggesting more successful ICA-based clean-up of MB data; iii) the MB accelerated data allowed a more detailed time series and network analyses through higher dimensionality decomposition (d=100), which was not achievable with the Standard sequence because of its lower temporal degrees of freedom (DOF); iv) MB time series

spectra after cleaning showed considerably less structured artefact (i.e., deviation from the expected clean 1/f-like spectrum) though preserving mean total time series power; v) network patterns were more reproducible across subjects; vi) results of spatial map analyses were not altered in MB, notwithstanding the lower static image SNR of MB due to its higher resolution.

An important observation emerging from this comparison is that the characteristics of the data do also influence the decisions regarding the dimensionality of group ICA decomposition. In fact, it must be taken into account that the cleaning procedure reduces the number of DOF in the data, limiting the possibility to perform high-dimensional group ICA and dual regression. For example, in chapter 4, in Standard sequence the data has 200 time points; after cleaning (on average 60.9 ± 14.9 components per subject manually identified as noise) the remaining DOF are around 140. Although a group ICA with temporal concatenation is feasible with d=100, the single subject data at the same dimensionality cannot be obtained by dual regression as the number of components is similar and in some cases could be higher than the actual number of DOF. For similar reasons in Chapter 6 we were able to do a reliable high-dimensionality analysis only at d=70.

The denoising with FIX was also demonstrated to be beneficial in clinical studies, as demonstrated in our application in mild to moderate Alzheimer's disease (AD) patients. In this population we observed the presence of a larger amount of artefacts with respect to aged healthy controls, possibly due predominantly to atrophy. The cleaning procedure with FIX revealed to be particularly useful to detect the typical alteration of the PCC functional connectivity in the DMN (evaluated with two different FC analysis methods), which were not detectable using uncleaned data or data cleaned with more common data-driven cleaning approaches (removal of the contribution of motion parameters or removal of the contribution of motion parameters, WM signal and CSF signal). It would be undoubtedly a corroboration of our findings to be able to replicate the differences we observed across cleaning modalities in a different population, with a different well-documented functional alteration.

Regarding the two different options for FIX denoising (soft vs aggressive), for data acquired on healthy subjects with good spatial and temporal resolution (chapters 3 and 4) we would in general suggest the use of the soft cleaning approach, which consists of: 1) removing the full space of the 24 motion parameters (Satterthwaite et al., 2013) from the data and the ICA time series; 2) estimating the contribution (spatial regression coefficients) of both good and bad components, in order to identify the unique variance of the artefacts; 3) subtracting the contribution of the bad components from the data (the outer product of their time series and spatial regression coefficients, summed over noise components). Conversely, in the application on patients using data acquired with a clinical scanner (chapters 5 and 6), we found that the aggressive option (i.e. the removal of

the full space of motion parameters and artefactual components from the data) revealed to be more effective. Therefore this difference could be due either to the characteristics of the data (number of timepoints acquired, field strength, resolution) or to the populations (healthy subjects versus AD patients), or a combination of the two and, although FIX demonstrated to be an effective cleaning procedure for different sequences and populations, further research is needed to define the optimized cleaning options for each specific application.

FIX is now publicly available; the current version (v1.06) is available as a "plugin" for FSL (the FMRIB Software Library) at link www.fmrib.ox.ac.uk/fslwiki/fsl/FIX. The FIX download includes training-weights files for "standard" fMRI acquisitions and for the MB RS-fMRI dataset delivered by the Human Connectome Project (HCP http://www.humanconnectomeproject.org/). In fact, partly due to the study performed in this thesis, FIX is now in use as part of the default HCP analysis pipeline (Smith et al., 2013), and FIX-cleaned data is the recommended version of the resting-state fMRI data that is publicly available –over 200 subjects worth of hour-long datasets having been released to date.

Finally, the combined use of ICA-based denoising and high-dimensional group ICA was applied in Alzheimer's disease, in order to investigate in more detail the functional connectivity of two selected RSNs (the DMN and the SMN) and their sub-networks. The creation of an automatic labelling algorithm allowed to automatically identify the sub-networks of interest with an objective and quantitative criterion and to perform a high-dimensional analysis that added complementary information to the low-dimensional one, relevant to loss of connectivity poorly detected by the latter. A future improvement of the algorithm could be the use of a standard template to avoid the need of manually label the low-dimensional components or the development of an extension of the classifier used by FIX for the automated labelling of group-level components at low and high dimensionality.

The study of the temporal information and the more detailed parcellation of the RSNs of interest allowed to detect FC changes in AD that were not observable with the more common approach of low-dimensional spatial map analyses, suggesting that these optimized FC analysis methods could give further insight into the detection of functional connectivity alterations in pathological conditions for evidence based diagnosis, follow-up and prognosis (Abou Elseoud et al., 2011; Tian et al., 2013). Of course, these results need further research to be confirmed and a wider analysis on other resting state networks, different AD stages, and other pathologies would be the natural progress of this study. In fact, this work focused on a homogeneous sample of AD patients in a mild to moderate stage of the disease. Certainly, future studies including people with Mild Cognitive Impairment (MCI) and severe AD patients, or longitudinal studies on AD patients would

better clarify if the connectivity changes we observed by the proposed method enhancements were early signs that anticipate changes well recognized in the low-dimensional spatial maps at higher AD severity.

Conclusion

The aim of this study was to optimize and validate objective methods for the investigation of the RSNs and the removal of artefacts in resting state fMRI data, applicable to the context of neurodegenerative diseases, especially Alzheimer's disease. With a preliminary study the amount of FC estimation errors in one of the most common FC analysis techniques (seed-based FC) was quantified and a thresholding method was proposed for a reliable single-subject FC analysis. Through the development of FMRIB's ICA-based X-noisefier (FIX), we then demonstrated that, by combining an accurate ICA component classifier with an effective approach for noise removal, we are able to remove artefacts directly from the raw data, automatically, without removing significant amounts of useful signal. Moreover, with multiband accelerated sequences and effective cleaning, we were able to perform higher dimensionality decompositions and more detailed RSN analyses than with a standard EPI acquisition. The proposed denoising approach was also demonstrated to be particularly beneficial in clinical applications, as it allowed to correctly detect FC alterations in mild to moderate Alzheimer's disease (AD) patients. Finally, we showed that high-dimensional ICA, supported by a component classification based on low-dimensional ICA, could be successfully applied in clinical studies (e.g. in AD) to gain additional knowledge regarding brain functional connectivity changes in diseased populations. A detailed parcellation of the brain and the analysis of the temporal information (e.g. amplitude and network) could give further insight into the detection of functional connectivity alterations in pathological conditions and their monitoring at different stages. The promising results obtained in describing the functional disconnections due to this neurodegenerative disease foster further investigation in this direction, towards the definition of reliable non-invasive biomarkers for AD.

Appendix - Processing pipelines and software used

RS-fMRI preprocessing with SPM (chapter 2)

- Image format conversion: dcm2nii part of MRIcron
  (http://www.mccauslandcenter.sc.edu/mricro/mrocron)
- Reorientation of T1 and EPI images with spm8
  (http://www.fil.ion.ucl.ac.uk/spm/software/spm8)
- Preprocessing with DPARSF (Data Processing Assistant for Resting State fMRI;
  http://www.rfmri.org/DPARSF):
  - o Removal of first 10 time points
  - o Slice Timing
  - o Realignment
  - o Coregistration on T1
  - o Normalisation to MNI space
  - o Resampling (3 x 3 x 3 mm^3)
  - o Spatial smoothing (FWHM = 4 mm)
  - o Removal of nuisance covariates (motion parameters, WM signal, CSF signal)
  - o Detrend
  - o Temporal filtering (0.08-0.1 Hz)

Seed-based correlation (chapters 2 and 5)

- REST -Resting State fMRI Data Analysis Toolkit; http://restfmri.net/forum/REST_V1.8

Individual trhesholding of seed-based FC maps (chapter 2)

- generation of surrogate time series: Matlab script (http://www.mathworks.it/)
  (http://www.mathworks.com/matlabcentral/fileexchange/4612-surrogate-data)
- seed-based FC with REST Toolbox (http://restfmri.net/forum/REST_V1.8)
- confidence interval estimation: Matlab scripts (http://www.mathworks.it/)
- zFC map thresholding: Matlab scripts (http://www.mathworks.it/)

RS-fMRI preprocessing with FSL (http://www.fmrib.ox.ac.uk/fsl) (chapters 3-6)

- Image format conversion: dcm2nii part of MRIcron
  (http://www.mccauslandcenter.sc.edu/mricro/mricron/)
- Brain extraction on T1 images: BET (Brain Extraction Tool) part of FSL
- MELODIC (part of FSL):
    o correction for head motion using MCFLIRT
    o correction for EPI distortions using FMRIB's Utility for Geometrically Unwarping EPIs (FUGUE)
    o Non-brain tissue was removal from EPI images with BET
    o high-pass temporal filter (cutoff period ~ 100.0 s)
    o spatial smoothing (no smoothing for dataset 1 and 2, FWHM = 5 mm for dataset 3)
- FIX classification and denoising: Matlab and shell scripts
  (http://fsl.fmrib.ox.ac.uk/fsl/fslwiki/FIX)
- coregistration of the RS-fMRI data to their high-resolution structural image with FLIRT linear registration (part of FSL), enhanced with brain-boundary-registration (BBR), and then to MNI152 standard space via application of the nonlinear FNIRT (part of FSL)

Group ICA and dual regression analysis
- temporal group ICA with MELODIC, part of FSL (performed on training dataset 1 and 2 and test dataset 3 with dimensionality estimation d - different d for low and high dimensional group ICA)
- dual regression, part of FSL, using group ICA maps (chapter 6) or template maps (chapter 4 and 5)
- Time series and network analyses: Matlab scripts (http://www.mathworks.it/), some of which are included in FSLNets (http://fsl.fmrib.ox.ac.uk/fsl/fslwiki/Fslnets)
- Spatial maps analyses with GLM and randomise, part of FSL

Abbreviations

ACC = anterior cingulate cortex

AD = Alzheimer's disease

ADRDA = Alzheimer's Disease and Related Disorders Association

BOLD = blood oxygen level-dependent

BSS = blind source separation

CDR = clinical dementia rating

CI = confidence interval

CNR = contrast-to-noise ratio

CSF = cerebrospinal fluid

DMN = default mode network

DOF= degrees of freedom

EPI = echo planar imaging

FC = functional connectivity

FE = fixed effects

fMRI = functional magnetic resonance imaging

FWHM = full width at half maximum

GLM = general linear model

GM = grey matter

HC = healthy controls

HCP = Human Connectome Project

HF = high frequency

iAAFT = iteratively refined amplitude adjusted Fourier transform

IC = independent component

ICA = independent component analysis

ICOV = inverse covariance matrix

IPL = inferior parietal lobule

k-NN = k-nearest neighbour algorithm

LF = low frequency

LOO = leave-one-out

MB = multiband

MCI = mild cognitive impairment

ME = mixed effects

MEG = magnetoencephalography

MMSE = mini-mental state examination

MNI = Montreal neurological institute

mPFC = medial prefrontal cortex

MPRAGE = magnetization prepared rapid gradient echo

MRI = magnetic resonance imaging

NINCDS = National Institute of Neurological and Communicative Disorders and Stroke

PCA = principal component analysis

PCC = posterior cingulate cortex

PET = positron emission tomography

pICA = probabilistic independent component analysis

ROI = region of interest

ROIs = regions of interest

RS = resting state

RS-fMRI = resting state functional magnetic resonance imaging

RSN = resting state network

SMN = sensory motor network

SNR = signal-to-noise ratio

SPECT = single photon emission computed tomography

SVM = support vector machine

TE = echo time

TNR = true negative rate

TPR = true positive rate

TR = repetition time

VBM = voxel based morphometry

WM = white matter

References

Aalkjaer C., Boedtkjer D., Matchkov V., 2011. Vasomotion - what is currently thought? Acta Physiologica (Oxford, England) 202(3),253-269.

Abou Elseoud A., Littow H., Remes J., Starck T., Nikkinen J., Nissila J., Timonen M., Tervonen O., Kiviniemi V., 2011. Group-ICA model order highlights patterns of functional brain connectivity. Frontiers in Systems Neuroscience 5,37.

Abou-Elseoud A., Starck T., Remes J., Nikkinen J., Tervonen O., Kiviniemi V., 2010. The effect of model order selection in group PICA. Human Brain Mapping 31(8),1207-1216.

Agosta F., Pievani M., Geroldi C., Copetti M., Frisoni G.B., Filippi M., 2012. Resting state fMRI in Alzheimer's disease: Beyond the default mode network. Neurobiology of Aging 33(8),1564-1578.

Amaro E.,Jr and Barker G.J., 2006. Study design in fMRI: Basic principles. Brain and Cognition 60(3),220-232.

Andersson, J.L.R., Jenkinson, M., Smith, S. 2007a. Non-linear registration aka spatial normalisation. FMRIB Technial Report TR07JA2.

Andersson, J.L.R., Jenkinson, M., Smith, S. 2007b. Non-linear optimisation. FMRIB Technical Report TR07JA1.

Andrews-Hanna J.R., Snyder A.Z., Vincent J.L., Lustig C., Head D., Raichle M.E., Buckner R.L., 2007. Disruption of large-scale brain systems in advanced aging. Neuron 56(5),924-935.

Bandettini P.A., 2012. Twenty years of functional MRI: The science and the stories. Neuroimage 62(2),575-588.

Bandettini P.A., Wong E.C., Hinks R.S., Tikofsky R.S., Hyde J.S., 1992. Time course EPI of human brain function during task activation. Magnetic Resonance in Medicine : Official Journal of the Society of Magnetic Resonance in Medicine / Society of Magnetic Resonance in Medicine 25(2),390-397.

Beall E.B. and Lowe M.J., 2007. Isolating physiologic noise sources with independently determined spatial measures. Neuroimage 37(4),1286-1300.

Beckmann C.F., 2012. Modelling with independent components. Neuroimage 62(2),891-901.

Beckmann C.F., DeLuca M., Devlin J.T., Smith S.M., 2005. Investigations into resting-state connectivity using independent component analysis. Philosophical Transactions of the Royal Society of London.Series B, Biological Sciences 360(1457),1001-1013.

Beckmann C.F. and Smith S.M., 2004. Probabilistic independent component analysis for functional magnetic resonance imaging. IEEE Transactions on Medical Imaging 23(2),137-152.

Bell A.J. and Sejnowski T.J., 1995. An information-maximization approach to blind separation and blind deconvolution. Neural Computation 7(6),1129-1159.

Berr C., Wancata J., Ritchie K., 2005. Prevalence of dementia in the elderly in europe. European Neuropsychopharmacology : The Journal of the European College of Neuropsychopharmacology 15(4),463-471.

Binnewijzend M.A., Schoonheim M.M., Sanz-Arigita E., Wink A.M., van der Flier W.M., Tolboom N., Adriaanse S.M., Damoiseaux J.S., Scheltens P., van Berckel B.N., and others, 2012. Resting-state fMRI changes in alzheimer's disease and mild cognitive impairment. Neurobiology of Aging 33(9),2018-2028.

Birn R.M., Diamond J.B., Smith M.A., Bandettini P.A., 2006. Separating respiratory-variation-related fluctuations from neuronal-activity-related fluctuations in fMRI. Neuroimage 31(4),1536-1548.

Biswal B., Yetkin F.Z., Haughton V.M., Hyde J.S., 1995. Functional connectivity in the motor cortex of resting human brain using echo-planar MRI. Magnetic Resonance in Medicine : Official Journal of the Society of Magnetic Resonance in Medicine / Society of Magnetic Resonance in Medicine 34(4),537-541.

Biswal B.B., Van Kylen J., Hyde J.S., 1997. Simultaneous assessment of flow and BOLD signals in resting-state functional connectivity maps. NMR in Biomedicine 10(4-5),165-170.

Brier M.R., Thomas J.B., Snyder A.Z., Benzinger T.L., Zhang D., Raichle M.E., Holtzman D.M., Morris J.C., Ances B.M., 2012. Loss of intranetwork and internetwork resting state functional connections with alzheimer's disease progression. The Journal of Neuroscience : The Official Journal of the Society for Neuroscience 32(26),8890-8899.

Bright M.G. and Murphy K., 2013. Removing motion and physiological artifacts from intrinsic BOLD fluctuations using short echo data. Neuroimage 64,526-537.

Buckner R.L., Andrews-Hanna J.R., Schacter D.L., 2008. The brain's default network: Anatomy, function, and relevance to disease. Annals of the New York Academy of Sciences 1124,1-38.

Buckner R.L., Snyder A.Z., Shannon B.J., LaRossa G., Sachs R., Fotenos A.F., Sheline Y.I., Klunk W.E., Mathis C.A., Morris J.C., and others, 2005. Molecular, structural, and functional characterization of alzheimer's disease: Evidence for a relationship between default activity, amyloid, and memory. The Journal of Neuroscience : The Official Journal of the Society for Neuroscience 25(34),7709-7717.

Bullmore E., 2012. The future of functional MRI in clinical medicine. Neuroimage 62(2),1267-1271.

Bullmore E. and Sporns O., 2009. Complex brain networks: Graph theoretical analysis of structural and functional systems. Nature Reviews.Neuroscience 10(3),186-198.

Busatto G.F., Diniz B.S., Zanetti M.V., 2008. Voxel-based morphometry in alzheimer's disease. Expert Review of Neurotherapeutics 8(11),1691-1702.

Cataldi M., Avoli M., de Villers-Sidani E., 2013. Resting state networks in temporal lobe epilepsy. Epilepsia .

Cha J., Jo H.J., Kim H.J., Seo S.W., Kim H.S., Yoon U., Park H., Na D.L., Lee J.M., 2013. Functional alteration patterns of default mode networks: Comparisons of normal aging, amnestic mild cognitive impairment and alzheimer's disease. The European Journal of Neuroscience 37(12),1916-1924.

Chao-Gan Y. and Yu-Feng Z., 2010. DPARSF: A MATLAB toolbox for "pipeline" data analysis of resting-state fMRI. Frontiers in Systems Neuroscience 4,13.

Cole D.M., Smith S.M., Beckmann C.F., 2010. Advances and pitfalls in the analysis and interpretation of resting-state FMRI data. Frontiers in Systems Neuroscience 4,8.

Cordes D., Haughton V., Carew J.D., Arfanakis K., Maravilla K., 2002. Hierarchical clustering to measure connectivity in fMRI resting-state data. Magnetic Resonance Imaging 20(4),305-317.

Cordes D., Haughton V.M., Arfanakis K., Wendt G.J., Turski P.A., Moritz C.H., Quigley M.A., Meyerand M.E., 2000. Mapping functionally related regions of brain with functional connectivity MR imaging. AJNR.American Journal of Neuroradiology 21(9),1636-1644.

Damoiseaux J.S., Prater K.E., Miller B.L., Greicius M.D., 2012. Functional connectivity tracks clinical deterioration in alzheimer's disease. Neurobiology of Aging 33(4),828.e19-828.e30.

Damoiseaux J.S., Rombouts S.A., Barkhof F., Scheltens P., Stam C.J., Smith S.M., Beckmann C.F., 2006. Consistent resting-state networks across healthy subjects. Proceedings of the National Academy of Sciences of the United States of America 103(37),13848-13853.

De Luca M., Beckmann C.F., De Stefano N., Matthews P.M., Smith S.M., 2006. fMRI resting state networks define distinct modes of long-distance interactions in the human brain. Neuroimage 29(4),1359-1367.

De Martino F., Gentile F., Esposito F., Balsi M., Di Salle F., Goebel R., Formisano E., 2007. Classification of fMRI independent components using IC-fingerprints and support vector machine classifiers. Neuroimage 34(1),177-194.

de Pasquale F., Della Penna S., Snyder A.Z., Lewis C., Mantini D., Marzetti L., Belardinelli P., Ciancetta L., Pizzella V., Romani G.L., and others, 2010. Temporal dynamics of spontaneous MEG activity in brain networks. Proceedings of the National Academy of Sciences of the United States of America 107(13),6040-6045.

Desjardins A.E., Kiehl K.A., Liddle P.F., 2001. Removal of confounding effects of global signal in functional MRI analyses. Neuroimage 13(4),751-758.

Di Martino A., Scheres A., Margulies D.S., Kelly A.M., Uddin L.Q., Shehzad Z., Biswal B., Walters J.R., Castellanos F.X., Milham M.P., 2008. Functional connectivity of human striatum: A resting state FMRI study. Cerebral Cortex (New York, N.Y.: 1991) 18(12),2735-2747.

Douaud G., Smith S., Jenkinson M., Behrens T., Johansen-Berg H., Vickers J., James S., Voets N., Watkins K., Matthews P.M., and others, 2007. Anatomically related grey and white matter abnormalities in adolescent-onset schizophrenia. Brain : A Journal of Neurology 130(Pt 9),2375-2386.

Drobyshevsky A., Baumann S.B., Schneider W., 2006. A rapid fMRI task battery for mapping of visual, motor, cognitive, and emotional function. Neuroimage 31(2),732-744.

Dzeroski S. and Zenko B., 2004. Is combining classi ers with stacking better than selecting the best one? Machine Learning 54(3),255-273.

Esposito R., Mosca A., Pieramico V., Cieri F., Cera N., Sensi S.L., 2013. Characterization of resting state activity in MCI individuals. Peerj 1,e135.

Farb N.A., Grady C.L., Strother S., Tang-Wai D.F., Masellis M., Black S., Freedman M., Pollock B.G., Campbell K.L., Hasher L., and others, 2013. Abnormal network connectivity in frontotemporal dementia: Evidence for prefrontal isolation. Cortex; a Journal Devoted to the Study of the Nervous System and Behavior 49(7),1856-1873.

Feinberg D.A., Moeller S., Smith S.M., Auerbach E., Ramanna S., Gunther M., Glasser M.F., Miller K.L., Ugurbil K., Yacoub E., 2010. Multiplexed echo planar imaging for sub-second whole brain FMRI and fast diffusion imaging. PloS One 5(12),e15710.

Feinberg D.A. and Yacoub E., 2012. The rapid development of high speed, resolution and precision in fMRI. Neuroimage 62(2),720-725.

Filippini N., MacIntosh B.J., Hough M.G., Goodwin G.M., Frisoni G.B., Smith S.M., Matthews P.M., Beckmann C.F., Mackay C.E., 2009. Distinct patterns of brain activity in young carriers of the APOE-epsilon4 allele. Proceedings of the National Academy of Sciences of the United States of America 106(17),7209-7214.

Fox M.D. and Greicius M., 2010. Clinical applications of resting state functional connectivity. Frontiers in Systems Neuroscience 4,19.

Fox M.D. and Raichle M.E., 2007. Spontaneous fluctuations in brain activity observed with functional magnetic resonance imaging. Nature Reviews.Neuroscience 8(9),700-711.

Fox M.D., Snyder A.Z., Vincent J.L., Corbetta M., Van Essen D.C., Raichle M.E., 2005. The human brain is intrinsically organized into dynamic, anticorrelated functional networks. Proceedings of the National Academy of Sciences of the United States of America 102(27),9673-9678.

Fox M.D., Zhang D., Snyder A.Z., Raichle M.E., 2009. The global signal and observed anticorrelated resting state brain networks. Journal of Neurophysiology 101(6),3270-3283.

Friedman J., Hastie T., Tibshirani R., 2008. Sparse inverse covariance estimation with the graphical lasso. Biostatistics (Oxford, England) 9(3),432-441.

Friston K.J., 2011. Functional and effective connectivity: A review. Brain Connectivity 1(1),13-36.

Friston K.J., Frith C.D., Frackowiak R.S., 1993. Principal component analysis learning algorithms: A neurobiological analysis. Proceedings.Biological Sciences / the Royal Society 254(1339),47-54.

Friston K.J., Holmes A.P., Poline J.B., Frith C.D., Frackowiak R.S., 1995. Statistical parametric maps in functional imaging: A general linear approach. Hum. Brain Mapp. 20(4),189--210.

Galvin J.E., Price J.L., Yan Z., Morris J.C., Sheline Y.I., 2011. Resting bold fMRI differentiates dementia with lewy bodies vs alzheimer disease. Neurology 76(21),1797-1803.

Gili T., Cercignani M., Serra L., Perri R., Giove F., Maraviglia B., Caltagirone C., Bozzali M., 2011. Regional brain atrophy and functional disconnection across alzheimer's disease evolution. Journal of Neurology, Neurosurgery, and Psychiatry 82(1),58-66.

Glover G.H., Li T.Q., Ress D., 2000. Image-based method for retrospective correction of physiological motion effects in fMRI: RETROICOR. Magnetic Resonance in Medicine : Official Journal of the Society of Magnetic Resonance in Medicine / Society of Magnetic Resonance in Medicine 44(1),162-167.

Golestani A.M. and Goodyear B.G., 2011. Regions of interest for resting-state fMRI analysis determined by inter-voxel cross-correlation. Neuroimage 56(1),246-251.

Good C.D., Johnsrude I.S., Ashburner J., Henson R.N., Friston K.J., Frackowiak R.S., 2001. A voxel-based morphometric study of ageing in 465 normal adult human brains. Neuroimage 14(1 Pt 1),21-36.

Gottlich M., Munte T.F., Heldmann M., Kasten M., Hagenah J., Kramer U.M., 2013. Altered resting state brain networks in parkinson's disease. PloS One 8(10),e77336.

Greicius M.D., Krasnow B., Reiss A.L., Menon V., 2003. Functional connectivity in the resting brain: A network analysis of the default mode hypothesis. Proceedings of the National Academy of Sciences of the United States of America 100(1),253-258.

Greicius M.D., Srivastava G., Reiss A.L., Menon V., 2004. Default-mode network activity distinguishes alzheimer's disease from healthy aging: Evidence from functional MRI. Proceedings of the National Academy of Sciences of the United States of America 101(13),4637-4642.

Greve D.N. and Fischl B., 2009. Accurate and robust brain image alignment using boundary-based registration. Neuroimage 48(1),63-72.

Gusnard D.A., Raichle M.E., Raichle M.E., 2001. Searching for a baseline: Functional imaging and the resting human brain. Nature Reviews.Neuroscience 2(10),685-694.

Hafkemeijer A., van der Grond J., Rombouts S.A., 2012. Imaging the default mode network in aging and dementia. Biochimica Et Biophysica Acta 1822(3),431-441.

He X., Qin W., Liu Y., Zhang X., Duan Y., Song J., Li K., Jiang T., Yu C., 2013. Abnormal salience network in normal aging and in amnestic mild cognitive impairment and alzheimer's disease. Human Brain Mapping .

Hlinka J., Palus M., Vejmelka M., Mantini D., Corbetta M., 2011. Functional connectivity in resting-state fMRI: Is linear correlation sufficient? Neuroimage 54(3),2218-2225.

Howseman A.M. and Bowtell R.W., 1999. Functional magnetic resonance imaging: Imaging techniques and contrast mechanisms. Philosophical Transactions of the Royal Society of London.Series B, Biological Sciences 354(1387),1179-1194.

Jenkinson M., Bannister P., Brady M., Smith S., 2002. Improved optimization for the robust and accurate linear registration and motion correction of brain images. Neuroimage 17(2),825-841.

Jenkinson M., Beckmann C.F., Behrens T.E., Woolrich M.W., Smith S.M., 2012. Fsl. Neuroimage 62(2),782-790.

Johnson K.A., Fox N.C., Sperling R.A., Klunk W.E., 2012. Brain imaging in alzheimer disease. Cold Spring Harbor Perspectives in Medicine 2(4),a006213.

Karbasforoushan H. and Woodward N.D., 2012. Resting-state networks in schizophrenia. Current Topics in Medicinal Chemistry 12(21),2404-2414.

Khalili-Mahani N., Chang C., van Osch M.J., Veer I.M., van Buchem M.A., Dahan A., Beckmann C.F., van Gerven J.M., Rombouts S.A., 2013. The impact of "physiological correction" on functional connectivity analysis of pharmacological resting state fMRI. Neuroimage 65,499-510.

Khalili-Mahani N., Zoethout R.M., Beckmann C.F., Baerends E., de Kam M.L., Soeter R.P., Dahan A., van Buchem M.A., van Gerven J.M., Rombouts S.A., 2012. Effects of morphine and alcohol on functional brain connectivity during "resting state": A placebo-controlled crossover study in healthy young men. Human Brain Mapping 33(5),1003-1018.

Kim S.G. and Ogawa S., 2012. Biophysical and physiological origins of blood oxygenation level-dependent fMRI signals. Journal of Cerebral Blood Flow and Metabolism : Official Journal of the International Society of Cerebral Blood Flow and Metabolism 32(7),1188-1206.

Kiviniemi V., Starck T., Remes J., Long X., Nikkinen J., Haapea M., Veijola J., Moilanen I., Isohanni M., Zang Y.F., and others, 2009. Functional segmentation of the brain cortex using high model order group PICA. Human Brain Mapping 30(12),3865-3886.

Kochiyama T., Morita T., Okada T., Yonekura Y., Matsumura M., Sadato N., 2005. Removing the effects of task-related motion using independent-component analysis. Neuroimage 25(3),802-814.

Kundu P., Inati S.J., Evans J.W., Luh W.M., Bandettini P.A., 2012. Differentiating BOLD and non-BOLD signals in fMRI time series using multi-echo EPI. Neuroimage 60(3),1759-1770.

Kwong K.K., Belliveau J.W., Chesler D.A., Goldberg I.E., Weisskoff R.M., Poncelet B.P., Kennedy D.N., Hoppel B.E., Cohen M.S., Turner R., 1992. Dynamic magnetic resonance imaging of human brain activity during primary sensory stimulation. Proceedings of the National Academy of Sciences of the United States of America 89(12),5675-5679.

Li R., Wu X., Fleisher A.S., Reiman E.M., Chen K., Yao L., 2012. Attention-related networks in alzheimer's disease: A resting functional MRI study. Human Brain Mapping 33(5),1076-1088.

Li T.Q. and Wahlund L.O., 2011. The search for neuroimaging biomarkers of alzheimer's disease with advanced MRI techniques. Acta Radiologica (Stockholm, Sweden: 1987) 52(2),211-222.

Lobo A., Launer L.J., Fratiglioni L., Andersen K., Di Carlo A., Breteler M.M., Copeland J.R., Dartigues J.F., Jagger C., Martinez-Lage J., and others, 2000. Prevalence of dementia and major subtypes in europe: A collaborative study of population-based cohorts. neurologic diseases in the elderly research group. Neurology 54(11 Suppl 5),S4-9.

Logothetis N.K. and Pfeuffer J., 2004. On the nature of the BOLD fMRI contrast mechanism. Magnetic Resonance Imaging 22(10),1517-1531.

Lowe M.J., Mock B.J., Sorenson J.A., 1998. Functional connectivity in single and multislice echoplanar imaging using resting-state fluctuations. Neuroimage 7(2),119-132.

Maldjian J.A., Laurienti P.J., Kraft R.A., Burdette J.H., 2003. An automated method for neuroanatomic and cytoarchitectonic atlas-based interrogation of fMRI data sets. Neuroimage 19(3),1233-1239.

Marrelec G., Krainik A., Duffau H., Pelegrini-Issac M., Lehericy S., Doyon J., Benali H., 2006. Partial correlation for functional brain interactivity investigation in functional MRI. Neuroimage 32(1),228-237.

Marx M., Pauly K.B., Chang C., 2013. A novel approach for global noise reduction in resting-state fMRI: APPLECOR. Neuroimage 64,19-31.

McKeown M.J., Makeig S., Brown G.G., Jung T.P., Kindermann S.S., Bell A.J., Sejnowski T.J., 1998. Analysis of fMRI data by blind separation into independent spatial components. Human Brain Mapping 6(3),160-188.

McKhann G.M., Knopman D.S., Chertkow H., Hyman B.T., Jack C.R.,Jr, Kawas C.H., Klunk W.E., Koroshetz W.J., Manly J.J., Mayeux R., and others, 2011. The diagnosis of dementia due to alzheimer's disease: Recommendations from the national institute on aging-alzheimer's association workgroups on diagnostic guidelines for alzheimer's disease. Alzheimer's & Dementia : The Journal of the Alzheimer's Association 7(3),263-269.

Minoshima S., Giordani B., Berent S., Frey K.A., Foster N.L., Kuhl D.E., 1997. Metabolic reduction in the posterior cingulate cortex in very early alzheimer's disease. Annals of Neurology 42(1),85-94.

Moeller S., Yacoub E., Olman C.A., Auerbach E., Strupp J., Harel N., Ugurbil K., 2010. Multiband multislice GE-EPI at 7 tesla, with 16-fold acceleration using partial parallel imaging with application to high spatial and temporal whole-brain fMRI. Magnetic Resonance in Medicine : Official Journal of the Society of Magnetic Resonance in Medicine / Society of Magnetic Resonance in Medicine 63(5),1144-1153.

Murphy K., Birn R.M., Bandettini P.A., 2013. Resting-state fMRI confounds and cleanup. Neuroimage 80,349-359.

Murphy K., Birn R.M., Handwerker D.A., Jones T.B., Bandettini P.A., 2009. The impact of global signal regression on resting state correlations: Are anti-correlated networks introduced? Neuroimage 44(3),893-905.

Niazy R.K., Xie J., Miller K., Beckmann C.F., Smith S.M., 2011. Spectral characteristics of resting state networks. Progress in Brain Research 193,259-276.

Ogawa S., Lee T.M., Kay A.R., Tank D.W., 1990. Brain magnetic resonance imaging with contrast dependent on blood oxygenation. Proceedings of the National Academy of Sciences of the United States of America 87(24),9868-9872.

Perlbarg V., Bellec P., Anton J.L., Pelegrini-Issac M., Doyon J., Benali H., 2007. CORSICA: Correction of structured noise in fMRI by automatic identification of ICA components. Magnetic Resonance Imaging 25(1),35-46.

Popa D., Popescu A.T., Pare D., 2009. Contrasting activity profile of two distributed cortical networks as a function of attentional demands. The Journal of Neuroscience : The Official Journal of the Society for Neuroscience 29(4),1191-1201.

Power J.D., Barnes K.A., Snyder A.Z., Schlaggar B.L., Petersen S.E., 2012. Spurious but systematic correlations in functional connectivity MRI networks arise from subject motion. Neuroimage 59(3),2142-2154.

Raichle M.E., MacLeod A.M., Snyder A.Z., Powers W.J., Gusnard D.A., Shulman G.L., 2001. A default mode of brain function. Proceedings of the National Academy of Sciences of the United States of America 98(2),676-682.

Raichle M.E. and Mintun M.A., 2006. Brain work and brain imaging. Annual Review of Neuroscience 29,449-476.

Raichle M.E. and Snyder A.Z., 2007. A default mode of brain function: A brief history of an evolving idea. Neuroimage 37(4),1083-90; discussion 1097-9.

Rubinov M. and Sporns O., 2010. Complex network measures of brain connectivity: Uses and interpretations. Neuroimage 52(3),1059-1069.

Rytty R., Nikkinen J., Paavola L., Abou Elseoud A., Moilanen V., Visuri A., Tervonen O., Renton A.E., Traynor B.J., Kiviniemi V., and others, 2013. GroupICA dual regression analysis of resting state networks in a behavioral variant of frontotemporal dementia. Frontiers in Human Neuroscience 7,461.

Saad Z.S., Gotts S.J., Murphy K., Chen G., Jo H.J., Martin A., Cox R.W., 2012. Trouble at rest: How correlation patterns and group differences become distorted after global signal regression. Brain Connectivity 2(1),25-32.

Salimi-Khorshidi G., Douaud G., Beckmann C.F., Glasser M., Griffanti L., Smith S.M., 2013. Automatic denoising of functional MRI data: Combining independent component analysis and hierarchical fusion of classifiers. Neuroimage 2014; 90C 449-468..

Sambataro F., Wolf N.D., Pennuto M., Vasic N., Wolf R.C., 2013. Revisiting default mode network function in major depression: Evidence for disrupted subsystem connectivity. Psychological Medicine ,1-11.

Satterthwaite T.D., Elliott M.A., Gerraty R.T., Ruparel K., Loughead J., Calkins M.E., Eickhoff S.B., Hakonarson H., Gur R.C., Gur R.E., and others, 2013. An improved framework for confound regression and filtering for control of motion artifact in the preprocessing of resting-state functional connectivity data. Neuroimage 64,240-256.

Satterthwaite T.D., Wolf D.H., Loughead J., Ruparel K., Elliott M.A., Hakonarson H., Gur R.C., Gur R.E., 2012. Impact of in-scanner head motion on multiple measures of functional connectivity: Relevance for studies of neurodevelopment in youth. Neuroimage 60(1),623-632.

Schreiber T. and Schmitz A., 2000. Surrogate time series. Physica D: Nonlinear Phenomena 142(3-4),346-382.

Setsompop K., Gagoski B.A., Polimeni J.R., Witzel T., Wedeen V.J., Wald L.L., 2012. Blipped-controlled aliasing in parallel imaging for simultaneous multislice echo planar imaging with reduced g-factor penalty. Magnetic Resonance in Medicine : Official Journal of the Society of Magnetic Resonance in Medicine / Society of Magnetic Resonance in Medicine 67(5),1210-1224.

Shehzad Z., Kelly A.M., Reiss P.T., Gee D.G., Gotimer K., Uddin L.Q., Lee S.H., Margulies D.S., Roy A.K., Biswal B.B., and others, 2009. The resting brain: Unconstrained yet reliable. Cerebral Cortex (New York, N.Y.: 1991) 19(10),2209-2229.

Shmueli K., van Gelderen P., de Zwart J.A., Horovitz S.G., Fukunaga M., Jansma J.M., Duyn J.H., 2007. Low-frequency fluctuations in the cardiac rate as a source of variance in the resting-state fMRI BOLD signal. Neuroimage 38(2),306-320.

Smith S.M., 2012. The future of FMRI connectivity. Neuroimage 62(2),1257-1266.

Smith S.M., 2002. Fast robust automated brain extraction. Human Brain Mapping 17(3),143-155.

Smith S.M., Beckmann C.F., Andersson J., Auerbach E.J., Bijsterbosch J., Douaud G., Duff E., Feinberg D.A., Griffanti L., Harms M.P., and others, 2013. Resting-state fMRI in the human connectome project. Neuroimage 80,144-168.

Smith S.M., Beckmann C.F., Ramnani N., Woolrich M.W., Bannister P.R., Jenkinson M., Matthews P.M., McGonigle D.J., 2005. Variability in fMRI: A re-examination of inter-session differences. Human Brain Mapping 24(3),248-257.

Smith S.M., Fox P.T., Miller K.L., Glahn D.C., Fox P.M., Mackay C.E., Filippini N., Watkins K.E., Toro R., Laird A.R., and others, 2009. Correspondence of the brain's functional architecture during activation and rest. Proceedings of the National Academy of Sciences of the United States of America 106(31),13040-13045.

Smith S.M., Jenkinson M., Woolrich M.W., Beckmann C.F., Behrens T.E., Johansen-Berg H., Bannister P.R., De Luca M., Drobnjak I., Flitney D.E., and others, 2004. Advances in functional and structural MR image analysis and implementation as FSL. Neuroimage 23 Suppl 1,S208-19.

Smith S.M., Miller K.L., Salimi-Khorshidi G., Webster M., Beckmann C.F., Nichols T.E., Ramsey J.D., Woolrich M.W., 2011. Network modelling methods for FMRI. Neuroimage 54(2),875-891.

Song X.W., Dong Z.Y., Long X.Y., Li S.F., Zuo X.N., Zhu C.Z., He Y., Yan C.G., Zang Y.F., 2011. REST: A toolkit for resting-state functional magnetic resonance imaging data processing. PloS One 6(9),e25031.

Sorg C., Riedl V., Perneczky R., Kurz A., Wohlschlager A.M., 2009. Impact of alzheimer's disease on the functional connectivity of spontaneous brain activity. Current Alzheimer Research 6(6),541-553.

Stephan K.E., Mattout J., David O., Friston K.J., 2006. Models of functional neuroimaging data. Current Medical Imaging Reviews 2(1),15-34.

Taylor K.S., Seminowicz D.A., Davis K.D., 2009. Two systems of resting state connectivity between the insula and cingulate cortex. Human Brain Mapping 30(9),2731-2745.

Thomas C.G., Harshman R.A., Menon R.S., 2002. Noise Reduction in BOLD-Based fMRI Using Component Analysis. Neuroimage 17, 1521-1537.

Tian L., Kong Y., Ren J., Varoquaux G., Zang Y., Smith S.M., 2013. Spatial vs. temporal features in ICA of resting-state fMRI - A quantitative and qualitative investigation in the context of response inhibition. PloS One 8(6),e66572.

Tohka J., Foerde K., Aron A.R., Tom S.M., Toga A.W., Poldrack R.A., 2008. Automatic independent component labeling for artifact removal in fMRI. Neuroimage 39(3),1227-1245.

Triantafyllou C., Hoge R.D., Krueger G., Wiggins C.J., Potthast A., Wiggins G.C., Wald L.L., 2005. Comparison of physiological noise at 1.5 T, 3 T and 7 T and optimization of fMRI acquisition parameters. Neuroimage 26(1),243-250.

van den Heuvel M.P. and Hulshoff Pol H.E., 2010. Exploring the brain network: A review on resting-state fMRI functional connectivity. European Neuropsychopharmacology : The Journal of the European College of Neuropsychopharmacology 20(8),519-534.

van den Heuvel M.P., Stam C.J., Boersma M., Hulshoff Pol H.E., 2008. Small-world and scale-free organization of voxel-based resting-state functional connectivity in the human brain. Neuroimage 43(3),528-539.

Van Dijk K.R., Hedden T., Venkataraman A., Evans K.C., Lazar S.W., Buckner R.L., 2010. Intrinsic functional connectivity as a tool for human connectomics: Theory, properties, and optimization. Journal of Neurophysiology 103(1),297-321.

Van Dijk K.R., Sabuncu M.R., Buckner R.L., 2012. The influence of head motion on intrinsic functional connectivity MRI. Neuroimage 59(1),431-438.

Van Essen D.C. and Ugurbil K., 2012. The future of the human connectome. Neuroimage 62(2),1299-1310.

Varsou O., Macleod M.J., Schwarzbauer C., 2013. Functional connectivity magnetic resonance imaging in stroke: An evidence-based clinical review. International Journal of Stroke : Official Journal of the International Stroke Society .

Veer I.M., Beckmann C.F., van Tol M.J., Ferrarini L., Milles J., Veltman D.J., Aleman A., van Buchem M.A., van der Wee N.J., Rombouts S.A., 2010. Whole brain resting-state analysis reveals decreased functional connectivity in major depression. Frontiers in Systems Neuroscience 4,10.3389/fnsys.2010.00041.

Wang K., Liang M., Wang L., Tian L., Zhang X., Li K., Jiang T., 2007. Altered functional connectivity in early alzheimer's disease: A resting-state fMRI study. Human Brain Mapping 28(10),967-978.

Wang L., Li H., Liang Y., Zhang J., Li X., Shu N., Wang Y.Y., Zhang Z., 2013. Amnestic mild cognitive impairment: Topological reorganization of the default-mode network. Radiology 268(2),501-514.

Weissenbacher A., Kasess C., Gerstl F., Lanzenberger R., Moser E., Windischberger C., 2009. Correlations and anticorrelations in resting-state functional connectivity MRI: A quantitative comparison of preprocessing strategies. Neuroimage 47(4),1408-1416.

Wolpert D., 1992. Stacked generalization. Neural Networks 5(2),241-259.

Woolrich M.W., Behrens T.E., Beckmann C.F., Smith S.M., 2005. Mixture models with adaptive spatial regularization for segmentation with an application to FMRI data. IEEE Transactions on Medical Imaging 24(1),1-11.

Xiong J., Parsons L.M., Gao J.H., Fox P.T., 1999. Interregional connectivity to primary motor cortex revealed using MRI resting state images. Human Brain Mapping 8(2-3),151-156.

Zamboni G., Wilcock G.K., Douaud G., Drazich E., McCulloch E., Filippini N., Tracey I., Brooks J.C., Smith S.M., Jenkinson M., and others, 2013. Resting functional connectivity reveals residual functional activity in alzheimer's disease. Biological Psychiatry 74(5),375-383.

Zarzoso, V. and Nandi, A.K. 1999. Blind source separation. In: A. K. Nandi (Ed.), Blind Estimation Using Higher-Order Statistics. Springer US, pp. 167-252.

Zhang H.Y., Wang S.J., Liu B., Ma Z.L., Yang M., Zhang Z.J., Teng G.J., 2010. Resting brain connectivity: Changes during the progress of alzheimer disease. Radiology 256(2),598-606.

Zhang H.Y., Wang S.J., Xing J., Liu B., Ma Z.L., Yang M., Zhang Z.J., Teng G.J., 2009. Detection of PCC functional connectivity characteristics in resting-state fMRI in mild alzheimer's disease. Behavioural Brain Research 197(1),103-108.

Zhang Y., Brady M., Smith S., 2001. Segmentation of brain MR images through a hidden markov random field model and the expectation-maximization algorithm. IEEE Transactions on Medical Imaging 20(1),45-57.